substantially decreased due to nonlinear behavior of the building, which generally occurs under high intensity ground motions.

However, unlike the linear system, describing the effectiveness of TMD using peak response reduction of the nonlinear structures alone seems insufficient [8]. Obviously, this measure cannot account for the effects of accumulated damage due to low cycle fatigue. That is of particular importance for the seismic application where the structure may experience a significant number of nonlinear vibration cycles. Therefore, in such circumstances, TMD is expected to effectively reduce not only the peak response of the structure but also the induced-damage of the structure.

In this study, damage reduction is proposed as an indicator to evaluate seismic effectiveness of TMD with inelastic structures. A 20-storey reinforced concrete building is modeled by an equivalent inelastic single-degree-of-freedom system. The numerical simulations of the building with and without TMD attached on top are performed. Two records of ground motion characterized by a harmonic and a distant earthquake are examined. The inelastic behavior of the structure is introduced by increasing the peak ground acceleration of ground motions. By considering the variation of the energy dissipation in the structure, the TMD's control characteristic and its inability to control high intensity ground motion as found in the literature are explained. Since the structure is excited in the inelastic range, the damage is quantified employing the well-accepted damage index [9]. By comparing the induced-damage indices for the structure with and without TMD, the effectiveness of TMD can be evaluated and explained.

2. An example reinforced concrete building

In this study, a 20-story reinforced concrete office building is considered. The plan and elevation of the building is shown in Fig. 1. The building utilizes a structural system with moment-resisting frames in the longitudinal direction and a coupled moment-resisting frameshear wall system in the transverse direction. The building is designed only for gravity and wind loads for Thailand with non-ductile reinforcement details. A uniformly distributed live load of 2,500 N/m² and a maximum wind pressure of approximately 1,400 N/m² are employed. Compressive strength of concrete of 30 MPa and yield strength of reinforcement of 40 MPa are used. The cross-sections of the shear walls and beams are 0.30×8.00 m and 0.30×0.60 m, respectively, while the dimensions of the columns vary from 0.95×0.95 m at the first floor to 0.45×0.45 m at the roof floor. The program IDARC [10] is used to model the structure. The fundamental period of the structure, determined from analysis in the transverse direction, is found to be 2.13 seconds. Pushover analysis using an inverted triangular load is also performed. Fig. 2 plots the roof displacement of the structure against the base shear of the structure. It should be noted that response due to designed wind load is well within the elastic range of the curve.

3. An equivalent inelastic SDOF

The 20-story building outlined in previous section is modeled by an equivalent inelastic single-degree-of-freedom (SDOF) system. The nonlinear pushover characteristics of the building are ascertained and then its load-deformation characteristic is replaced by the elastic-perfectly plastic behavior of the SDOF system. Although there exist many

formulations in the literatures for selection of the equivalent inelastic SDOF, the formulation proposed by Fajfar and Fischinger [11] is adopted in this study.

The equation of motion that governs the response of the structure when subjected to ground excitation can be expressed as

$$\mathbf{M}\ddot{\mathbf{u}}(t) + \mathbf{C}\dot{\mathbf{u}}(t) + \mathbf{Q}(t) = -\mathbf{M}\mathbf{r}\ddot{\mathbf{x}}_{g}(t) \tag{1}$$

where

M and C are, respectively, the mass and damping matrices of the structure; $\ddot{\mathbf{u}}(t)$ and $\dot{\mathbf{u}}(t)$ are, respectively, the acceleration and velocity vectors of the structure relative to the ground;

- Q(t) is the storey restoring force vector of the structure;
- r is the influence coefficient vector which represents the displacement vector, $\mathbf{u}(t)$, resulting from a unit support displacement and
- $\ddot{x}_{g}(t)$ is the acceleration of the input ground motion.

The base shear force of the structure is determined from $V(t) = \{1\}^{T}Q(t)$.

Using the transformation of the roof displacement of the structure, $u^*(t)$, to the displacement of the SDOF, x(t), by

$$x(t) = \frac{\Phi^{\mathsf{T}} \mathbf{M} \Phi}{\Phi^{\mathsf{T}} \mathbf{M} \mathbf{r}} u^{*}(t)$$
 (2)

in which Φ is the assumed shape vector of the structure normalized with respect to $u^*(t)$, the above equation of motion of the structure, Eq. (1), can be rewritten as

$$m\ddot{x}(t) + c\dot{x}(t) + q(t) = -m\ddot{x}_{g}(t) \tag{3}$$

where

 $m = \Phi^{T} \mathbf{M} \mathbf{r}$ is an equivalent mass;

$$c = \Phi^{T} \mathbf{C} \Phi \cdot \frac{\Phi^{T} \mathbf{M} \mathbf{r}}{\Phi^{T} \mathbf{M} \Phi}$$
 is an equivalent damping;

 $q(t) = \Phi^{T} \mathbf{Q}(t)$ is an equivalent restoring force and

 $\ddot{x}(t)$ and $\dot{x}(t)$ are the acceleration and the velocity of the equivalent SDOF.

Based on the load-displacement relationship of the structure obtained from pushover analysis with an inverted-triangle load distribution as shown in Fig. 2, the corresponding properties of the equivalent elastic-perfectly plastic SDOF previously mentioned can be computed as listed in Table 1 and plotted as the dotted-line in the same figure.

4. Earthquake ground motions

Two different ground motions, characterized by harmonic acceleration and distant earthquake acceleration, are employed as the input ground motions. Both are scaled to have various peak ground accelerations (PGA) in order to study the influence of the degree of inelasticity in the structure on the effectiveness of TMD. Harmonic ground motion is generated for 50 seconds from a constant amplitude sine wave with the same period as that of the structure, while the acceleration record at the SCT station of the 1985 Mexico City earthquake is used to represent distant earthquake ground motion. The dominant period of this acceleration record is very close to that of the structure. These intentionally lead to extreme conditions where the structure vibrates in resonance with the excitations and consequently TMD is expected to be effective for suppression of both displacement and energy of the structure.

5. Damage quantification

For earthquake excitation, it is generally necessary to permit some degree of induced-damage in the structure, otherwise the design would be too costly. However, the damage should be kept below a certain amount in order to avoid collapse.

To investigate the effectiveness of TMD in reducing damage to the structure induced by ground excitation, the damage index as suggested by Park et al. [9] is adopted for the system Eq. (1), which can be globally described by

$$DI = \frac{u_m^*}{u_u^*} + \beta \frac{\int dE}{u_u^* V_y} \tag{4}$$

where

 u_m^* and u_u^* are the maximum and the ultimate displacements of the structure at roof, respectively;

 $\int dE$ is the cumulative hysteresis energy of the structure;

 V_y is the base shear at yielding of the structure and

 β is the strength deterioration parameter (≈ 0.27 by Ciampoli, et al. [12]).

This damage equation accounts for damage due to maximum inelastic displacement, as well as damage due to cumulative low-cycle fatigue. The value of DI can vary from 0 to 1.0, which corresponds respectively to the damage level of the structure from no damage to collapse [13].

6. Structure with tuned mass damper (TMD)

A TMD is installed on top of the structure to reduce the displacement and the damage induced by ground excitations. For computational convenience, the equivalent inelastic SDOF obtained in Section 3 is employed to represent the 20-story R/C building as outlined in Section 2. Thus the equations of motion describing the structure-TMD interaction can be simply expressed by

$$m\ddot{x}(t) + c\dot{x}(t) + q(t) = -m\ddot{x}_{\sigma}(t) + c_{T}\dot{z}(t) + k_{T}z(t)$$
 (5)

and
$$m_T \ddot{z}(t) + c_T \dot{z}(t) + k_T z(t) = -m_T \left[\ddot{x}_g(t) + \ddot{x}(t) \right]$$
 (6)

where -

 $\textit{m}_{\textit{T}}$, $\textit{c}_{\textit{T}}$ and $\textit{k}_{\textit{T}}$ are the mass, damping, and stiffness of the TMD, respectively;

and $\ddot{z}(t)$, $\dot{z}(t)$, and z(t) are the relative acceleration, velocity and displacement of the TMD.

In the following numerical investigation, a mass ratio of 1.40%, corresponding to an effective mass ratio of 0.03 between the TMD mass and the structure's first-mode generalized mass, is considered. Assuming linear behavior of the controlled structure, the stiffness and damping coefficients of TMD are optimized for harmonic base excitation [14]. This yields the optimal values of the TMD parameters as listed in Table 1 along with the properties of the example structure.

7. Effectiveness of TMD under a harmonic ground motion

The effectiveness of TMD is evaluated under harmonic ground motion. The inability to control high intensity ground motion is demonstrated and explained. The use of damage

reduction of the structure as the effectiveness measure of TMD is introduced instead of using displacement reduction alone.

7.1 Displacement Reduction

Figs 3 and 4 show the typical displacement histories of the structure with and without TMD under harmonic ground motion with PGAs of 0.01g and 0.05g, respectively. The motion frequency is intentionally set to be the natural frequency of the structure. In these figures, the former represents the case where the structure is vibrated within the elastic range and significant displacement reduction of the structure can be gained from the application of TMD, whereas the latter represents the case where the structure is vibrated well within the inelastic range and the displacement reduction of the structure by application of TMD is substantially decreased. To show the influence of degree of inelasticity in the structure on the performance of TMD, Fig. 5 compares the displacement ratio of the structure with and without TMD for various PGAs of ground motion. In the figure, the displacement ratio of the structure is calculated from the ratio of the steady-state displacement of the inelastic structure with or without TMD to that of the corresponding elastic structure without TMD, while the input PGA is represented by the normalized PGA, $\left|\ddot{x}_{g}\right|/(q_{y}/m)$. To ascertain the effectiveness of TMD in terms of displacement reduction of the structure, Fig. 6 plots the steady-state displacement reduction of the structure due to the application of TMD as a function of normalized PGA. It is obvious from Figs. 5 and 6 that TMD is very effective in reducing the displacement of the structure by as much as 77% when normalized PGA is less than 0.042. This is the case where the structure is vibrated within its elastic range. However, beyond this range, the TMD's effectiveness gradually decreases as the PGA increases and

becomes as small as 10% when normalized PGA is greater than 0.176. These findings coincide with those found by previous studies [4,7] in which the effectiveness of TMD is reported to be substantially deteriorated when the structure's motion is characterized by significant inelastic vibration. This control deficiency can be demonstrated through inspection of the energy dissipation of TMD as shown in Fig. 7. In the figure, the energy dissipation in the structure due to inherent damping, yielding and TMD are normalized by the corresponding kinetic energy of the structure and are plotted against the normalized PGA. The figure shows that TMD slightly loses its effectiveness in dissipating the energy from the structure once yielding occurs in the structure. This is because yielding raises the apparent damping of the structure and consequently disturbs the tuning condition of TMD. Although the dissipation reduction of TMD seems significant in this considered range of PGA, the large amount of dissipation due to yielding causes the contribution of TMD to become a comparatively small portion. As a result, a displacement reduction of the structure of only 10% is obtained from the application of TMD.

7.2 Damage Reduction

It is clear from Figs 5 and 6 that TMD can completely protect the building from yielding up to a normalized PGA of 0.156. Although the displacement reduction in this range indicates deterioration of TMD's effectiveness, this is of particular importance for seismic applications in which the objective of TMD installation is to suppress the damage to the structure rather than its displacement.

Therefore, the following introduces the damage reduction of the structure to describe the effectiveness of TMD instead of the displacement reduction. Employing the

damage model previously outlined, Fig. 8 compares the damage index of the structure with and without TMD under harmonic ground motion, while Fig. 9 shows the damage reduction gained from TMD. In the figure, the damage reduction is calculated from the difference between damage to the structure with TMD and without TMD divided by that without TMD, $(DI_{w/o}-DI_{TMD})/DI_{w/o}$. It is pointed out that, for normalized PGA less than 0.042, the damage reduction of the structure due to TMD is not defined since there is no damage to the corresponding structure without TMD. Unlike the displacement reduction as in Fig. 6, the figure shows complete damage reduction due to TMD for normalized PGA between 0.042 and 0.156. This implies the usefulness of TMD even when the structure is subjected to moderate input ground motion. However, further increasing the PGA causes yielding in the structure with TMD and damage reduction of about 40-70% is obtained for normalized PGA between 0.156 and 0.306. In this range of input PGA, the damage reduction decreases as the PGA increases. It is also observed that, for normalized PGA between 0.306 and 0.443, the computed damage of the structure without TMD exceeds the collapse limit, i.e. DI>1.0, while that of the structure with TMD is still within the limit. This corresponds to the case where the TMD can prevent the structure from collapse. Beyond this range of input PGA (normalized PGA greater than 0.443), the structure with TMD also collapses and therefore the application of TMD to the structure provides no benefit.

8. Effectiveness of TMD under a distant earthquake

In this section, ground motion recorded from the distant earthquake in Mexico City (1985) at SCT station in the N-S direction is employed as the input ground excitation. This record

is found to have its predominant period close to the first natural period of the structure. The effectiveness of TMD is again evaluated in terms of displacement and damage reduction of the structure

8.1 Displacement Reduction

Fig. 10 plots the displacement ratio of the structure with and without TMD against the input PGA of ground motion. In this figure, the displacement ratios are calculated using peak displacement instead of steady-state displacement as in Fig. 5. It can be seen from the figure that TMD is very effective in reducing the peak displacement of the structure when the structure is vibrated within the elastic range. However, its effectiveness gradually decreases as the inelasticity in the structure increases. It is noticed that, for normalized PGA higher than 0.40, the structure with TMD exhibits larger displacement than that without TMD. This leads to negative displacement reduction of TMD as shown in Fig. 11.

8.2 Damage Reduction

Fig. 12 compares the damage indices of the structure with and without TMD under the SCT ground motion for various PGAs, while Fig. 13 shows the damage reduction gained from the application of TMD. The figures reveal that TMD always reduces the damage to the structure for the entire range of PGA considered. Similar to the case of the harmonic ground motion, TMD perfectly protects the structure from damage for normalized PGA less than 0.20, and yields about 20-40% reduction of the damage for normalized PGA from 0.20 to 0.685. It is interesting to note that, for normalized PGA greater than 0.40, TMD provides positive effectiveness in damage reduction of the structure although its effectiveness in terms of displacement reduction is found to be negative (see also Fig. 11). This is because the

damage index of the structure under the SCT ground motion is mainly governed by the energy term, i.e. the second term of Eq. (4), which is effectively reduced by TMD. It should also be noted that, for this ground excitation, TMD prevents collapse for normalized PGA from 0.685 to 0.841. Beyond this range of the input PGA, the structure with TMD collapses and therefore the application of TMD becomes useless.

9. Conclusions

The effectiveness of the TMD for control of the 20-storey reinforced concrete building subjected to both harmonic and the 1985 Mexico City (SCT) ground motions is investigated. Using numerical simulation, the obtained results indicate that the commonly used displacement reduction of the structure fails to prescribe the effectiveness of the TMD when damage occurs in the structure. This is because it does not provide sufficient information on the damage state of the controlled structure which is the main concern in engineering applications.

Therefore, direct use of damage reduction of the structure becomes more relevant and it is employed as the indicator of TMD effectiveness in this paper. Based on the ground motions considered, which have predominant periods close to that of the structure, the TMD is found to provide damage protection for the structure up to a certain level of input PGA. With a higher level of input PGA, it also significantly reduced the damage to the structure, which would suffer substantial damage in its absence. With further increase of input PGA, it is found that the application of TMD can prevent the structure from collapse.

By comparing these damage characteristics to those of the structure with higher yield strength of base shear, this application of TMD is equivalent to an increase in the yield strength of the structure of about 45% and 20% for the harmonic and the SCT ground motions, respectively. This is of practical significance in view of the current trend toward performance based design in which the TMD may be installed to achieve the target performance of buildings designed for seismic loads.

Acknowledgements

The authors are grateful to the Thailand Research Funds (TRF) for the research scholar grant for this project. They would like to thank Mr. P. Vaijunya for providing the design of the example structure used in this study.

References

- [1] ENR. Handcock Tower Now to get dampers. *Engineering News-Record*, 1975, Oct. 30:11.
- [2] Kwok KCS, MacDonald PA. Full-scale measurements of acceleration response of Sydney Tower. *Engineering Structures* 1990; **12**:153-162.
- [3] Kaynai AM, Veneziano D, Biggs JM. Seismic effectiveness of tuned mass dampers.

 Journal of Structural Engineering, ASCE 1981; 107(8):1465-1484.
- [4] Sladek JR and Klingner RE. Effect of tuned mass dampers on seismic response.

 Journal of Structural Engineering, ASCE 1983; 109(8):2004-2009.

- [5] Chowdhury AH, Iwuchukwu MD, Garske JJ. Past and future of seismic effectiveness of tuned mass dampers. *Proceedings of the 2nd International Symposium on Structural Control*, Ontario, Canada, 1985; 105-127.
- [6] Villaverde R, Koyoama LA. Damped resonant appendages to increase inherent damping in buildings. Earthquake Engineering and Structural Dynamics 1993; 22:491-507.
- [7] Soto-Brito R, Ruiz SE. Influence of ground motion intensity on the effectiveness of tuned mass dampers. Earthquake Engineering and Structural Dynamics 1999; 28:1255-1271.
- [8] Lukkunaprasit P, Wanitkorkul A. Inelastic buildings with tuned mass dampers under moderate ground motions from distant earthquakes. Earthquake Engineering and Structural Dynamics 2001; 30(4):537-551.
- [9] Park YJ, Ang AHS, Wen YK. Mechanistic seismic damage model for reinforced concrete. *Journal of Structural Engineering, ASCE* 1985; 111(4):722-739.
- [10] Valles RE, Reinhorn AM, Kunnath SK, Li C, Madan A. IDARC2D Version 4.0: A computer program for the inelastic damage analysis of buildings. *Technical Report NCEER-96-0010*, University of New York at Buffalo, USA, 1996.
- [11] Fajfar P, Fischinger M. N2- A method for non-linear seismic analysis of regular buildings. Proceedings of the 9th World Conference on Earthquake Engineering, Tokyo, Japan, 1988; 111-116.
- [12] Ciampoli M, Giannini R, Nuti C, Pinto PE. Seismic reliability of non-linear structures with stochastic parameters by directional simulation. *Proceedings of the 5th*

- International Conference on Structural Safety and Reliability, San Francisco, USA, 1989; 1121-1128.
- [13] Park YJ, Ang AHS, Wen YK. Damage-limiting aseismic design of buildings.

 Earthquake Spectra 1987; 3:565-619.
- [14] Warburton GB. Optimum absorber parameters for various combinations of response and excitation parameters. Earthquake Engineering and Structural Dynamics 1982; 10:381-401.

LIST OF TABLES AND FIGURES

<u>TABLE</u>	TITLE		
Table 1	Properties of the structure, the equivalent inelastic SDOF and TMD.		
FIGURE	TITLE		
Figure 1	Elevation and plan of a 20-storey reinforced concrete building		
Figure 2	Pushover curve of structure		
Figure 3	Displacement histories of structure with and without TMD under harmonic		
	ground motion with PGA of 0.01g		
Figure 4	Displacement histories of structure under harmonic ground motion with PGA		
	of 0.05g		
Figure 5	Normalized displacement ratio of structure against normalized PGA		
Figure 6	Displacement reduction of structure with TMD against normalized PGA		
Figure 7	Normalized energy dissipation in structure with TMD against normalize		
	PGA		
Figure 8	Damage index of structure against normalized PGA		
Figure 9	Damage reduction of structure with TMD against normalized PGA		
Figure 10	Displacement ratio of the structure against normalized PGA		
Figure 11	Displacement reduction of the structure with TMD against normalized PGA		
Figure 12	Damage index of structure against normalized PGA		
Figure 13	Damage reduction of structure with TMD against normalized PGA		

Table 1 Properties of the structure, the equivalent inelastic SDOF and TMD.

Structure	System, Eq.(1)	$W = 378.0 \text{ MN}, V_y = 43.5 \text{ MN},$ $u_y^* = 0.258 \text{ m}, u_u^* = 1.68 \text{ m}, \text{ ductility} = 6.5$
	SDOF, Eq.(3)	$m = 17.9 \times 10^4 \text{ tons}, \ \omega = 2.95 \text{ rad/s}, \ \xi = 0.02$ $q_y = 27.4 \text{ MN}, \ x_y = 0.175 \text{ m}, \ x_u = 1.14 \text{ m}$
Tuned Mass Damper (TMD)		$m_T = 5.37 \times 10^4 \text{ tons, } k_T = 4.41 \times 10^5 \text{ kN/m,}$ $\omega_T = 2.87 \text{ rad/s, } \xi_T = 0.105$

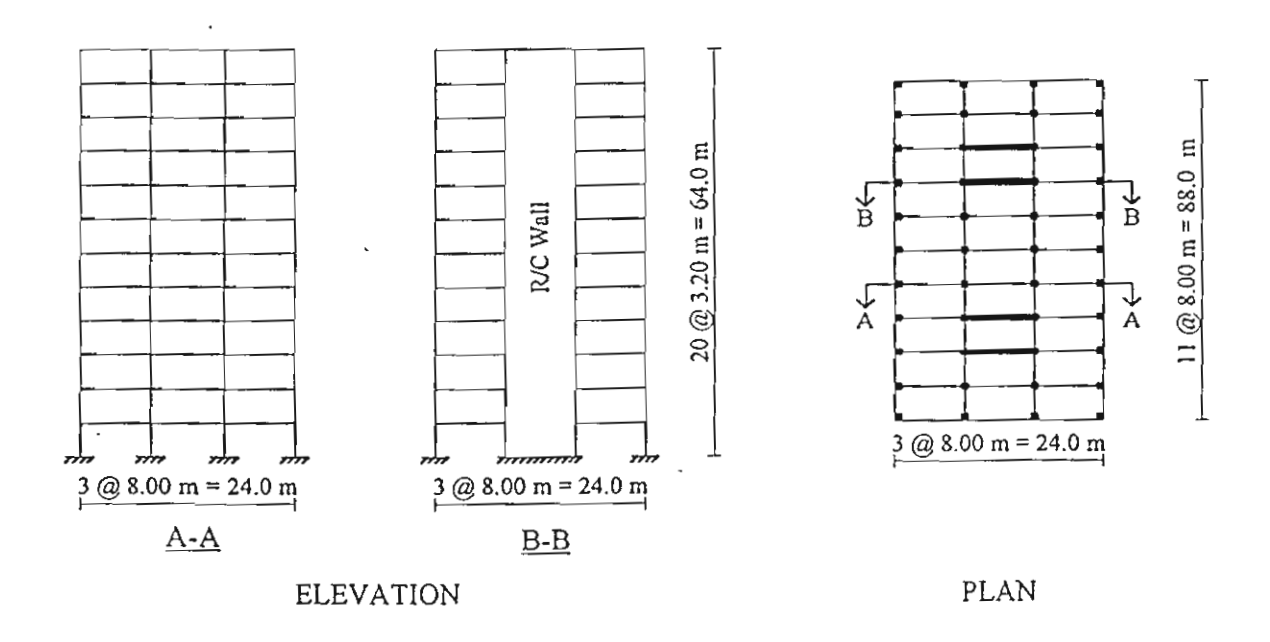


Figure 1 Elevation and plan of a 20-storey reinforced concrete building

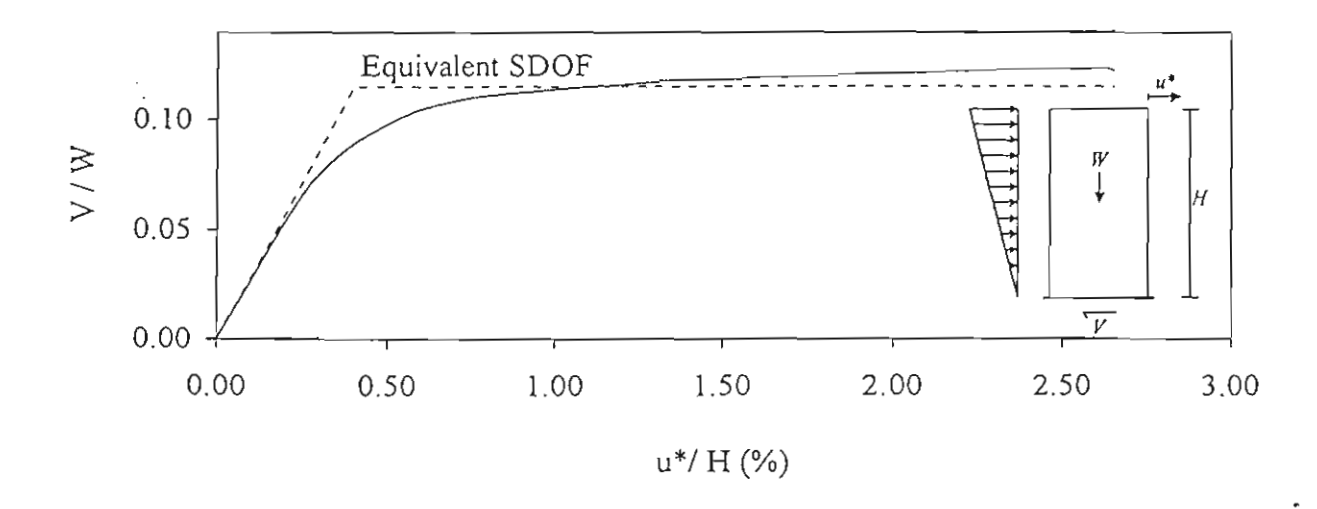


Figure 2 Pushover curve of structure

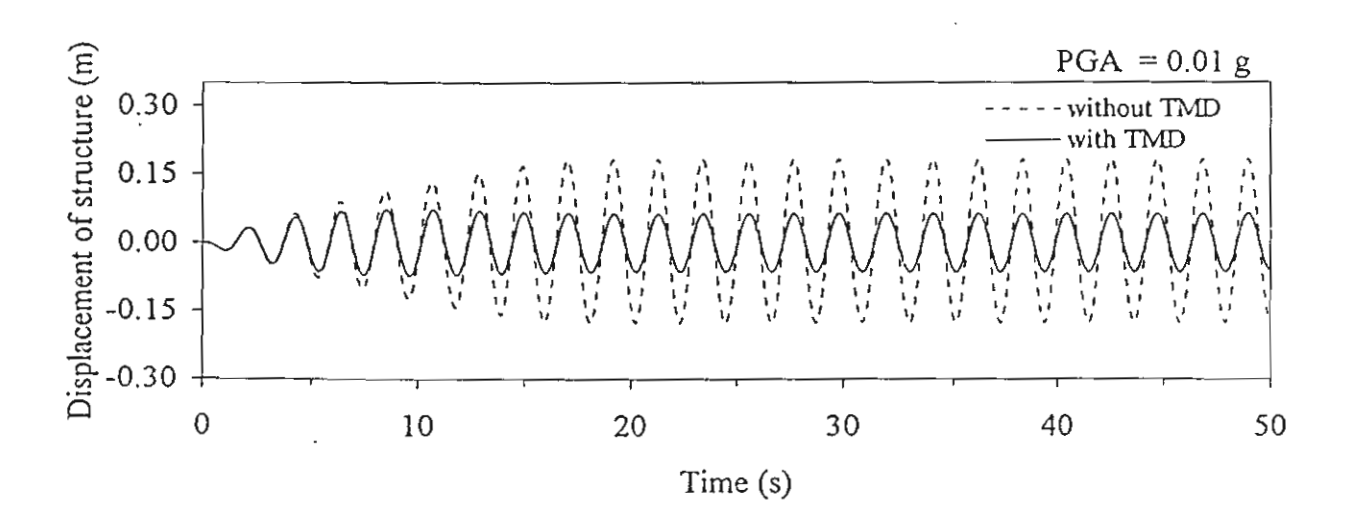


Figure 3 Displacement histories of structure with and without TMD under harmonic ground motion with PGA of 0.01g

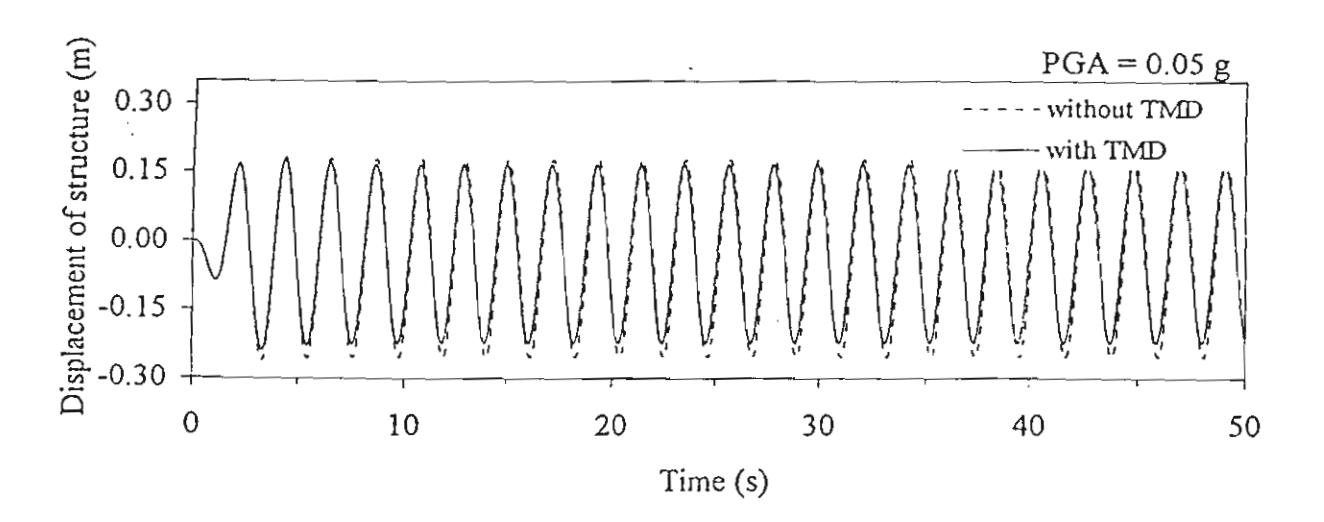


Figure 4 Displacement histories of structure under harmonic ground motion with PGA of 0.05g

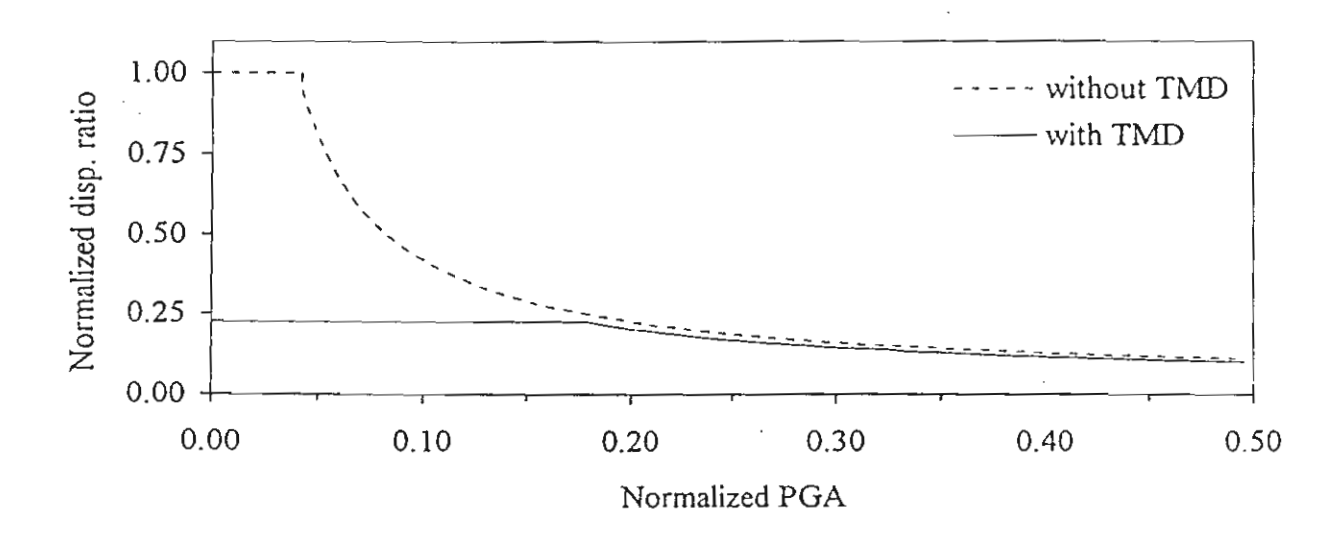


Figure 5 Normalized displacement ratio of structure against normalized PGA

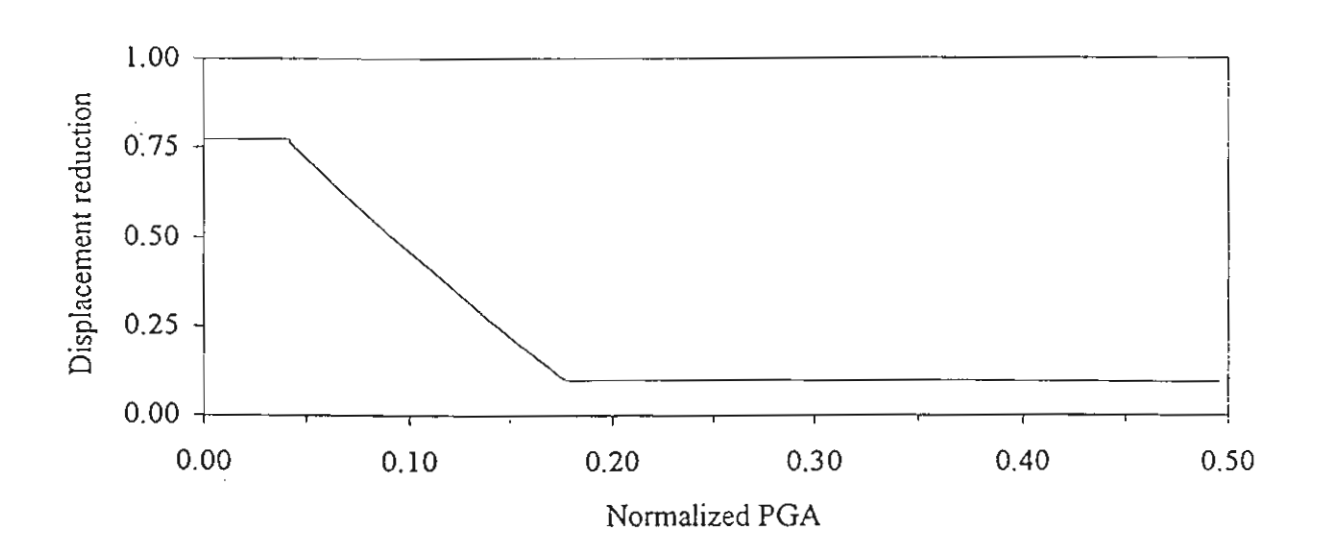


Figure 6 Displacement reduction of structure with TMD against normalized PGA

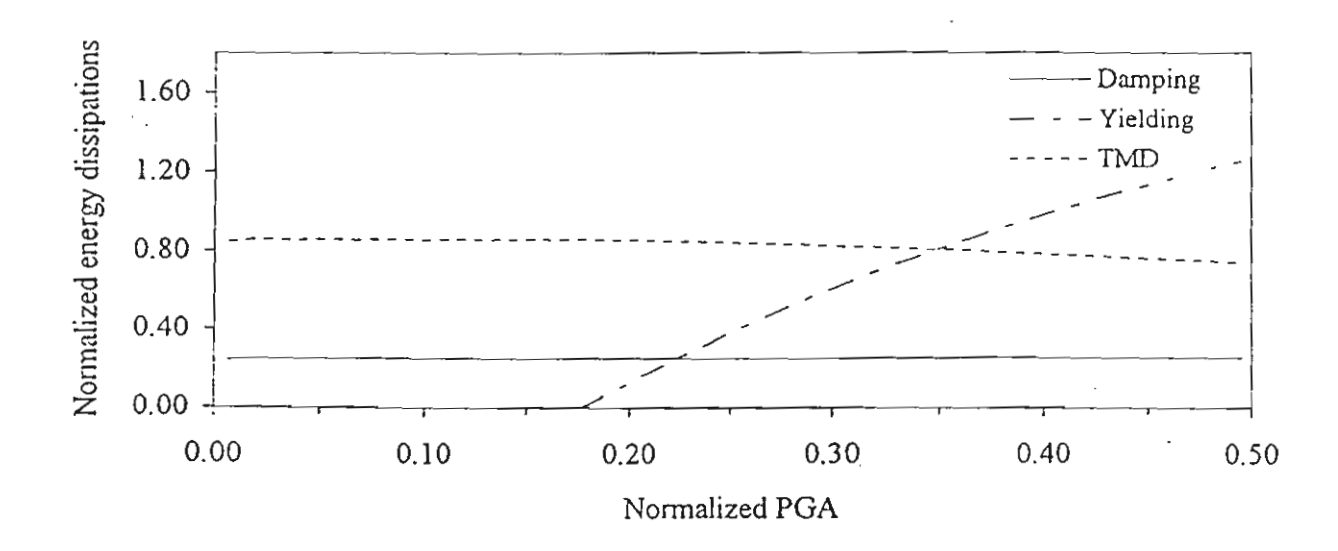


Figure 7 Normalized energy dissipation in structure with TMD against normalized PGA

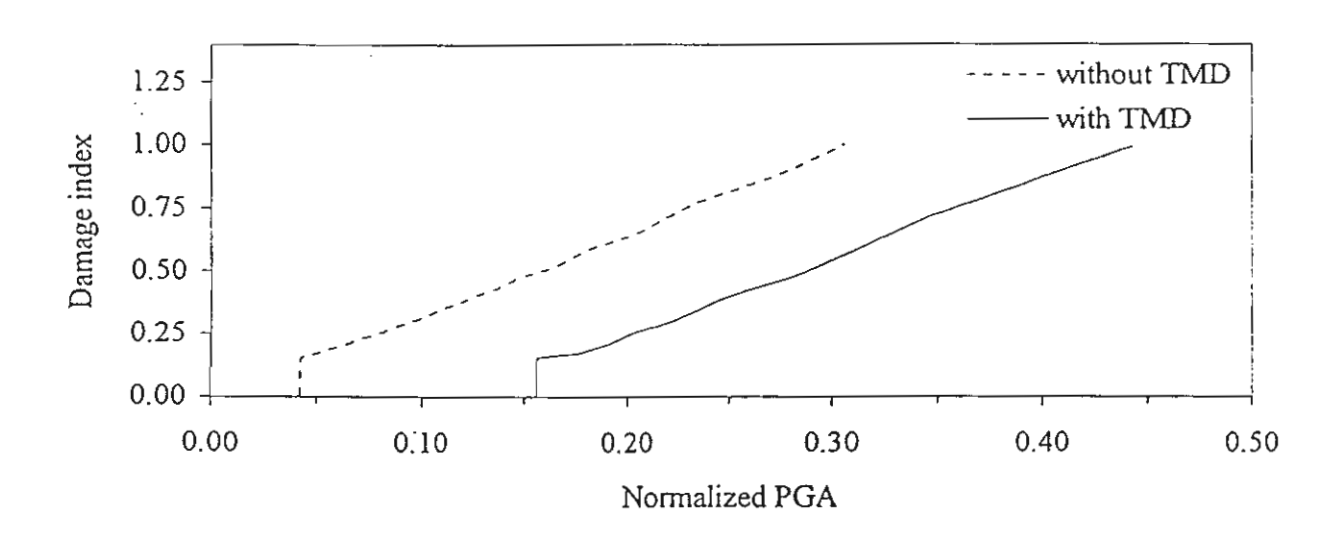


Figure 8 Damage index of structure against normalized PGA

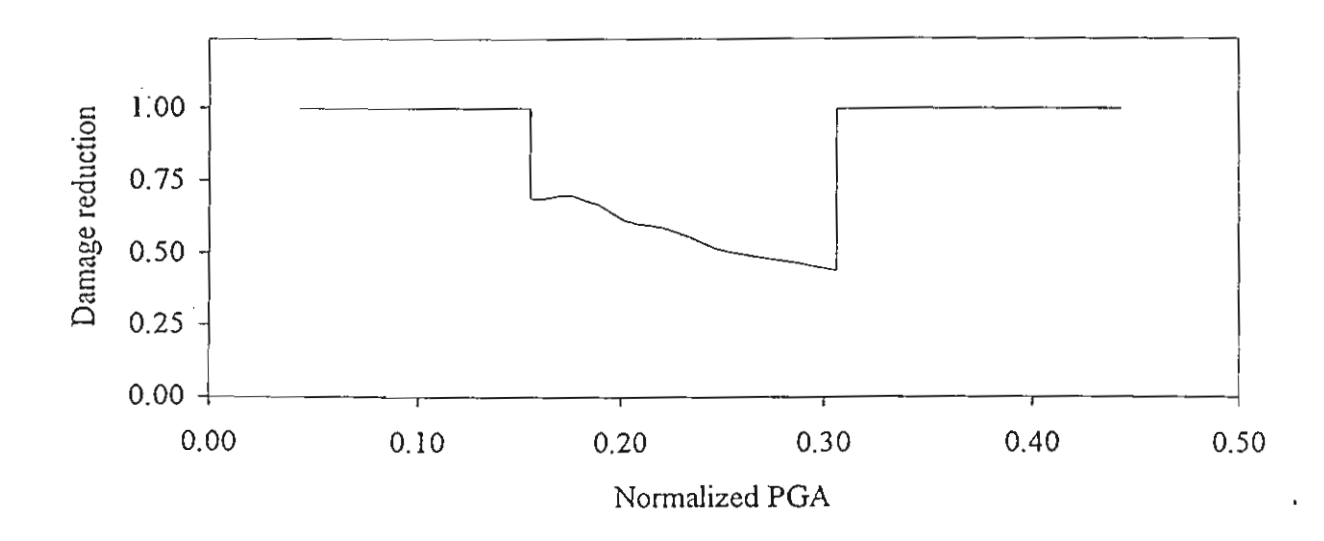


Figure 9 Damage reduction of structure with TMD against normalized PGA

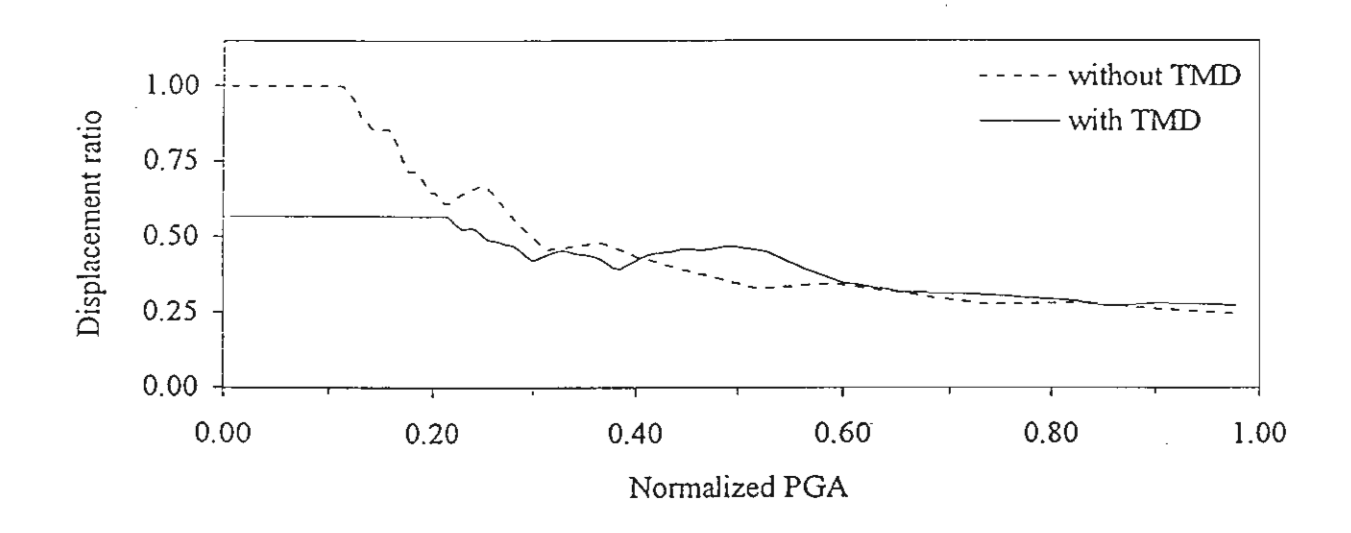


Figure 10 Displacement ratio of the structure against normalized PGA

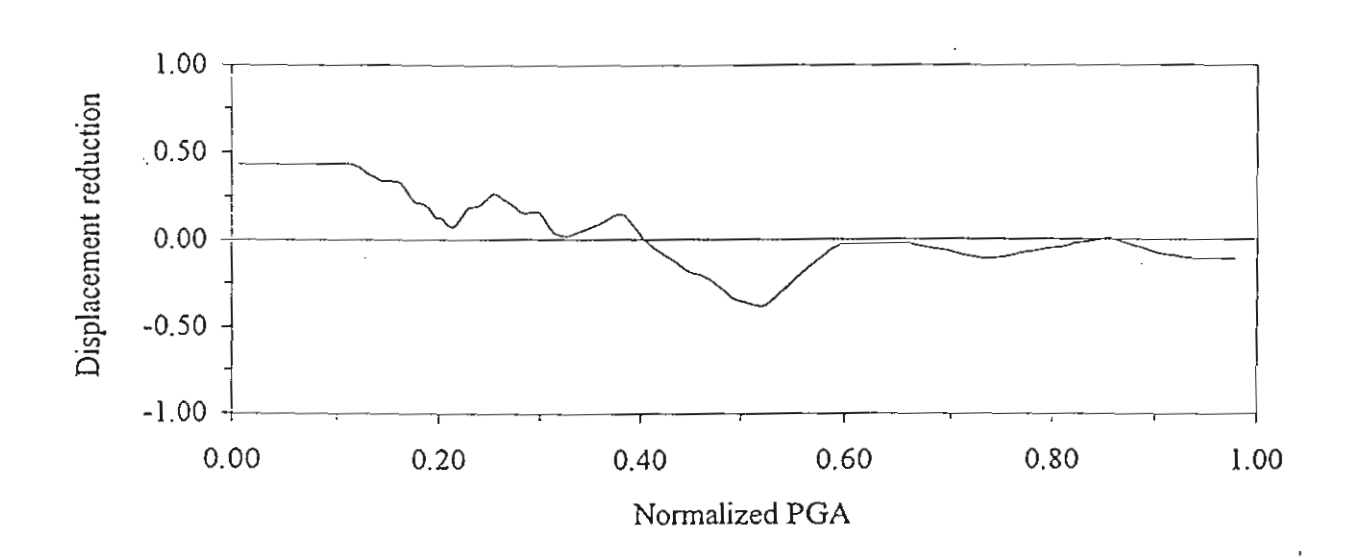


Figure 11 Displacement reduction of the structure with TMD against normalized PGA

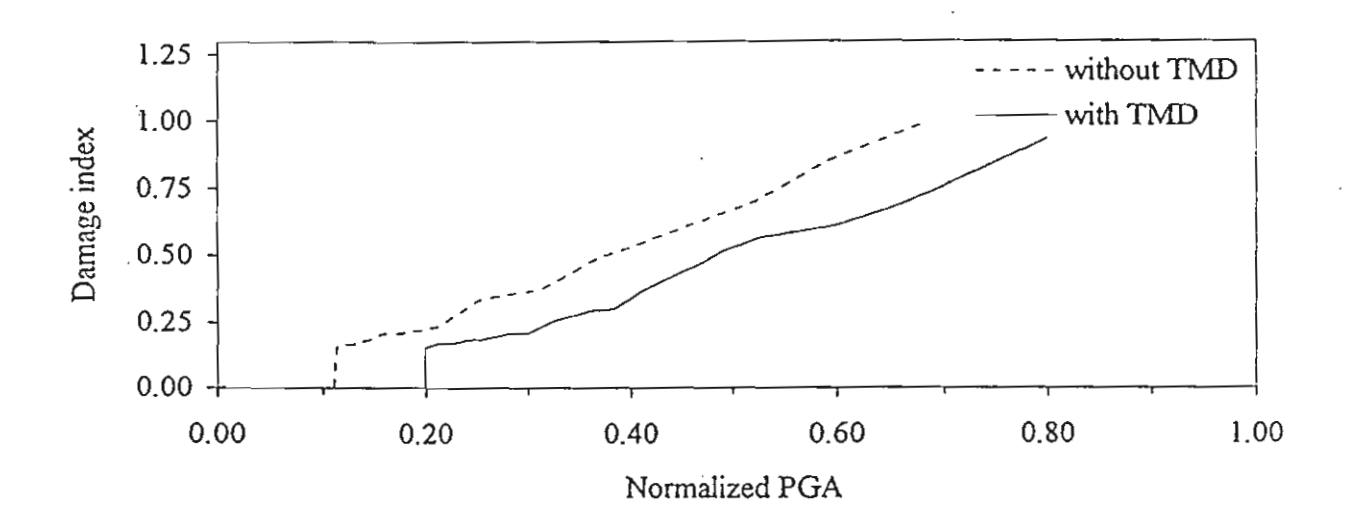


Figure 12 Damage index of structure against normalized PGA

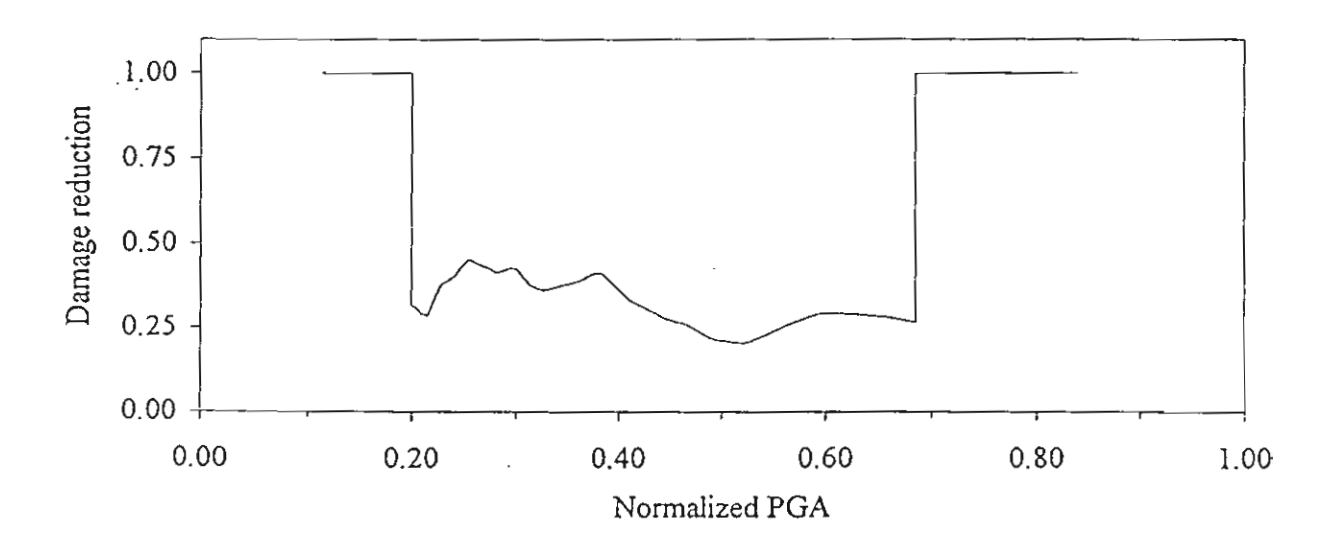


Figure 13 Damage reduction of structure with TMD against normalized PGA

ภาคผนวก ค

บทความที่ได้จัดเตรียมต้นฉบับ

- n. Lukkunaprasit, P., and Sittipunt, C. "Ductility Enhancement of Moderately Confined Concrete Tied Columns with Hook-Clips" (submitted to ACI Structural Journal)
- Lukkunaprasit, P., and Thepmangkorn, J. "Load History Effect on Cyclic Behavior of R.C. Tied Columns. (to be submitted to J. Struct. Engrg., ASCE)
- P. Lukkunaprasit, P., and Wanitkorkul, A. "Retrofit of steel momentresisting frames subjected to long-distance earthquakes considering weld fractures" (to be submitted to J. of Earthquake Engineering)

Ductility Enhancement of Moderately Confined Concrete Tied Columns with Hook-Clips

Panitan Lukkunaprasit, Chadchart Sittipunt

Department of Civil Engineering, Chulalongkorn University, Bangkok 10330,

Thailand; e-mail address: lpanitan@chula.ac.th

BIOGRAPHICAL SKETCH

ACI member Panitan Lukkunaprasit is a professor of civil engineering at Chulalongkorn University, Thailand. His current research work involves seismic behavior and design of reinforced concrete columns and dynamic nonlinear analysis of structures.

ACI member Chadchart Sittipunt is an assistant professor in the Department of Civil Engineering at Chulalongkorn University, Bangkok, Thailand. He received his Ph.D. from the University of Illinois at Urbana-Champaign in 1993.

ABSTRACT

An experimental investigation of the effectiveness of hook-clips in improving the performance of conventional 90-deg hook ties and ACI crossties in moderately confined reinforced concrete tied columns is described. The tie configurations provided in the five large-scale specimens tested included 90-deg hook ties and ACI crossties, with and without hook-clips, and 135-deg

hook ties. The columns were subjected to moderate levels of compression and cyclic lateral loads. The hook-clips were found to be effective in improving the performance of concrete columns confined with 90-deg hook ties and ACI crossties, resulting in the displacement ductility factor and energy dissipation capacity to be increased by about 85% and 400%, respectively.

Keywords: 90-deg hook; ACI crosstie; hook-clip; reinforced concrete column;
ductility; energy dissipation.

INTRODUCTION

Although extensive studies of reinforced concrete (r.c.) columns confined with 135-deg hook ties have been carried out, 1-6 little work has focused on the performance of 90-deg hook ties, in spite of the fact that crossties with a 135-deg hook at one end and a 90-deg hook at the other (ACI crossties) are permitted by the ACI Code7, even in areas of high seismic risk. Razvi and Saatcioglu⁸ tested two specimens with 90-deg hook ties, and the results indicated that they were inferior to columns confined by 135-deg hooks at axial strains in excess of about 0.015. Sheikh and Yeh9 investigated the behavior of tied columns with different reinforcement and tie configurations under medium to high axial load levels and flexure. Crossties with 90-deg hooks were reported to cause brittle failure and to be harmful rather than beneficial, especially at high axial loads. Lynn et al.10 tested eight fullscale reinforced concrete columns having details widely used before the mid-1970's in the U.S.A. and including 90-deg hook tie details among others. Cyclic load-displacement curves were obtained for light and moderate level axial loads. The poor performance of 90-deg hook ties was evident, leading to rapid loss of gravity load resistance. Wehbe et al. 11 tested four r.c. tied columns bound by 135-deg hook hoop ties and ACI crossties with moderate confinement. In all specimens, it was observed that opening of the 90-deg 'crosstie hooks initiated failure, leading to buckling of the outer longitudinal steel. Subsequently, the 135-deg hooks also started to open up.

The deficiency of 90-deg hook ties in columns was witnessed in past earthquakes in bridges, reinforced concrete buildings and steel reinforced concrete structures. 12-14 Despite their poor performance, 90-deg hook ties are still used extensively worldwide in low to moderate seismic risk regions because of the ease of their placement compared with the 135-deg hooks. Ninety-degree hook ties are even more appealing in developing countries where laying of reinforcing bars is quite commonly not practiced to a high level of precision, making it extremely difficult to put 135-deg hook ties in place when the vertical bars are misaligned. Recently, Lukkunaprasit¹⁵ introduced a simple device called a "hook-clip" to be clipped onto the conventional 90-deg hook ties or crossties at the sites. Experimental tests on axially loaded short columns revealed that the performance of r.c. tied columns with 90-deg hooks and hook-clips was comparable to that of columns with 135-deg hook ties.

RESEARCH SIGNIFICANCE

In view of the importance of vertical load resistance members, it is essential to have ductility in columns to ensure vertical load resistance even in zones with low to moderate seismic risk. Enhancement of performance of 90-deg hook tied columns would contribute to reduced damage due to earthquakes in such seismic risk regions. Furthermore, while there exist numerous test data on r.c. tied columns with ductile detailing for areas of high seismicity, there is a paucity of test results for lower ductility

demand suitable for moderate seismic risk regions. The experimental results from this study would form a valuable addition to the database of r.c. tied columns under cyclic loading. The effectiveness of hook-clips in improving the performance of conventional 90-deg hook ties and ACI crossties in columns for a moderate level of ductility was investigated. Enhancement in displacement ductility and energy dissipation capacity was also examined.

THE HOOK-CLIP

To prevent premature opening of 90-deg hooks, a supplementary tie or "hook-clip" has been devised which is to be embedded in the concrete core with its hooks holding the legs of the hook ties. The clip resists opening of the 90-deg hook after loss of the concrete cover. Fig. 1(a) shows the details of the clip proposed for binding 9 mm diameter ties or smaller. The hook-clip may be employed to clip the legs of any hoop tie or crosstie with 90-deg hooks (see Fig. 1(b)). With the clips prefabricated, they can be applied easily at the site, without any welding.

EXPERIMENTAL PROGRAM

Test specimens

Five column specimens 400mm by 400mm in cross section and 1500mm in height served as test specimens. Each test unit was reinforced with 16 longitudinal deformed bars of 20mm (DB20) nominal diameter. Transverse reinforcement consisted of 9mm diameter hoop ties and ACI crossties, with consecutive crossties alternated end for end along the axis of the column. The ties were supplied with either 90-deg or 135-deg hooks, depending on specimens. Each hook had an inside radius of twice the tie diameter and an extension of 6 bar

diameters, but not less than 60mm. The reinforcement detailing was in accordance with the non-seismic detailing provisions in the ACI Code⁷. Fig. 2 depicts a typical column cross section, and Table 1 lists the relevant data of the test specimens.

It should be noted that a relatively large bar size (viz. 20mm diameter) was used for the longitudinal reinforcement so that when the bars buckled, a large outward thrust would be exerted on the ties, which would, in turn, try to pull the hock-clips out of the confined core. The tie spacing provided (120mm) was smaller than that stipulated by ACI Code for non-seismic detailing, which allows as much as 300mm for the specimens tested. The closer spacing was chosen in view of the higher demand on the ties in providing lateral restraint for the longitudinal bars when buckled in shorter unsupported lengths. Consequently, a higher demand was also imposed on the hook-clips in order to prevent the ties from opening. Nevertheless, as can be seen in Table 2, the lateral reinforcement provided, A_{sh} , was only 39%-52% of the minimum amount required by ACI in areas of high seismicity.

Special care was taken to achieve the following tolerances in construction: cross sectional dimensions ± 1 percent; column height ± 1 percent; tie dimensions in the critical region ± 1.2 percent; tie spacing in the critical region ± 3 percent; widths and lengths of hook-clips ± 3 percent; and verticality of specimen $\pm 1/500$.

Material properties

All specimens were made of normal-strength materials. Normal-weight concrete with a maximum aggregate size of 20mm was used. The concrete compressive strengths of the standard concrete cylinders on the day of testing, f_{sa} , were in the range of 30.5-38.9 MPa.

The reinforcing steel used consisted of deformed bars with an average yield strength, f_y , of 472 MPa for longitudinal reinforcement, and smooth round bars with yield strengths, f_{yh} , in the range of 297 to 318 MPa for transverse steel. The average modulus of elasticity of the reinforcing bars was 212,000 MPa. The clips were fabricated from 5mm diameter mild steel bars whose yield strength and modulus of elasticity were 450 MPa and 204,500 MPa, respectively.

It should be noted that, except for the slight variation in concrete strengths (about 15% from the mean value) and the hook configurations, all specimens were basically the same in physical properties. Specimens CF90/0.30, CF135/0.30 and CFL90/0.30 were designed to investigate the ductility performance of conventional 90-deg hooks, 135-deg hooks and 90-deg hooks with hook-clips, respectively. The label 0.30 designates an axial stress level of 0.30 f_{ca} (based on gross cross sectional area). The performance of hook-clips was re-confirmed with another set of specimens, CFL90/0.37 and CF135/0.37, which were compressed to a higher axial stress level of 0.37 f_{ca} .

Test setup

Fig. 3 shows the schematic diagram of the test setup. The column footing was tied down to a strong floor by six high-strength steel bars post-tensioned to a total force of 3000 kN. In addition, a strut-and-tie system was employed to further provide lateral restraint to the foundation to minimize its movement. The axial load on each specimen was applied by means of a hydraulic jack bearing against the column top and a load transfer girder sitting on top of the jack. The reaction from the loading jack was resisted by two Ø40mm high-strength steel bars which tied the transfer girder to the foundation. A calibrated 1000-kN hydraulic actuator was employed to supply the cyclic lateral force, which was applied through a shaft placed in an embedded sleeve near the top of the column. Although the specimens were set up with extra care to minimize the eccentricity of the lateral force to within 4mm on average, a lateral bearing system was also utilized to prevent any out-of-plane movement of the column during testing.

Instrumentation

Linear variable differential transformers (LVDTs) were employed to measure the lateral displacements of the column along its height. The second and third hoop ties above the base were instrumented with electrical resistance strain gages, placed at the locations shown in Fig. 2. For specimens CFL90/0.37 and CF135/0.37, additional strain gages were also attached to the crossties at the second, third and fourth levels, in the direction of loading. An angle measuring device was used to monitor the inclination of the column top.

The vertical load was measured by means of a calibrated pressure gage. The 1000 kN hydraulic actuator for horizontal load application was fitted with a load cell. Signals, from the load cell, LVDTs and strain gages were connected to a computerized data acquisition system.

Testing procedure

The test specimens were first subjected to preliminary loadings under 50 percent of the specified axial load and a very small lateral load (in the order of 30 kN) in order to determine accidental eccentricities of the loadings, as well as to assure proper functioning of all measurement devices. Any necessary corrective measures would then be applied to ensure that the accidental eccentricity in the vertical load was within a tolerance of one percent of the column width, on average.

Actual testing was carried out following the general procedure proposed by Watson and Park⁵. After the application of the specified axial load, the lateral force was load-controlled to \pm 75 percent of the theoretical lateral yield value, $H_{\rm u}$, computed on the basis of the ACI Code without any strength reduction. The experimental yield displacement, $\Delta_{\rm y}$, was then extrapolated from the average of the measured displacements at \pm 0.75 $H_{\rm u}$ and \pm 0.75 $H_{\rm u}$ (Fig. 4). Subsequently, each specimen was subjected to displacement-controlled cyclic loading, starting from the displacement ductility level of 1. The displacement ductility level was incremented at an interval of 1, in general, with two cycles of loading performed for each ductility level until the ultimate capacity was reached. Failure was defined as the state when the capacity of the specimen during the loading cycle considered dropped by more

than 20 percent of the maximum capacity of the specimen. The associated displacement is denoted by Δ_{u} , and the displacement ductility factor is

$$\mu_A = \Delta_{\mu} / \Delta_{\nu} \tag{1}$$

Loading was applied at a very slow rate, with one cycle completed in about one hour. The slow rate of loading permitted control of the constant axial force by manual operation of the hydraulic pump.

TEST RESULTS

Test observations

Specimen CF90/0.30 (with 90-deg hooks but without hook-clips) exhibited normal flexural and shear cracks when loaded through 2 cycles at ductility 1.0, and only a few small spalling cracks developed at the edges in the plastic hinge zone. However, during the first push cycle at ductility 2.0, widespread spalling cracks occurred, which were caused by the popping out of the 90-deg hooks of the hoop tie and crosstie in the second tie set above the footing. At the end of the second cycle at ductility 2.0, those cracks became excessive. During the next push cycle at ductility 3.0, a major part of the concrete cover in the plastic hinge zone on the compression face spalled off, exposing the 90-deg hooks. The member consequently lost its load carrying capacity. The buckling mode of the vertical bars was not clear at this stage. However, after being loaded through another half cycle, it could clearly be seen that the longitudinal bars had buckled over approximately twice the tie spacings, indicating the inadequacy of the 90-deg hooks in the critical hoop tie and ACI crosstie in restraining longitudinal bars at the tie position (Fig. 5).

Specimens CF135/0.30 (with 135-deg hooks) and CFL90/0.30 (with 90-deg hooks and hook-clips) behaved in a similar manner up to ductility level 2.0 with stable hysteresis loops and little strength degradation. In contrast to specimen CF90/0.30, which had already developed significant spalling cracks at this ductility level, only a few small ones occurred in CFL90/0.30 and CF135/0.30. When specimen CF135/0.30 was pushed through the first cycle of ductility level 3.0, the spalling cracks, which had developed earlier at ductility level 2 as small cracks along one edge near the base, rapidly propagated with increasing width and length. Spalling cracks and swelling of the concrete cover around the third tie set above the base also developed due to expansion of the hoop tie. During the last cycle at ductility 3.0, more spalling near the base occurred, and swelling of the concrete in the vicinity of the 90-deg end of the ACI crosstie in the second tie set was evident. next (incomplete) push cycle to ductility level 4.0 saw excessive spalling and swelling of the concrete covering between the first and third tie sets, with opening of the 90-deg hook in the ACI crossties and eventual buckling of the longitudinal bars (Fig. 6). It was also observed that the 135-deg hook of the most severely stressed hoop tie was so deformed that it opened up substantially, indicating deficient anchorage of the hook due to the short extension leg provided for non-seismic design.

Specimen CFL90/0.30 exhibited remarkable behavior. Up to the second cycle, at ductility level 3.0, the overall appearance of the column was still in fairly good condition except for minor surface spalling of the cover at the base on the compression faces (which had occurred since ductility level 2), and some wide vertical spalling cracks near the edges in the plastic hinge zone. Swelling of the concrete cover on the compression face was observed near the location of one 90-deg end of the ACI crosstie at the second tie set above the base, indicating expansion action of the ties and hooks. However,

reinforcing bars were not exposed until the specimen was loaded to ductility level 4, when extensive spalling of the concrete cover took place. Bending of an inner longitudinal bar due to buckling could also be clearly observed at this stage (Fig. 7). Of particular significance is the integrity of the hook-clips in holding the legs of the 90-deg hook tie even at a substantial drift of 4% as witnessed in Fig. 8. It was remarkable that the longitudinal bars possessed significant post-buckling strength and the ties and hook-clips were resilient in confining the core, so that a significant amount of the peak load could be sustained, without abrupt failure, through one full cycle before eventual failure by total buckling of the longitudinal bars. The buckling shape of the longitudinal bars in the plastic hinge zone resembled that of specimen CF135/0.30 (Fig. 9).

Specimen CF135/0.37 displayed extensive spalling cracks near the edges in the plastic hinge zone when loaded to ductility level 2. Swelling of the concrete cover was significant along the third hoop level, but less so at the second hoop level. The edges spalled off during the first cycle of μ_4 = 3, but the longitudinal bars were still not visible. Just before the completion of the second cycle at ductility level 3, there was a drastic drop in lateral load resistance, followed by rapid widening of a major shear crack which had previously been minute, leading to eventual failure.

The overall appearance of CFL90/0.37, on the other hand, was much better than that of its counterpart, CF135/0.37. Similar crack patterns were observed in general, but the extent of cracking and damage was significantly less in the former than in the latter. At $\mu_{\rm d}$ = 2, only a few minor spalling cracks occurred over small areas at the base and at the third tie level. The cracks developed into significant ones at the third hoop tie level at ductility factor 3, with a clearly noticeable drop in lateral load

resistance. This prompted a reduction of the displacement increment to $0.5\Delta_y$ for the next (and last) loading cycle. Buckling of vertical bars in the plastic hinge zone led to an excessive drop in capacity and termination of the test after 1% cycles of loading at ductility level 3.5.

Lateral load-displacement hysteretic response

The lateral load-displacement hysteretic responses for the test specimens are shown in Fig. 10a - 10b and 11. The curves clearly indicate flexural dominated characteristics. It is interesting to note that specimens CF135/0.30 and CFL90/0.30 experienced stable hysteresis loops up to ductility level 3.0, with similar general characteristics. While the specimen with 135-deg hooks and (unclipped) ACI crossties suffered sharp decrease in lateral load resistance during the next (and last) loading cycle to ductility level 4.0, the specimen with hook-clips exhibited a stable hysteresis loop in the same cycle, with little strength degradation. The latter was able to sustain 2 complete cycles at this ductility level, although significant degradation in strength and stiffness occurred in the second cycle at μ_d = 4.0. The actual ductility factor that could have been attained by this specimen was estimated to be 3.7 which was based on equivalent energy dissipation and the condition that the loss in strength not to exceed 20 percent.

The sudden drop in lateral load resistance was even more pronounced in specimen CF90/0.30 when it was being pushed to $3\Delta_y$. The rapid decrease in load resistance was caused by the opening of the 90-deg hook of the ACI crosstie in the second tie set above the base, when the longitudinal bars buckled over approximately two tie spacings.

Specimen CFL90/0.37 exhibited a more stable hysteretic response than CF135/0.37, with much less strength degradation, when loaded from the second cycle at ductility 2.0 to the second loading cycle at μ_{Δ} = 3. Reduction of the peak load at ductility factor 3 was 22 percent for specimen CF135/0.37, compared with only 8 percent for specimen CFL90/0.37. However, prior to unloading from the second cycle at μ_{Δ} = 3, specimen CF135/0.37 rapidly lost its load capacity (by more than 45 percent) due to buckling of the vertical bars at a displacement of +2.54 Δ_y . The specimen with hook-clips, on the other hand, could still carry 85 percent of the peak load, and even sustained one complete cycle at μ_{Δ} = 3.5 with a remarkable sustained capacity before final failure.

Ductility performance

The displacement ductility factors attained by specimens CF90/0.30, CF135/0.30 and CFL90/0.30, under an axial stress level of 0.3 f_{ca} , were 2, 3 and 3.7, respectively (see Table 3). It may be noted that the displacement ductility of CFL90/0.30 closely agreed with the value of 3.8 predicted by the formula suggested by Wehbe, et al. 11 for members with seismic detailing, indicating the effectiveness of the hook-clips in enhancing ductility performance of columns with 90-deg hook ties. The ductility performance of specimens without clips was expected to be unsatisfactory due to the use of non-seismic detailing, and hence it was not compared with that predicted by the Wehbe et al. equation.

The effectiveness of the hook-clips was again confirmed by specimen CFL90/0.37, which was able to sustain the same displacement ductility factor

as specimen CF135/0.30 even though it was subjected to a higher level of axial load.

Strains in transverse steel

Focus was first placed on measurement of the hoop tie strains in the plastic hinge zones in specimens CF90/0.30, CFL90/0.30 and CF135/0.30. It was unfortunate that some strain gages got damaged (some caused by the spalling concrete) which resulted in incomplete data so that comparison of the maximum axial strains in the hoop ties could not be made. Furthermore it was found that the strains in the hoop ties were much influenced by bending of the ties caused by the lateral pressure exerted by the core and/ or buckling of the longitudinal bars. In the last two specimens, therefore, attention was paid to the measurement of the strains in the crossties which were predominantly in tension. It was found that the most severely strained crosstie in specimen CFL90/0.37 developed a maximum strain of 1.5 times that in CF135/0.37. In fact, the former attained a strain of 0.0015, slightly higher than the yield value of 0.0014. Better anchorage of the 90-deg hook ends with hook-clips after spalling of the concrete cover obviously resulted from effective restraint of the hook ends by the hook-clips, leading to the ability to develop higher strains in the crossties, and enhanced confinement of the concrete core.

Energy dissipation capacity

The ability of structures to withstand cyclic loading is commonly measured in terms of the energy dissipation capacity, which is defined as the summation of the energy E_i dissipated within each cycle i. The normalized energy dissipation capacity, E_N , is

$$E_N = \left(\sum_{i=1}^n E_i\right) / \left(II_{max} \Delta_y\right)$$

in which n is the number of cycles to failure, and H_{max} is the peak lateral load during cyclic loading.

The normalized energy dissipation capacities of the specimens tested are tabulated in Table 3 and the cumulative normalized energy capacities versus loading cycles are plotted in Fig. 12. Those cycles which resulted in a drop in lateral load resistance of more than 20 percent of the peak lateral load were excluded in the computation. It is remarkable that the energy dissipation capacity of specimen CFL90/0.30 was larger than the unclipped specimens CF90/0.30 and CF135/0.30 by about 400 and 90 percent, respectively. At a higher axial load level of 0.37 $f_{ca}A_g$, the increase in the dissipated energy was less. At any rate, the energy dissipation capacity of CFL90/0.37 was still 1.5 times that of CF135/0.37.

Effectiveness of hook-clips

From the test results, together with the following observations, it is evident that the hook-clips were effective in improving the performance of the 90-deg hooks in the hoop ties and ACI crossties:

- a) At each ductility level, the number and extent of spalling cracks were significantly lower in the specimens with hook-clips than in those without, indicating less pop-out action of the 90-deg ends of the ACI crossties and 90-deg hooks in the hoop ties due to containment by the hook-clips.
- b) In contrast to CF90/0.30 with conventional 90-deg hooks, the clips in the CFL90/0.30 specimen were able to prevent premature opening of the 90-deg

hooks, leading to effective restraint of the vertical bars at the tie positions, and resulting in the vertical bars buckling by about half the buckling length of those without clips, when buckling commenced, as depicted in Fig. 7. The shorter buckling length allowed the specimen to sustain a higher load at the same deformation.

- c) The ductility performance of the specimen with 90-deg hook ties and hook-clips far excelled that of the specimen without hook-clips. In fact, the former even performed better than the CF135/0.30, which was confined with 135-deg ties and ACI crossties (without hook-clips). The reason is that the ACI crossties with hook-clips in specimen CFL90/0.30 were effectively restrained from opening up by the hook-clips, in contrast to the unclipped ACI crossties in specimen CF135/0.30 which popped out at an earlier stage, leading to loss of structural integrity.
- d) The crossties with hook-clips were able to develop larger strains than those without clips as mentioned earlier.

CONCLUSIONS

The hook-clips were found to be effective in improving the performance of reinforced concrete columns confined with 90-deg hook ties and ACI crossties, as evidenced by the significant enhancement of the ductility and energy dissipation capacity and the fact that, for the tie configurations studied, the buckling lengths of the longitudinal bars in specimens with hook-clips were about half of those in specimens without them when bar buckling commenced. In fact, for the specimens tested, the overall performance of the specimens with hook-clips under a moderate ductility demand was even superior to that of columns confined with 135-deg hook ties and conventional ACI crossties. The effective restraint of the 90-deg ends of crossties by hook-clips enabled the most severely strained crossties in the plastic hinge

region to develop a strain slightly higher than the yield value. The effectiveness of the hook-clips should be beneficial, even in regions of high seismicity, pending further investigation.

ACKNOWLEDGMENTS

The authors are grateful to the Thailand Research Fund (TRF) for the TRF Senior Research Scholar Grant to the senior author for this research project. Special appreciation goes to the following companies for their support with materials and equipment: VSL (Thailand), TEM LERT, and INTERCONSULT. The contributions of Mr. J. Thepmangkorn, Mr. C. Lawpattanapong, Mr. T. Deesomsuk, and Mr. N. Lee and Mr. N. Phol, among other students, are acknowledged for carrying out the tests and computations. Comments made by Prof. Dr. S. Wood in the revision process are also greatly appreciated.

CONVERSION FACTORS

1 MPa = 145 psi

1 mm = 0.0394 in.

1 kN = 0.2248 kips

REFERENCES

1. Kent, D. C., and Park, R., "Flexural Members with Confined Concrete,"

Journal of the Structural Division, ASCE, 97, ST7, 1971, pp.1969-1990.

- 2. Sheikh, S. A., and Uzumeri, S. M., "Strength and Ductility of Tied Concrete Columns," Journal of the Structural Division, ASCE, 106, ST5, 1980, pp.1079-1102.
- 3. Park, R.; Priestley, M. J. N.; and Gill, W. D., "Ductility of Square Confined Concrete Columns," Journal of the Structural Division, ASCE, 108, ST4, 1982, pp.929-950.
- 4. Mander, J. B.; Priestley, M. J. N.; and Park, R., "Theoretical Stress-Strain Model for Confined Concrete," Journal of Structural Engineering, ASCE, 114, 8, 1988, pp.1804-1826.
- 5. Watson, S., and Park, R., "Simulated Seismic Load Tests on Reinforced Concrete Columns," Journal of Structural Engineering, ASCE, Vol.120, No.6, 1994, pp.1825-1849.
- 6. Watson, S.; Zahn, F. A.; and Park, R., "Confining Reinforcement for Concrete Columns," Journal of Structural Engineering, ASCE, Vol.120, No.6, 1994, pp.1798-1824.
- 7. ACI Committee 318 (1999), Building Code Requirements for Reinforced

 · Concrete (ACI 318-99), American Concrete Institute, Farmington Hills,

 Michigan.
- 8. Razvi, S. R., and Saatcioglu, M., "Confinement of Reinforced Concrete Columns with Welded Wire Fabric," ACI Structural Journal, V.86, No.5, 1989, pp.615-623.
- 9. Sheikh, S. A., and Yeh, C., "Tied Concrete Columns under Axial Load and Flexure," Journal of Structural Engineering, ASCE, 116, 10, 1990, pp.2780-2800.
- 10. Lynn, C. A.; Moehle, J. P.; Mahin, S. A.; and Holmes, W. T., "Seismic Evaluation of Existing Reinforced Concrete Building Columns," *Earthquake Spectra*, 12, 4, 1996, pp.715-739.

- 11. Wehbe, N. I.; Saiid M. S.; and Sanders, D. H., "Seismic Performance of Rectangular Bridge Columns with Moderate Confinement," ACI Structural Journal, V.96, No.2, 1999, pp.248-258.
- 12. EQE International, The January 17, 1995 Kobe Earthquake, An EQE Summary Report, EQE International, San Francisco, 1995.
- 13. Seible, F.; Priestley, M. J. N.; and MacRae, G., The Kobe Earthquake of January 17, 1995, Initial Impressions From A Quick Reconnaissance, Report No. SSRP-95/03, University of California, San Diego, 1995.
- 14. Azizinamini, A., and Ghosh, S. K., "Steel Reinforced Concrete Structures in 1995 Hyogoken-Nanbu Earthquake," Journal of Structural Engineering, ASCE, 123, 8, 1997, pp.986-992.
- 15. Lukkunaprasit, P., "An Innovative Hook-Clip for Performance Improvement of Tied Columns in Developing Countries," Proceedings of the 12th World Conference on Earthquake Engineering, Auckland, New Zealand, 2000.

Table 1 - Details of test specimens

Specimen	Concret strength	Dimensions			Longitudinal reinforcement		Transverse reinforcement				Hook	P/f _{cs} A _s
	f _{cs} ,	Width,	Depth,	Height,	Ръ	f _y ,	Diameter,	5,	f _{yh} ,	A _{sh} /sh _c ,	configuration	3.14
	MPa	mm	mm	mm	%	MPa	mm	mm	MPa	%		
CF 90 / 0.30	38,9	398	397	1500	3.14	471	9	120	305	0.453	90° + ACI crosstics; no clips	0.30
CF 135 / 0.30	35.7	398	396	1490	3.14	471	9	120	305	0.453	135° + ACI crossties; no clips	0.30
CFL 90 / 0.30	31.7	398	398	1500	3.14	471	9	120	306	0.453	90° + ACI crossties with clips	0.30
CF 135 / 0.37	30.5	399	397	1500	3.14	475	9	120	318	0.453	135° + ACI crossties; no clips	0.37
CFL 90 / 0.37	32.4	398	397	1500	3.14	471	9	120	297	0.453	90° + ACI crossiles with clips	0.37

Note: ρ_l = longitudinal reinforcement ratio; s = center-to-center spacing between sets of ties; h_e = cross-sectional dimension of column core measured center-to-center of confining reinforcement; P = axial load; and A_g = gross area of column section.

Table 2 - Lateral reinforcement ratio in comparison with ACI Code⁷ (seismic design)

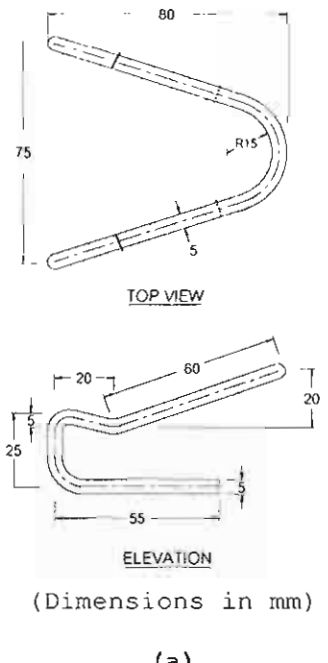
Chasimon	D/f A	Lateral reinforcement ratio A,h/(shc)						
Specimen	P/f _{ca} A _g	Provided	ACI Code	A _{sh} /A _{sh,ACI}				
CF 90 / 0.30	0.30	0.0045	0.0115	0.39				
CF 135 / 0.30	0.30	0.0045	0.0105	0.43				
CFL 90 / 0.30	0.30	0.0045	0.0093	0.49				
CF 135 / 0.37	0.37	0.0045	0.0086	0.52				
CFL 90 / 0.37	0.37	0.0045	0.0098	0.46				

Note: $A_{sh,ACI}$ = minimum total cross-sectional area of rectangular hoops and crossties as specified by the ACI Code.⁷

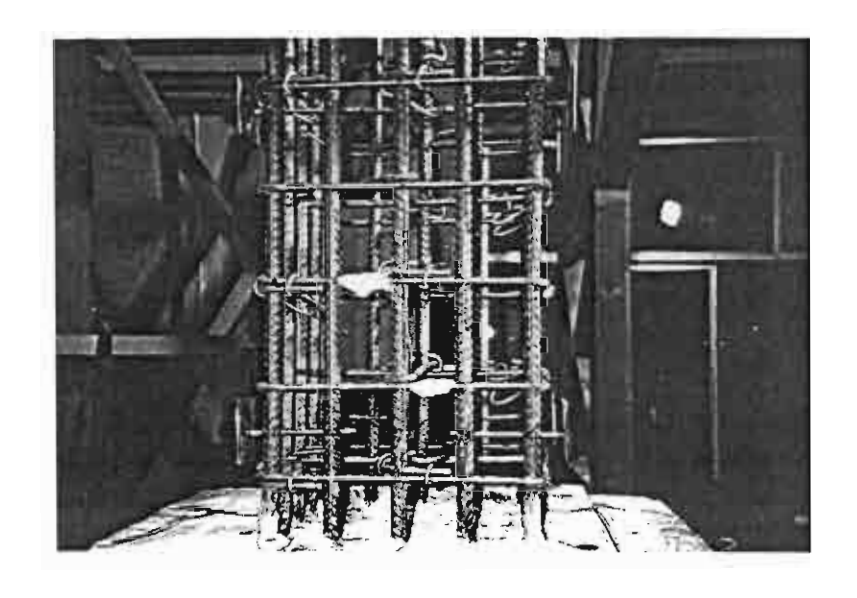
Table 3 - Test results

Specimen	Δy,	Δu, mm	μ _{Δ,exp.}	µ _{∆,caL}	H _{max} ,	En, kN-mm	E _N /(H _{max} \(\Delta_y\)	Failure mode
CF 90 / 0.30	14.3	28.4	2.0	-	315	16908	3.8	Flexure
CF 135 / 0.30	14.2	42.6	3.0	-	314	44806	10.1	Flexure
CFL 90 / 0.30	15.0	55.5	3.7	3.8	284	83032	19.3	Flexure
CF 135 / 0.37	14.2	42.4	2.5	-	295	27821	6.6	Flexure
CFL 90 / 0.37	13.2	39.6	3.0	3.5	303	41448	10.4	Flexure

Note: $\mu_{\Delta,exp}$ = displacement ductility factor from experiment; and $\mu_{\Delta,cal}$ = calculated displacement ductility factor in accordance with the formula proposed by Wehbe et al. 11



(a)



(b)

Fig.1-(a) Details of hook-clip; and (b) Hook-clips engaging 90° hoop ties and crossties

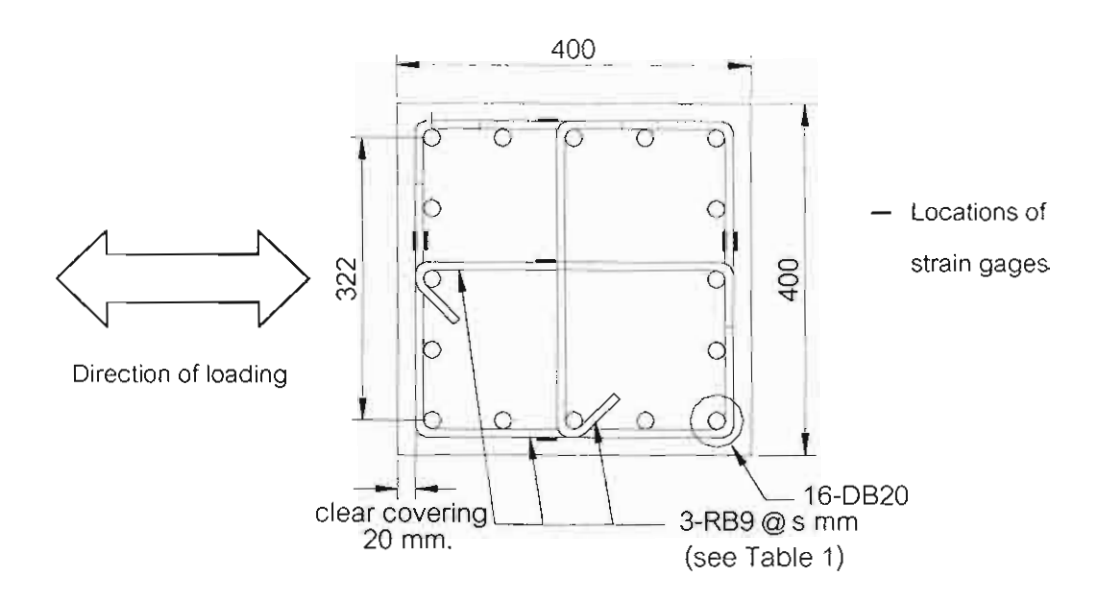


Fig. 2-Column reinforcement detail

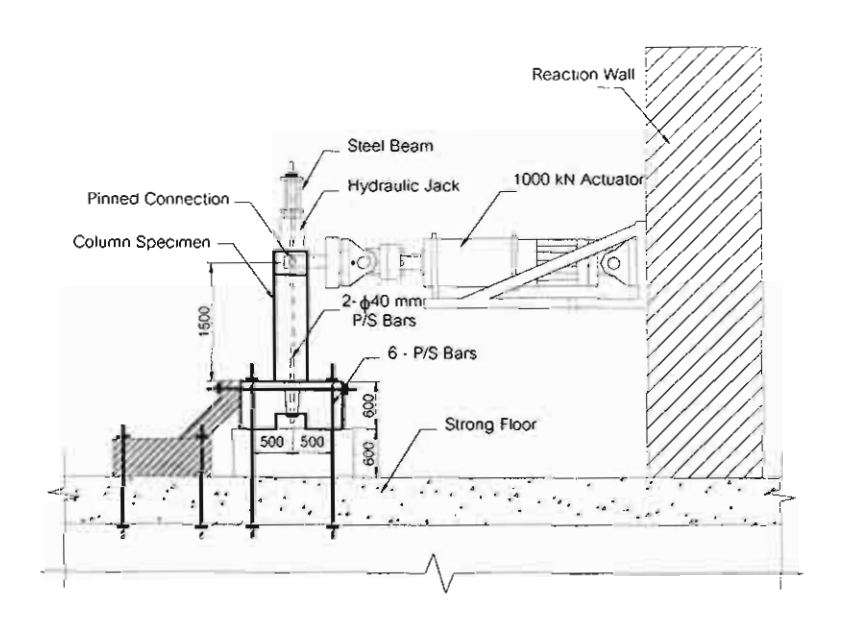


Fig.3-Test setup

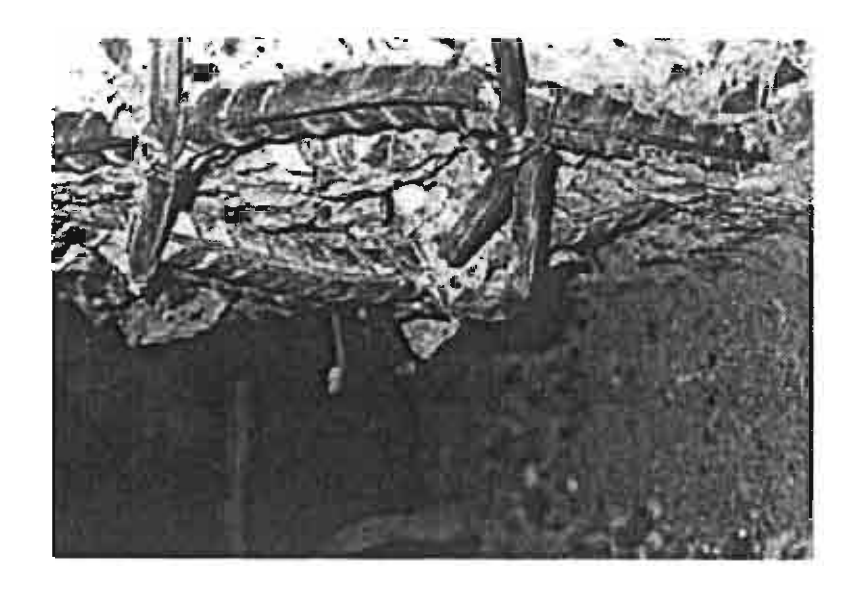


Fig. 5-Failure mode of CF90/0.30

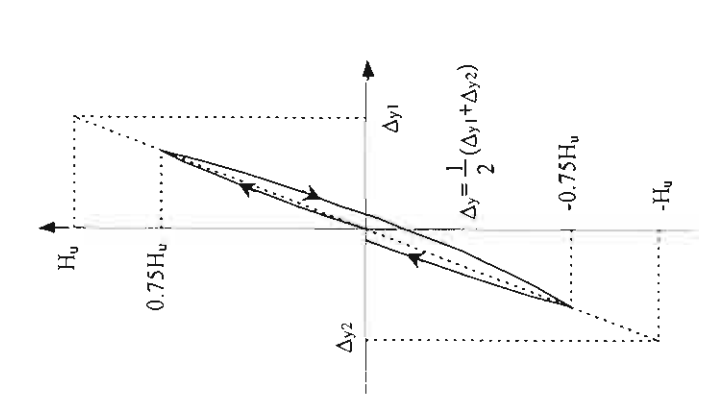


Fig.4-Definition of first-yield displacement

(after Watson and Park⁵)

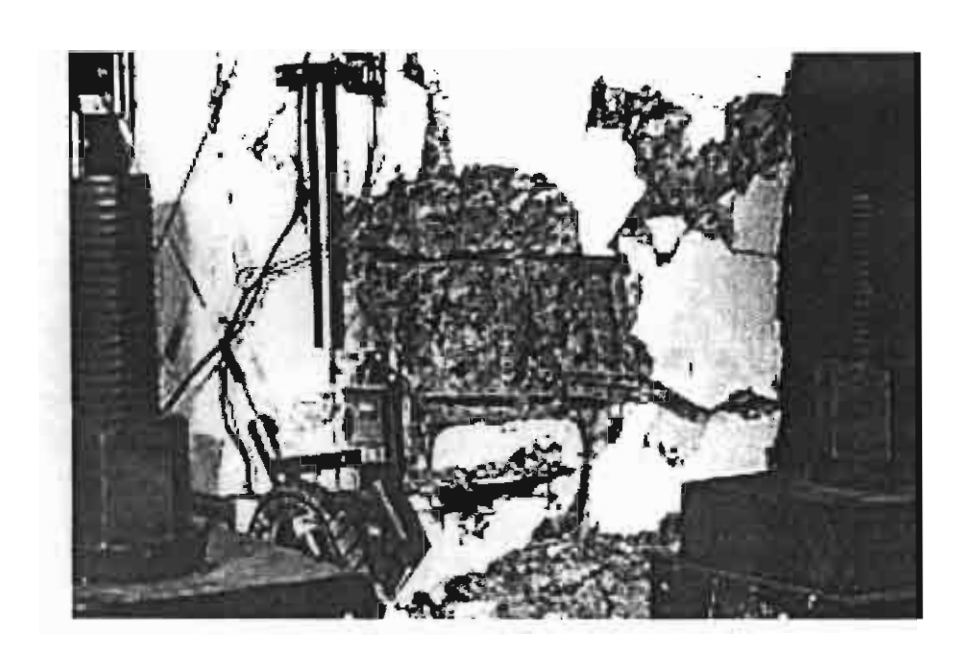


Fig. 6 - Failure mode of CF135/0.30

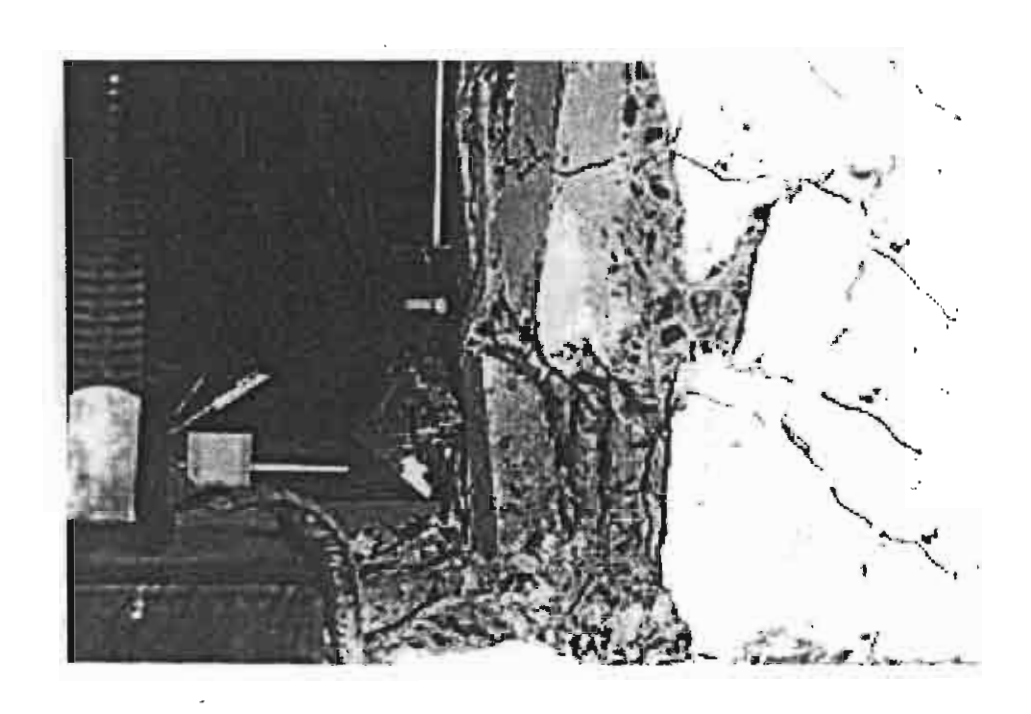


Fig. 7 - CFL90/0.30-Buckling of vertical bar in single tie spacing

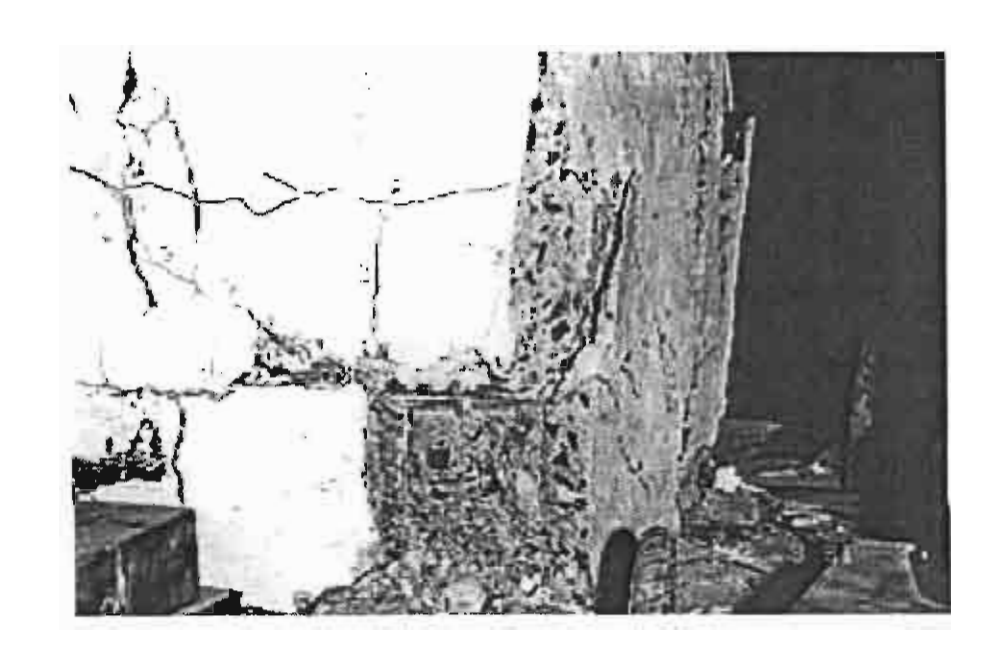


Fig. 8 - CFL90/0.30-Effective restraining of 90-deg hook legs by hookclips at a large drift of 4%

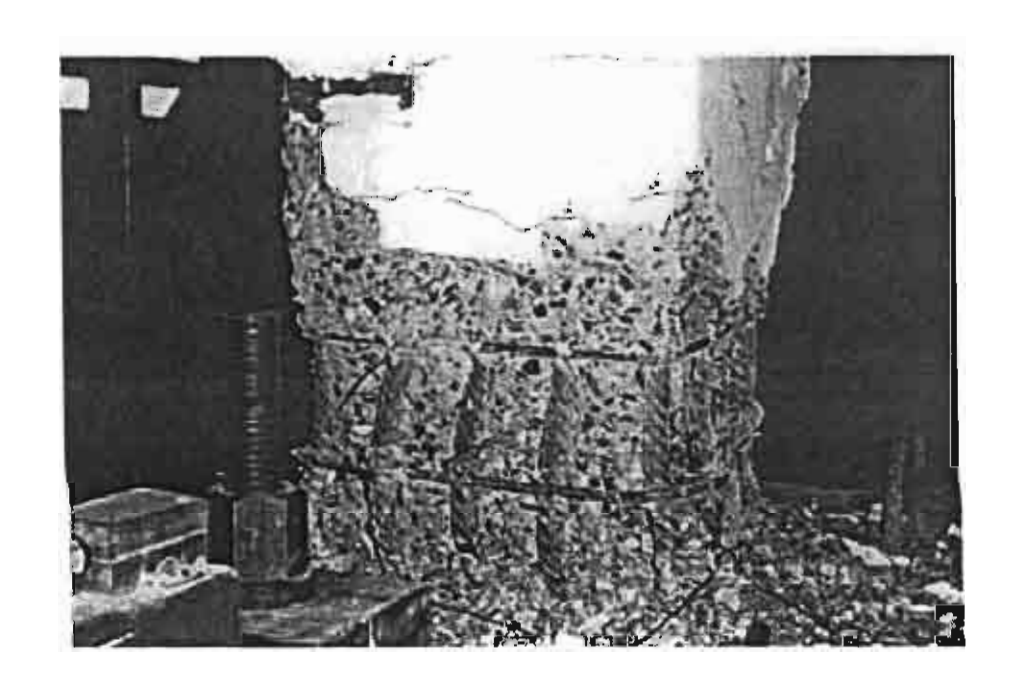
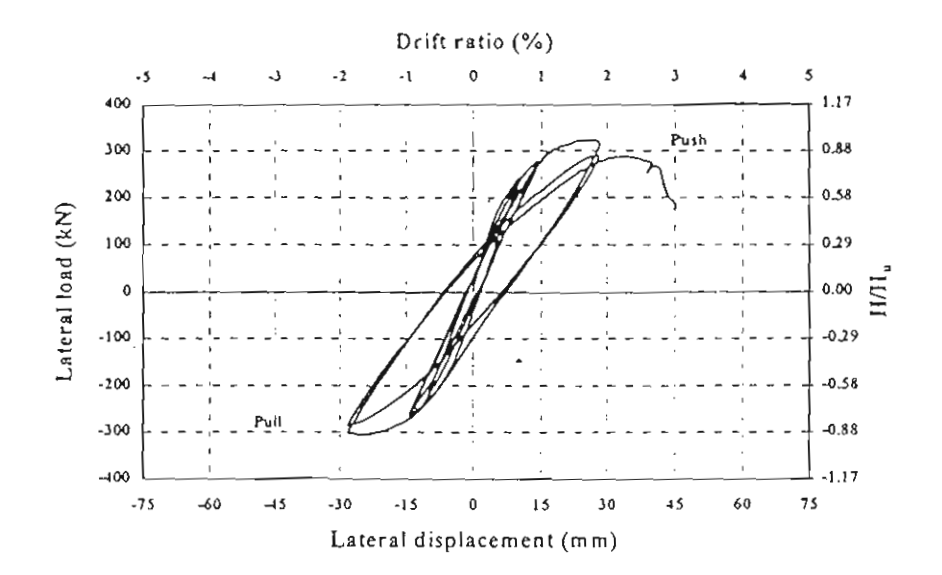
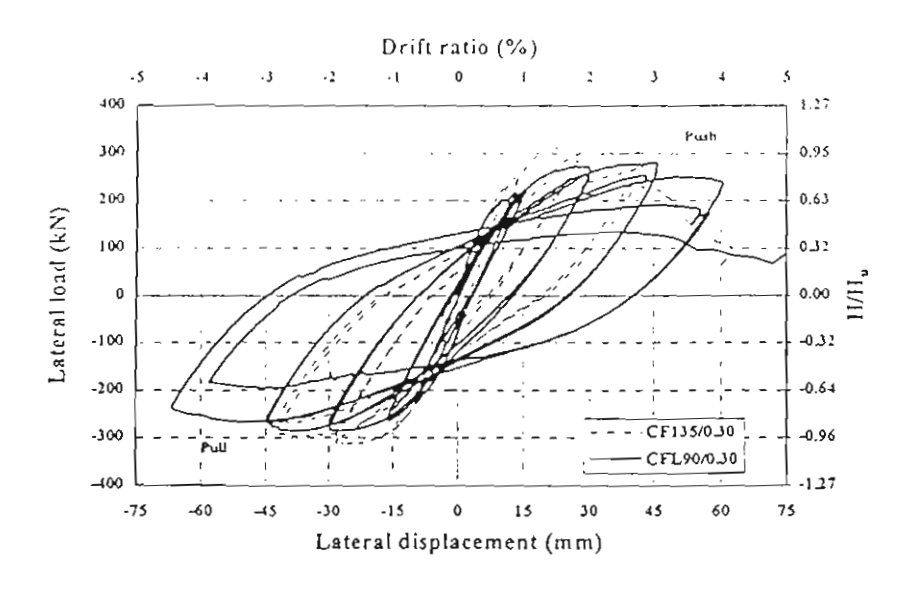


Fig. 9 - CFL90/0.30-Effectiveness of hook-clips in restraining hook opening at failure



(a)



(b)

Fig.10 - Lateral load-displacement hysteresis: (a)CF90/0.30; (b)CF135/0.30 (dashed line) and CFL90/0.30 (solid line)

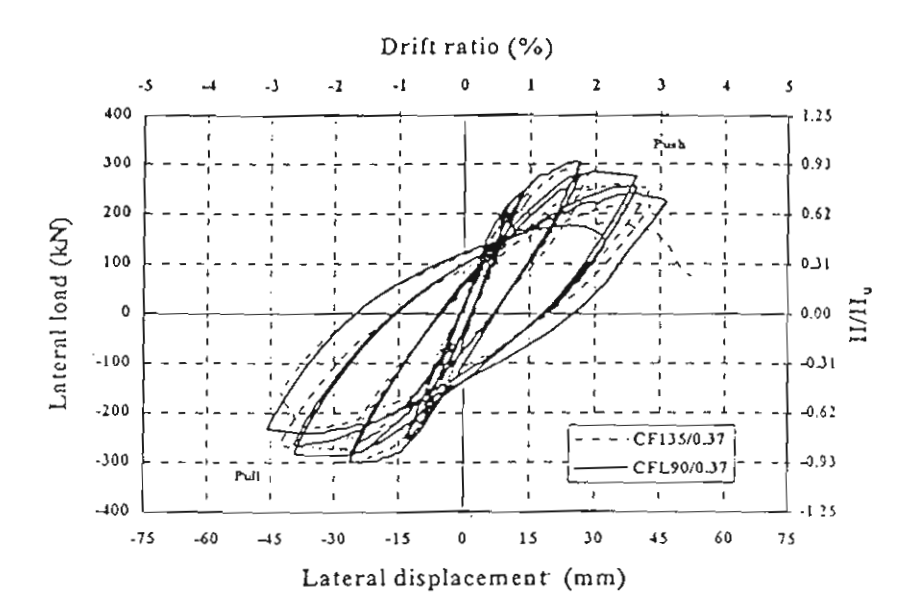
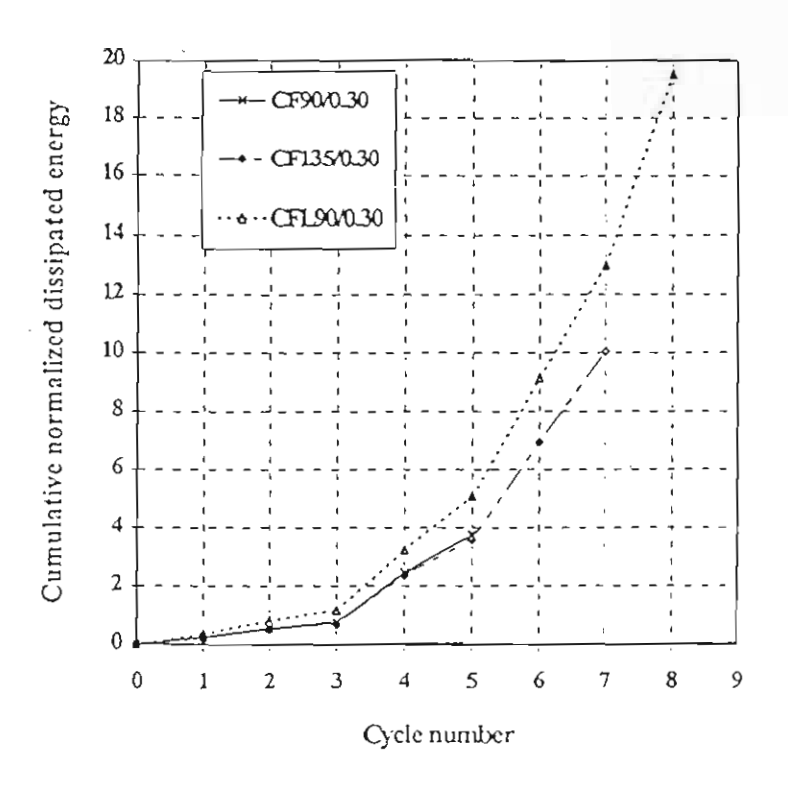


Fig. 11 - Lateral load-displacement hysteresis for specimens CF135/0.37 (dashed line) and CFL90/0.37 (solid line)



(a)

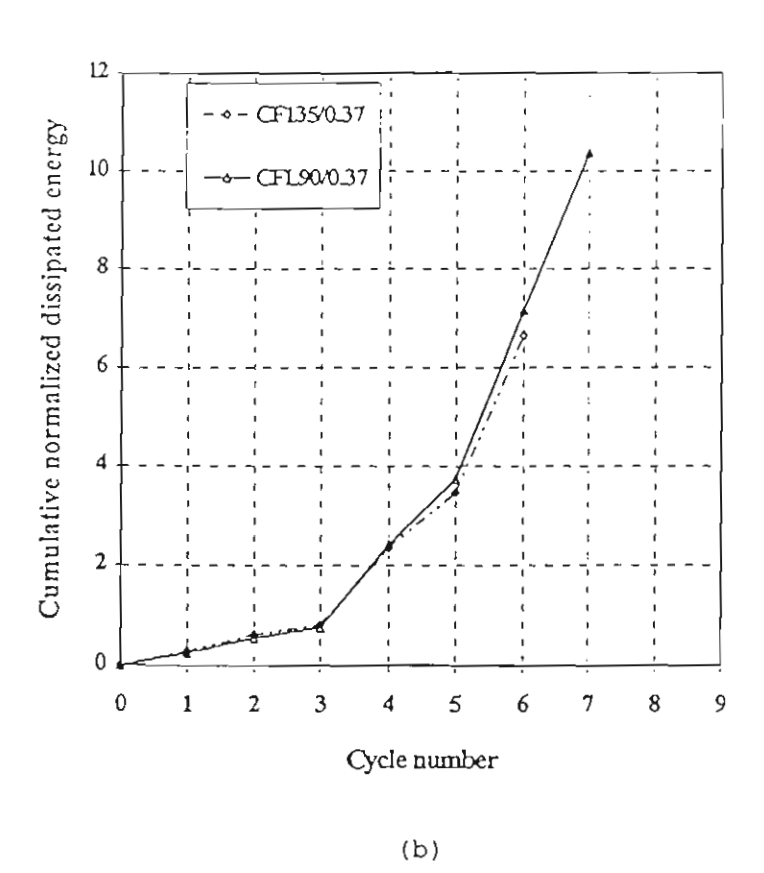


Fig.12-Cummulative normalized dissipated energy: (a) Specimens CF90/0.30, CF135/0.30, and CFL90/0.30; and (b) Specimens CF135/0.37 and CFL90/0.37.

List of Notations

 A_{σ} = gross area of column section

 A_{sh} = total cross-sectional area of transverse reinforcement

 $A_{Sh,ACI}$ = minimum total cross-section area of rectangular hoops and crossties as specified by the ACI Code

 E_i = dissipated energy within cycle i

 E_{t} = normalized dissipation energy capacity

 $F_{\rm rs}$ = compressive strength on day of testing of the standard concrete cylinder

 f_y = yield strength of longitudinal reinforcement steal

 $f_{\rm vh}$ = yield strength of transverse reinforcement steel

 H_{tt} = theoretical lateral yield load

 H_{max} = peak lateral load during cyclic loading

 $h_{\rm c}$ = cross-sectional dimension of column core measured center-tocenter of confining reinforcement

P = axial load

s = center-to-center spacing between sets of ties measured along the axis of the column

 Δ_{ν} = ultimate tip displacement of column

 Δ_v = yield displacement of column

 $\mu_{\rm d}$ = displacement ductility factor

 $\mu_{3,cai}$ = calculated displacement ductility factor in accordance with the formula proposed by Wehbe et al. 11

 $\mu_{\rm d,emp}$ = displacement ductility factor from experiment

 ρ_{t} = longitudinal reinforcement ratio

List of Tables

- Table 1 Details of test specimens
- Table 2 Lateral reinforcement ratio in comparison with ACI Code (seismic design)
- Table 3 Test results

List of Figures

- Fig. 1 (a) Details of hook-clip; and (b) Hook-clips engaging 90° hoop ties and crossties
- Fig. 2 Column reinforcement detail
- Fig. 3 Test setup
- Fig. 4 Definition of first-yield displacement (after Watson and Park⁵)
- Fig. 5 Failure mode of CF90/0.30
- Fig. 6 Failure mode of CF135/0.30
- Fig. 7 CFL90/0.30-Buckling of vertical bar in single tie spacing
- Fig. 8 CFL90/0.30-Effective restraining of 90-deg hook legs by hook-clips at a large drift of 4%
- Fig. 9 CFL90/0.30-Effectiveness of hook-clips in restraining hook opening at failure
- Fig.10 Lateral load-displacement hysteresis : (a) CF90/0.30; and (b) CF135/0.30 (dashed line) and CFL90/0.30 (solid line)
- Fig.11 Lateral load-displacement hysteresis for specimens CF135/0.37 and CFL90/0.37
- Fig. 12 Cummulative normalized dissipated energy: (a) Specimens CF90/0.30, FC135/0.30, and CFL90/0.30; and (b) Specimens CF135/0.37 and CFL90/0.37.

Load History Effect on Cyclic Behavior of R.C. Tied Columns

By P. Lukkunaprasit¹, Fellow, ASCE, and J. Thepmangkorn²

Abstract: The effect of two commonly used load histories on the ductility and energy dissipation capacity of reinforced concrete tied columns was investigated. Based on regression analyses of the test results reported in the literature, the effective confinement reinforcement ratio was found to provide a good correlation with the performance indexes studied. The parameters accounted for include the material strength ratio, the amount of the transverse reinforcement, the axial load level and the effectiveness of the tie configurations. For moderate values of the effective confinement steel ratio, load history with increments of two times the yield displacement was found to be slightly more severe than that with one yield displacement increments. The effect of load history tends to be less significant for higher values of the effective confinement steel ratio.

INTRODUCTION

The influence of load history on the cyclic behavior of reinforced concrete (r.c.) members has been recognized for some time. Gosain et al. (1977) proposed the modified work index, I'_w , as a measure for evaluating the severity of the loading for r.c. members. They also pointed out limitations of the method when applied to significantly different load histories. For instance, loading to a deflection of 10 times yield displacement twice would likely yield more severe damage than loading four times to a deflection of 5 times the yield value, even though both loadings yield approximately the same value of work index. Noting the weak correlation of I'_w with the test data, Darwin and Nmai (1986) proposed an energy dissipation index, D_i , designed to provide an objective measure of beam response. It was found that D_i was strongly controlled by the maximum shear stress, v_m , the concrete strength, f'_c , and the transverse steel capacity, v_s , in the form

¹ Prof., Department of Civ. Engrg., Chulalongkorn Univ., Bangkok 10330, Thailand

² Former graduate student, Department. of Civ. Engrg., Chulalongkorn Univ., Bangkok 10330, Thailand.

of the parameter $(v_s f_c')^{0.5}/v_m^{1.5}$. Hwang and Scribner (1984) carried out experimental investigations on the effect of load history on reinforced concrete cantilever beams. The sequence of application of large and small deformations was found to have relatively small effect on the strength and stiffness degradation, and total energy dissipation capacity of the member. The most significant factor was the maximum displacement the members experienced. A limited investigation by Wight and Sozen (1975) seemed to suggest the same result.

It may be noted that most of the studies mentioned dealt with beams, with relatively little work carried out on columns. In the majority of studies on the cyclic behavior of reinforced concrete tied columns, the material properties, the amount of confinement steel and the effect of axial load level, are normally taken as the main parameters (e.g. Soesianawati et al., 1986; Azizinamini et al., 1992; Watson et al., 1994; Wehbe et al., 1999). The effect of tie configuration effectiveness has recently been considered by Sheikh and Khoury (1997). However, no single standard load history has been employed, and it is difficult to compare the performance of r.c. members tested by different investigators using different load histories. Furthermore, constitutive relationships have been normally assumed to be independent of load histories. It was thus the primary objective of this study to investigate the effect of load histories on the ductility and energy indexes of r.c. tied columns under cyclic loading. A parameter which influences the cyclic performance of r.c. tied columns was also identified.

PERFORMANCE EVALUATION

To evaluate the performance of columns on a rational basis, it is theoretically preferable to resort to a common and systematic approach in determining the various response parameters such as the yield displacement, the ultimate displacement, etc. Following the procedures outlined by Sheikh and Khoury (1993), the envelope curve (which results from the average of values in both directions) to hysteresis loop is first constructed. The displacement ductility factor, μ_{4} , is defined as

$$\mu_{\Delta} = \frac{\Delta_{u}}{\Delta_{y}} \tag{1}$$

where Δ_u is the displacement reached when the capacity of the specimen dropped to 80% of the peak value, which is considered as the failure load, and Δ_y is taken as the displacement value attained at the peak lateral load, H_{max} , assuming an initial stiffness K_i as shown in Fig. 1.

In computation, the initial stiffness may be difficult to obtain accurately due to some fluctuations in displacement data at small loads. Assuming that the initial response is essentially elastic at a lateral load not exceeding 30 percent of the maximum capacity of the specimen, the secant modulus at this load level was taken as a good approximation of the initial stiffness for practical purposes.

The dissipated energy, E, is defined as the cumulative energy dissipated within each cycle i, shown as the hatched area E_i in Fig. 1. Thus

$$E = \sum_{i=1}^{n} E_i \tag{2}$$

in which n is the number of cycles to failure. The normalized dissipated energy, E_N , is

$$E_N = \frac{1}{H_{\text{max}} \Delta_{\mathbf{y}}} \sum_{i=1}^{n} E_i \tag{3}$$

Rather than computing the dissipated energy, Gosain et al. (1977) proposed the following work index as an alternative performance indicator

$$I_W = \sum_{i=1}^n [(H_i \Delta_i) / (H_{max} \Delta_y)]$$
 (4)

where H_i and Δ_i are the maximum values of the lateral load and displacement in cycle i, respectively, averaged in both directions. Eq. (4) was further simplified to

$$N_{\Delta} = \sum_{i=1}^{n} (\Delta_i / \Delta_y) \tag{5}$$

which can be interpreted as the cumulative ductility ratio (Sheikh and Khoury, 1993).

Effective confinement steel ratio

It has been pointed out that while the ACI Code provisions for the design of confinement steel for high seismic risk regions are conservative for low axial loads, they may not be sufficient for high levels of axial load. Watson and Park (1994) proposed a design equation which accounts for the ductility performance in terms of curvature ductility factor, μ_{ϕ} , the influence of axial load level as well as material and dimensional parameters. Sheikh and Khoury (1997) developed a procedure for the design of confinement steel considering axial load level, tie configuration, and the expected curvature ductility performance.

Based on the concept of Sheikh and Khoury, it is suggested that the effective confinement steel, A_{sh} (k'_e), for a targeted ductility demand, μ_{Δ} , be given by the ACI confinement steel, $A_{sh,ACI}$, modified by the axial load and ductility level functions, i.e.

$$A_{sh}(k'_{e}) = A_{sh,ACI} g(\mu_{\Delta}) Y_{p}$$
 (6)

where k'_e is the confinement effectiveness coefficient normalized with respect to 0.75, which is the upper bound value assumed by the ACI Code for the efficiency of rectilinear ties in comparison with that of closely-spaced spirals; $g(\mu_{\Delta})$ is a nonlinear function of the displacement ductility demand; and Y_P is the axial load parameter given by (Sheikh and Khoury, 1997)

$$Y_p = 1 + 13(P/P_0)^5 (7)$$

in which P is the axial load, and P_0 is the ultimate load capacity.

Several researchers have proposed different formulae to account for the non-uniformity in confining pressure resulting from bending of ties under lateral pressure, which causes reduction in confinement effectiveness. The simple empirical formula proposed by Saatcioglu (1996) for the confinement effectiveness coefficient, k_e , was used in this study:

$$k_e = 0.15 \sqrt{\left(\frac{b_c}{s_t}\right) \left(\frac{b_c}{s_l}\right)} \le 1 \tag{8}$$

where b_c is the confined core dimension, center-to-center, of the perimeter hoop; s_t is the spacing of ties; and s_l is the spacing of the laterally supported longitudinal reinforcement.

Eq. (6) can be rewritten as

$$\mu_{\Delta} = f(\rho_{\Delta}) \tag{9}$$

where $f(\rho_A)$ is a nonlinear function of the effective confinement steel ratio to be obtained from a regression analysis of test results. The 'effective confinement reinforcement ratio', ρ_A , is defined as

$$\rho_A = \frac{A_{sh} k_e'}{A_{sh,ACI} Y_p} \tag{10}$$

This important parameter enables comparison of performance of column specimens with different transverse reinforcements (including tie arrangements) and different axial load levels.

Test Samples

Based on the number of test results available in the literature which needs to be large enough for a regression analysis, and the availability of digitized hysteresis loops, the number of test specimens that could be used in this study was only 17. The test samples can be broadly grouped into two categories in accordance with displacement histories (Fig. 2), viz.,

History type 1: increments of $1\Delta_y$ with basically two cycles repeated for each displacement increment

History type 2: increments of $2\Delta_y$ with basically two cycles repeated for each displacement increment

Histories types 1(a) and 2(a) are the basic ones. The others differ from the basic displacement histories in minor details. The extra third cycle at $6\Delta_y$ for specimen B2 with History Type 1(b) was accompanied by a much reduction in the lateral load capacity, and hence did not contribute to the energy computation. History Types 2(b) and 2(c) include extra cycles at $1\Delta_y$ which contributed less than 1% of the total energy. Judging from the stable hysteresis loops, the first two cycles at ductility level $7\Delta_y$ for specimen B1 with History Type 2(c) were approximated as equivalent to one cycle of $8\Delta_y$, assuming that one complete cycle at ductility level $8\Delta_y$ could have been attained if the loading history had strictly followed the $2\Delta_y$ increments.

Table 1 summarizes the details of test specimens whose results are used in the analyses. The main parameters, besides the displacement histories, include:

- a) material strength ratio f'_c / f_{yh} in the range of 0.060-0.136, where f'_c is the concrete compressive strength and f_{yh} is the yield strength of the transverse steel;
- b) shear span-to-depth ratio: 3.0 or larger;
- c) longitudinal reinforcement ratio: 1.51-2.45%;
- d) transverse steel in the range of 29% 236% of that specified in ACI code (1999);
- e) axial load level of 0.08–0.77 of the concrete gross section capacity;
- f) tie configurations as shown in Fig. 3.

All column specimens were made of normal strength concrete with conventional hoops and/ or ties, and all exhibited flexure mode of failure. The data on hysteresis loops were obtained from the web site: www.ce.washington.edu/~peera1.

ANALYSIS OF RESULTS

Displacement ductility factor

The calculated values of the displacement ductility factor, $\mu_{A,cal}$, are tabulated in Table 2 and plotted in Fig. 4 as functions of the effective confinement reinforcement ratio, ρ_A . The values of $\mu_{A,exp}$ reported (or implied) by the researchers are also included in Table 2. It may be observed that for load history Type 1, the discrepancy in $\mu_{A,cal}$ and $\mu_{A,exp}$ is in the range of 5.8-20.0%, which is acceptable. However, for load history Type 2, the agreement became worse for some specimens. For instance, for specimen UNIT2 by Soesianawati et al. (1986), the test result suggests a value of $\mu_{A,exp}$ of 6.0, much smaller than the computed value of 9.0. To be capable of reaching a ductility factor of 9.0, the specimen would have had to be able to sustain 10 (main) cycles (with adequate capacity) rather than 6, which was actually sustained. Obviously it is doubtful if the specimen could actually be able to develop a ductility of 9.0. Therefore, it was deemed more appropriate to use the values of $\mu_{A,exp}$ as reported by the researchers for the load histories Type 2.

The plot in Fig. 4 shows that the most of the data points for $\mu_{A,cal}$ for Type 1 load history are contained in a small band when they are plotted against ρ_A , while those for Type 2 load history are much more scattered. A second order curve fitting of Type 1 load history data points, yields

$$\mu_{\Delta,cal} = -12.86 \,\rho_A^2 + 15.54 \rho_A + 1 \tag{11}$$

with the goodness-of-fit index, R^2 , equal to 0.33. It is assumed here that the displacement ductility factor of 1.0 is attained for an un-confined section. The rather low R^2 is to be expected because the parameter ρ_A reflects several factors including the amount of transverse reinforcement, strength ratio, axial load level and tie configuration effectiveness, the latter being difficult to quantify precisely.

One may note that the plot of $\mu_{A,exp}$ versus ρ_A (also shown in Fig. 4) agrees quite well with that of $\mu_{A,cal}$ except for larger values of ρ_A , where there are few data points.

Clearly more data are definitely needed. As for Type 2 load history, no meaningful curve fitting is possible with the few sample points. Nevertheless, as expected, testing with displacement increments of $2\Delta_y$ seems to yield slightly higher ductility factor than testing with $1\Delta_y$ increments.

Energy Dissipation Capacity

The plots in Fig. 5 and Fig. 6 clearly indicate tendency for the normalized energy dissipation capacity and cumulative ductility ratio to increase nonlinearly with the effective confinement steel ratio. Results of second order curve fitting for the indexes based on the computed values of Δ_y (as explained earlier) are shown in the plots as solid lines. Assuming zero energy dissipation for a specimen without transverse reinforcement, which is a fairly good approximation, the equation of best fit, for displacement increments of $1\Delta_y$ is given by

$$E_{N,cal} = 83.67 \,\rho_A^2 + 49.58 \,\rho_A \tag{12}$$

and for the cumulative ductility ratio, the fitted curve is

$$N_{A,cal} = 193.61 \,\rho_A^2 - 59.77 \,\rho_A^2 + 20.33 \tag{13}$$

with corresponding R² values of 0.83 and 0.59, respectively.

For comparison, the fitted curves for the indexes based on the experimental values of Δ_y are also given as the dashed lines. Again, due to the paucity of data, only sample points for Type 2 load history are shown in the plots without any curve fitting performed. The fitted curves for normalized energy dissipation capacity based on the experimental and computed values of μ_{Δ} agree well, to within about 10% in the range of available data points. The same is true for the cumulative ductility ratio.

The limited data seem to suggest that the loading history with increments of $2\Delta_y$ is somewhat more severe than that with $1\Delta_y$ increments. For specimens with effective confinement steel ratio less than about 0.40, the energy dissipation capacity for Type 2

loading history may be smaller than that for Type 1 loading history by about 30% - 40%. The fact that the reduced value of μ_{Δ} results in an increase in the normalized energy dissipation capacity was earlier reported by Darwin and Nmai (1986). However, at larger values of ρ_{A} , e.g for highly confined columns, the effect of load history tends to be less significant. Due to the scatter in the test results and the paucity of data points, it is obvious that more tests are needed on highly confined specimens under small axial load levels.

As would be expected, there is a close correlation between the work index and cumulative ductility ratio as depicted in Fig. 7.

CONCLUSIONS

The following conclusions can be drawn:

- 1. For a given loading history, the displacement ductility factor, μ_{Δ} , and the energy dissipation parameters were found to correlate with the effective confinement reinforcement ratio. This is of practical significance in enabling prediction of displacement ductility and energy dissipation capacity for a given column, taking into account the effect of axial load and tie configuration effectiveness, among other basic variables.
- 2. The ductility factor for loading history Type 2 (with increments of $2\Delta_y$) tends to be somewhat higher than that for Type 1 (with $1\Delta_y$ increments) for the same effective confinement steel ratio. However, since the number of samples in the former case is small, further study is needed.
- 3. The load history with $2\Delta_y$ increments is slightly more severe than that with $1\Delta_y$ increments for moderate values of effective confinement steel ratio. The effect of load history tends to be less significant at higher values of the effective confinement steel ratio, pending further investigation.

ACKNOWLEDGMENTS

The authors are grateful to the Thailand Research Fund (TRF) for the TRF Senior Research Scholar Grant to the senior author for this research project.

REFERENCES

- Azizinamini, A., Corley, W. G., and Johal L. S. P. (1992). "Effects of transverse reinforcement on seismic performance of columns." *ACI Struct. J.*, 89(4), 422-450.
- American Concrete Institute (1999). "Building code requirements for reinforced concrete." ACI 318-99, Farmington Hills, Michigan.
- Darwin, D., and Nmai, C.K. (1985). "Energy dissipation in RC beams under cyclic load." J. Struct. Div., ASCE, 112(8), 1986, 1829-1846.
- Gosain, N. K., Brown, R. H., and Jirsa, J. O. (1977). "Shear requirement for load reversals on RC members." J. Struct. Div., ASCE, 103(ST7), 1461-1476.
- Hwang, T. H., and Scribner, C. F. (1984). "R/C member cyclic response during various loadings." J. Struct. Engrg., ASCE, 110(3), 477-489.
- Soesianawati, M. T., Park, R., and Priestley M. J. N. (1986). "Limited ductility design of columns." *Report 86-10*, Dept. of Civ. Engrg., Univ. of Canterbury, Christchurch, New Zealand.
- Sheikh, S. A., and Khoury, S. S. (1993). "Confined concrete columns with stubs." *ACI Struct. J.*, 90(4), 414-431.
- Saatcioglu, M. (1996). "Design of seismic resistant concrete columns for confinement." Proceedings of the ASCE CCMS Symposium held in conjunction with Structural Congress XIV, 233-245.
- Sheikh, S. A., and Khoury, S. S. (1997). "A performance-based approach for the design of confining steel in tied columns." *ACI Struct. J.*, 94(4), 421-431.
- Wight, J. K., and Sozen, M. A. (1975). "Strength decay of RC columns under shear reversal." J. Struct. Div., ASCE, 101(ST5), 1053-1065.
- Watson, S., and Park, R. (1994), "Simulated seismic load tests on reinforced concrete columns." J. Struct. Engrg., ASCE, 120(6), 1825-1849.
- Watson, S., Zahn, F. A., and Park, R. (1994), "Confining reinforcement for concrete columns." J. Struct. Engrg., ASCE, 120(6), 1798-1824.
- Wehbe, N. I., Saiid, M. S., and Sanders, D. H. (1999), "Seismic performance of rectangular bridge columns with moderate confinement." *ACI Struct. J.*, 96(2), 248-258.

Table 1. Details of test specimens used in analyses

	Specimen	Ag (m²)	Concrete Strength (Mpa)	Longitudinal Steel		Lateral Steel			Axial	Shear		Load	
Referance				f _y (Mpa)	ρ _ι (%)	f _{yk} (Mpa)	A _{sh} /(s*h _c)	A _{sh} /A _{sh,ACI}	Load Level P/(f _c 'A _g)	span-to-d epth ratio	Tie Config.	History	k,
(1)	(2)	(3)	(4)	(5)	(6)	(7)	(8)	(9)	(10)	(11)	(12)	(13)	(14)
Soesianawati et al.	UNIT 2	0.160	44 0	446	1.51	360	0 00601	0.55	0.30	4.00	RO _	2(a)	0.58
(1986)	UNIT 3	0.160	44 0	446	1.51	364	0 00393	0 36	0.30	4.00	RO	2(a)	0.54
Watson et al.	UNIT 5	0.160	41.0	474	1.51	372	0 00579	0 58	0 50	4.00	RO	l(a)	0.57
(1994)	UNIT 6	0 160	40.0	474	1.51	388	0.00273	0 29	0.50	4.00	RO	l(a)	0 52
	UNIT 7	0.160	42 0	474	1.51	308	0 011111	0 91	0.70	4.00	RO	l(a)	0.53
	UNIT 8	0.160	39 0	474	1.51	372	0.00609	0.65	0.70	4.00	RO	l(a)	0.59
	UNIT 9	0 160	40.0	474	1.51	308	0 02051	1 76	0.70	4.00	RO	2(a)	0.71
Azizinamini et al.	NC-2	0 209	39 3	439	t 94	454	0.01152	f 01	0.21	3.00	RD1	I(a)	0.43
(1992)	NC-4	0 209	39 8	439	l 94	616	0 00650	0 68	0.31	3.00	RD1	1(a)	0.42
Wehbe et al.	A1	0 232	31.7	448	2.22	455	0 00323	0 52	0.08	3.83	RC	2(b)	0.46
(1999)	A2	0 232	27 2	448	2.22	455	0.00323	0.60	0.24	3.83	RC	l(a)	0.46
	BI	0 232	29 7	448	2 22	455	0.00428	0 73	0.09	3 83	RC	2(c)	0.53
	B2	0 232	28 l	448	2.22	455	0 00428	0.77	0 23	3.83	RC	I(b)	0.53
Sheikh and Khoury	AS-3	0.093	33 2	509	2.45	509	0.00844	1 44	0.60	4 83	RD2	l(a)	0.35
(1993)	AS-17	0.093	31 4	509	2.45	509	0.00844	1.52	0.77	4.83	RD2	l(a)	0.35
	AS-18	0 093	32.8	509	2 45	465	0.01501	2.36	0.77	4.83	RD2	l(a)	0.36
	AS-19	0 093	32.3	509	2 45	486	0.00691	1.15	0.47	0.00	RD2	l(a)	0.35

Table 2. Summary of displacement ductility and energy indexes

Referance	Specimen	Displacement ductility		Normalized dissipated energy		Cumulative ductility ratio		Work index	
		$\mu_{\Delta,exp}$	μ _{Δ,cal}	E _{N,exp}	E _{N,cal}	N _{A,exp}	N _{A,cat}	I _{W,exp}	I _{W,cal}
(1)	(2)	(3)	(4)	(5)	(6)	(7)	(8)	(9)	(10)
Soesianawati et al.	UNIT 2	6.0	9.0	20.1	30.3	19.1	28.8	17.4	26.2
(1986)	UNIT 3	5.8	8.6	11.8	17.4	12.7	t 8.7	11.9	17.6
Watson et al.	UNIT 5	5.7	5.4	30.7	29.3	30.2	28.9	27.7	26.5
(1994)	UNIT 6	4.0	4.5	17.3	19.5	18.9	21.3	17.2	19.4
	UNIT 7	3.2	3.2	13.4	13.1	10.4	10.2	9.7	9.5
	UNIT 8	3.9	3.5	11.3	10.1	10.3	9.2	9.6	8.6
	UNIT 9	9.1	7.3	61.5	49.5	41.0	33.0	38.3	30.8
Azizinamini et al.	NC-2	7.1	6.7	68.1	64.2	63.8	60.1	56.4	53.2
(1992)	NC-4	4.2	4.1	18.5	17.9	23.9	23.2	21.4	20.7
Wehbe et al.	AI	5.3	4.6	22.2	19.3	23.7	20.6	21.2	18.5
(1999)	A2	5.2	5.5	29.5	30.4	33.2	34.3	30.6	31.6
	Ві	6.7	5.1	43.2	32.8	38.9	29.6	35.0	26.6
	B2	6.1	5.6	52.0	45.0	53.3	46.2	49.0	42.4
Sheikh and Khoury	AS-3	4.7	4.7		-	23.0	23.0		-
(1993)	AS-17	3.8	3.8	-	-	24.0	24.0	-	
	AS-18	6.7	6.7	-	-	44.0	44.0		
	AS-19	4.0	4.0		-	18.0	18.0		-

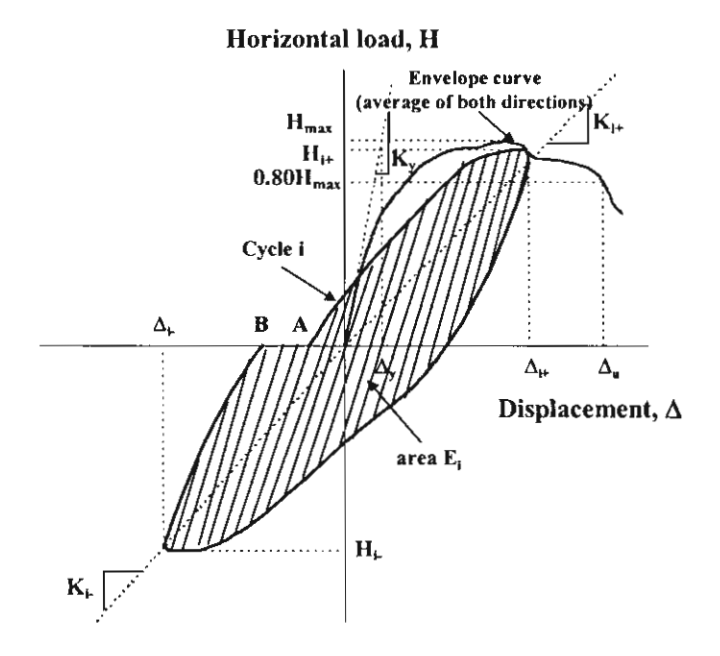


Fig. 1 Definition of yield displacement (Δ_y) and ultimate displacement (Δ_u)

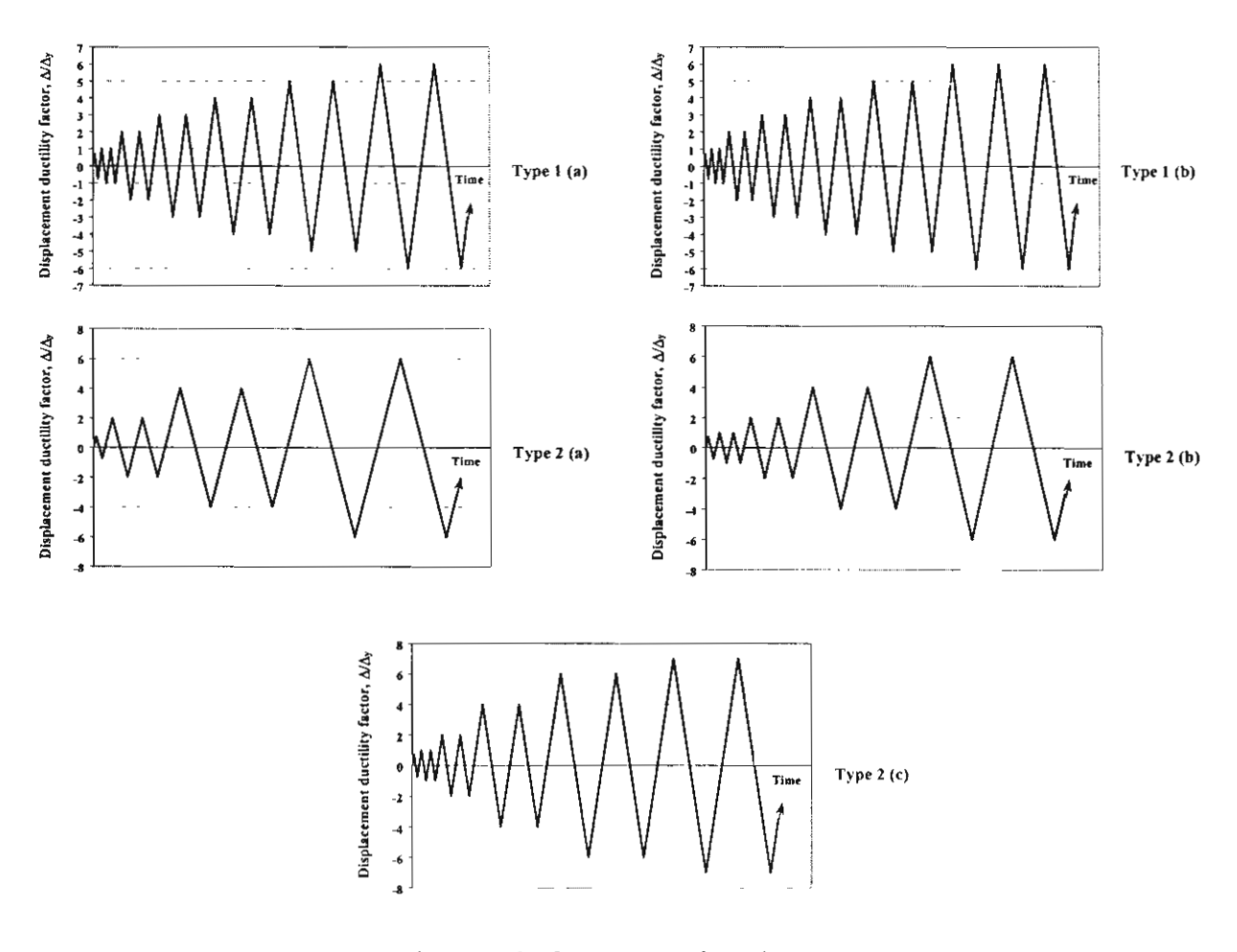


Fig. 2 Displacement histories

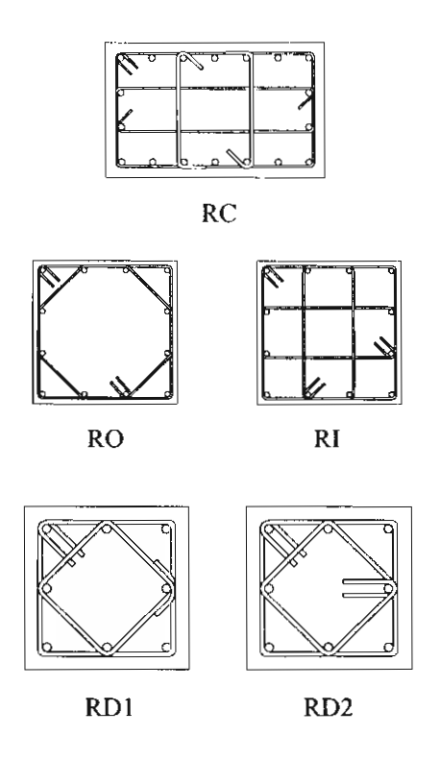


Fig. 3 Tie configurations

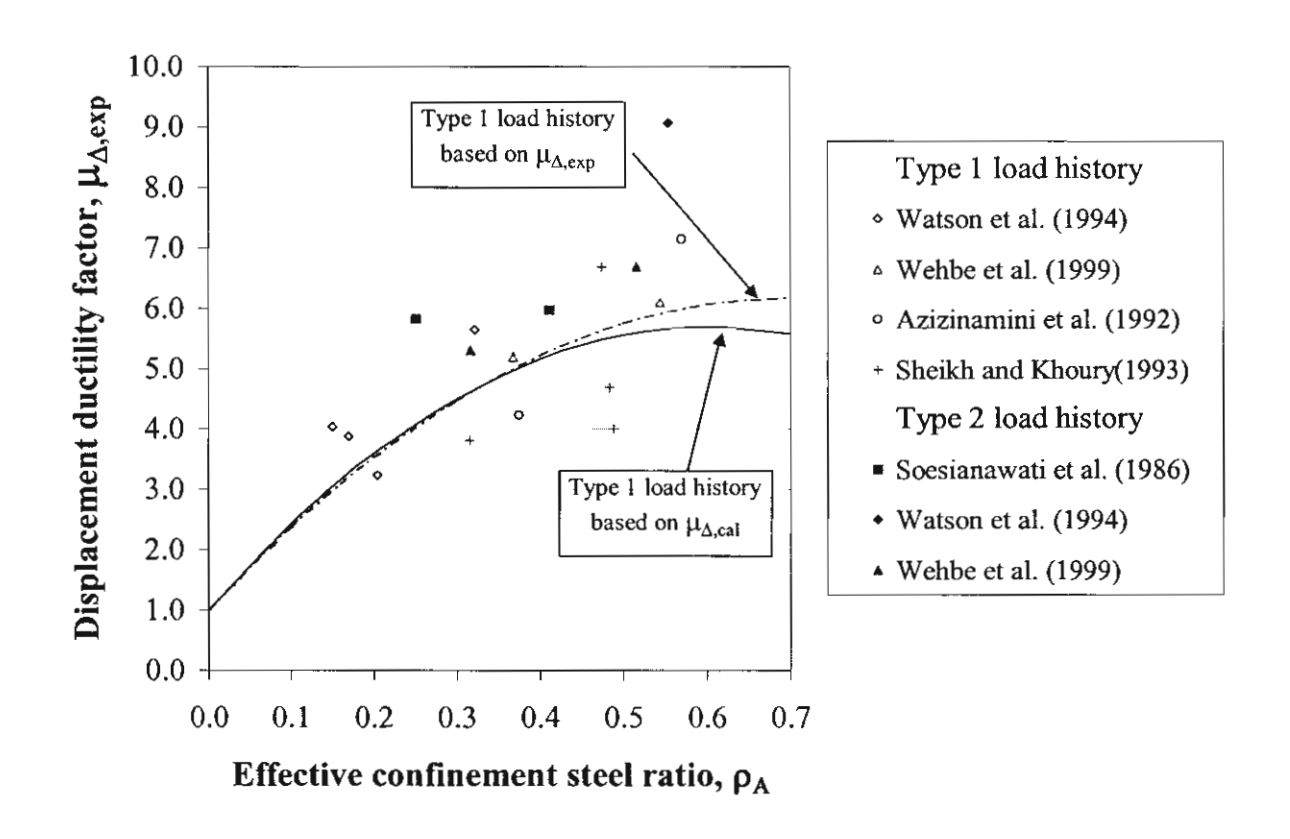


Fig. 4 Displacement ductility factor as function of ρ_A

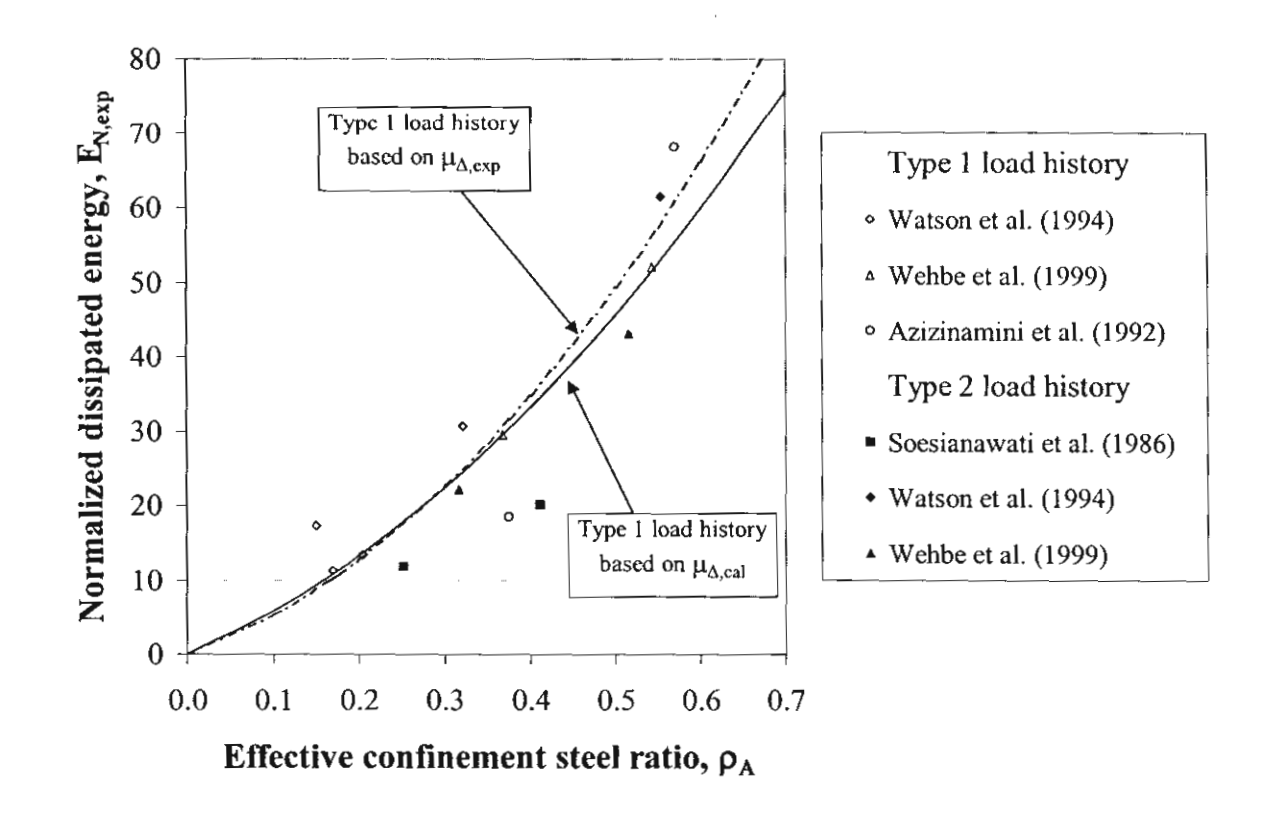


Fig. 5 Normalized dissipated energy as function of ρ_A

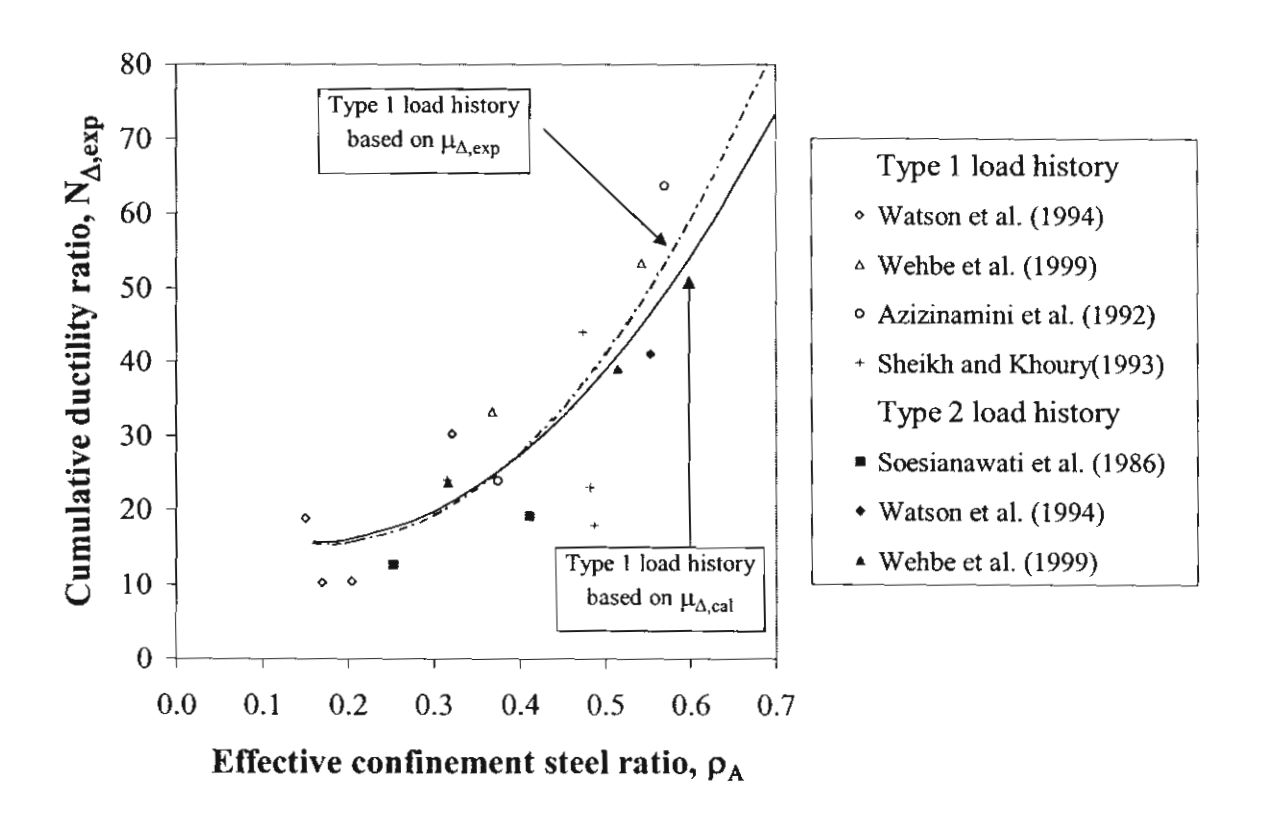


Fig. 6 Cumulative ductility ratio as function of ρ_A

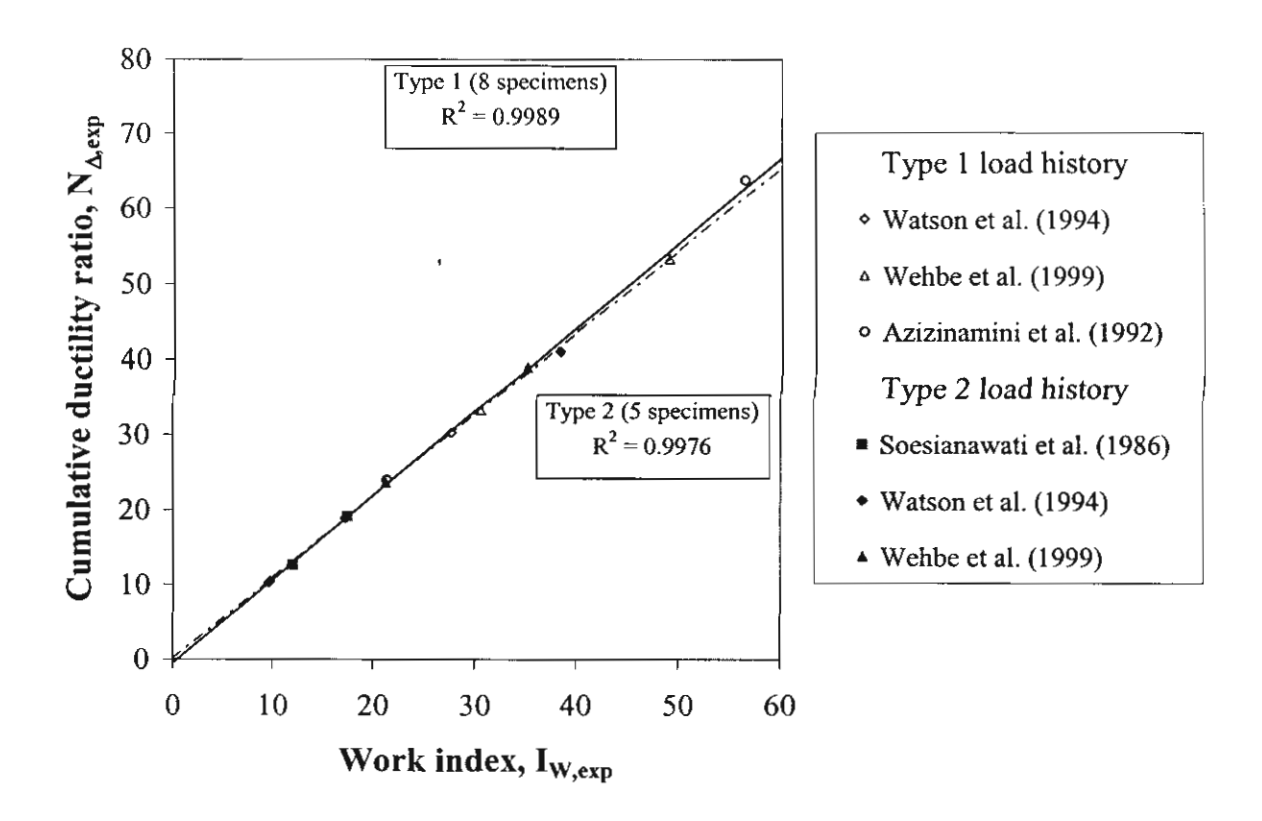


Fig. 7 Cumulative ductility ratio as function of Iw

RETROFIT OF STEEL MOMENT-RESISTING FRAMES SUBJECTED TO LONG-DISTANCE EARTHQUAKES CONSIDERING WELD FRACTURES

ASSAWIN WANITKORKUL

Department of Civil Engineering, Chulalongkorn University Phaya Thai Rd., Patumwan, Bangkok 10330, Thailand

PANITAN LUKKUNAPRASIT

Department of Civil Engineering, Chulalongkorn University Phaya Thai Rd., Patumwan, Bangkok 10330, Thailand

ANDRE FILIATRAULT

Department of Structural Engineering, University of California, San Diego La Jolla, CA 92093-0085, USA

It has been generally accepted that steel moment-resisting frames behave in a ductile manner under seismic excitations. However, during the 1994 Northridge earthquake, weld fractures at the beam-to-column connections occurred in many steel buildings. Such brittle failures obviously preclude the traditional ductile-behaviour assumption and have a significant effect on the responses of steel moment-resisting frames. In this paper, the performance of a friction damping system for retrofitting steel moment-resisting frames was investigated under long-distance earthquakes with frequency contents resembling the 1985 Mexico city (SCT), the 1995 Bangkok, or the 1977 Romania ground motions, all scaled to a peak ground acceleration of 0.17g. Responses of the building under the 1940 El Centro N-S component were also included for comparison. The results of the study show that a friction damping system can reduce the seismic responses significantly. The device can also prevent the total collapse and joint failures of the building equipped with friction dampers, while the one without dampers would collapse, even under a moderate peak ground acceleration of only 0.17g.

Keywords: weld fractures; joint failures; beam-column joints; long-distance earthquakes; friction dampers; energy ratio.

1. Introduction

As a result of the 1994 Northridge earthquake in California, many steel moment-resisting frames were seriously damaged. Brittle weld fractures in beam-to-column connections occurred in several steel structures. According to EERI [1997], two types of weld cracks can be distinguished. First is a fracture near the interface of the beam and column flange. This common fracture results in the severing of the beam flange from the column flange and passes through the weld or through the adjacent heat-affected material. Another type is a fracture through the

column. This type of fracture would be very dangerous if the crack extended all the way through the column which would reduce its compressive capacity. These fractures can violate the ductile-behaviour assumption of steel moment-resisting frames, which is usually presumed in an analysis, and they had an important effect on the seismic response of steel structures during the Northridge earthquake.

In recent decades, several analytical and experimental studies have led to the implementation of friction damping systems in many structures for retrofit, e.g., Pall and Marsh [1982], FitzGerald et al. [1989], Filiatrault and Cherry [1990], Grigorian et al. [1993], Pall A.S. and Pall R. [1996], Reinhorn and Li [1996]. The effectiveness of friction dampers in seismic retrofit has been widely recognized. However, most past studies did not consider the brittle weld fracture behaviour of steel moment-resisting frames, which can reduce the performance of steel structures. From the literature, it can be observed that there has been no research on retrofit of steel structures using friction dampers and taking into account the weld-fracture phenomena except the one by Filiatrault et al. [2001], which studied the performance of passive energy dissipating systems for retrofit of steel moment-resisting frames considering weld fracture effect. Those authors found that a friction damping system can significantly reduce responses of the building; however, major damage or total collapse in some cases still occurred and connection retrofit would still be required. The short duration, impulsive-type ground motions with average peak ground acceleration about 1 g, which represented the near field ground motions, were used. These findings, however, cannot be generalized for systems subjected to moderate ground motions induced by long-distance earthquakes, which may occur in many large cities in moderate seismic risk regions, such as Bangkok and Singapore.

This study investigates the performance of a passive friction damping system for retrofitting steel moment-resisting frames with weld fracture behaviour subjected to moderate ground motions from distant earthquakes. The effectiveness of friction dampers in reducing damage in structures is demonstrated through numerical examples obtained from nonlinear dynamic analyses. Only weld fracture at the beam-to-column interface was modeled into the studied building.

2. Building, Retrofit Scheme, and Model Assumptions

2.1. Building and retrofit scheme

The steel structure studied here is the same as considered by Filiatrault *et al.* [2001]. The building is a 6-storey steel moment-resisting frame, rectangular in plan, and is braced by two exterior moment-resisting frames. It is designed according to the 1994 UBC code requirements for a building located in seismic zone 4 on soil type S2. Gravity loads acting on the frame during the earthquake are assumed equal to 3.8 kPa from roof dead load, 4.5 kPa from floor dead load, 0.7 kPa from floor live load, and 1.7 kPa from weight of the exterior cladding. Steel grade A36 (nominal Fy = 248 MPa) is used for all members. Building details are shown in Fig. 1. For retrofit, chevron-brace members are introduced in the central bay of the two exterior moment-resisting frames as shown in Fig. 1. The steel section HSS 12 x 12 x 5/8 (300 mm x 300 mm x 15 mm) is used for all chevron-brace elements. Friction dampers are incorporated at one end of all bracing members.

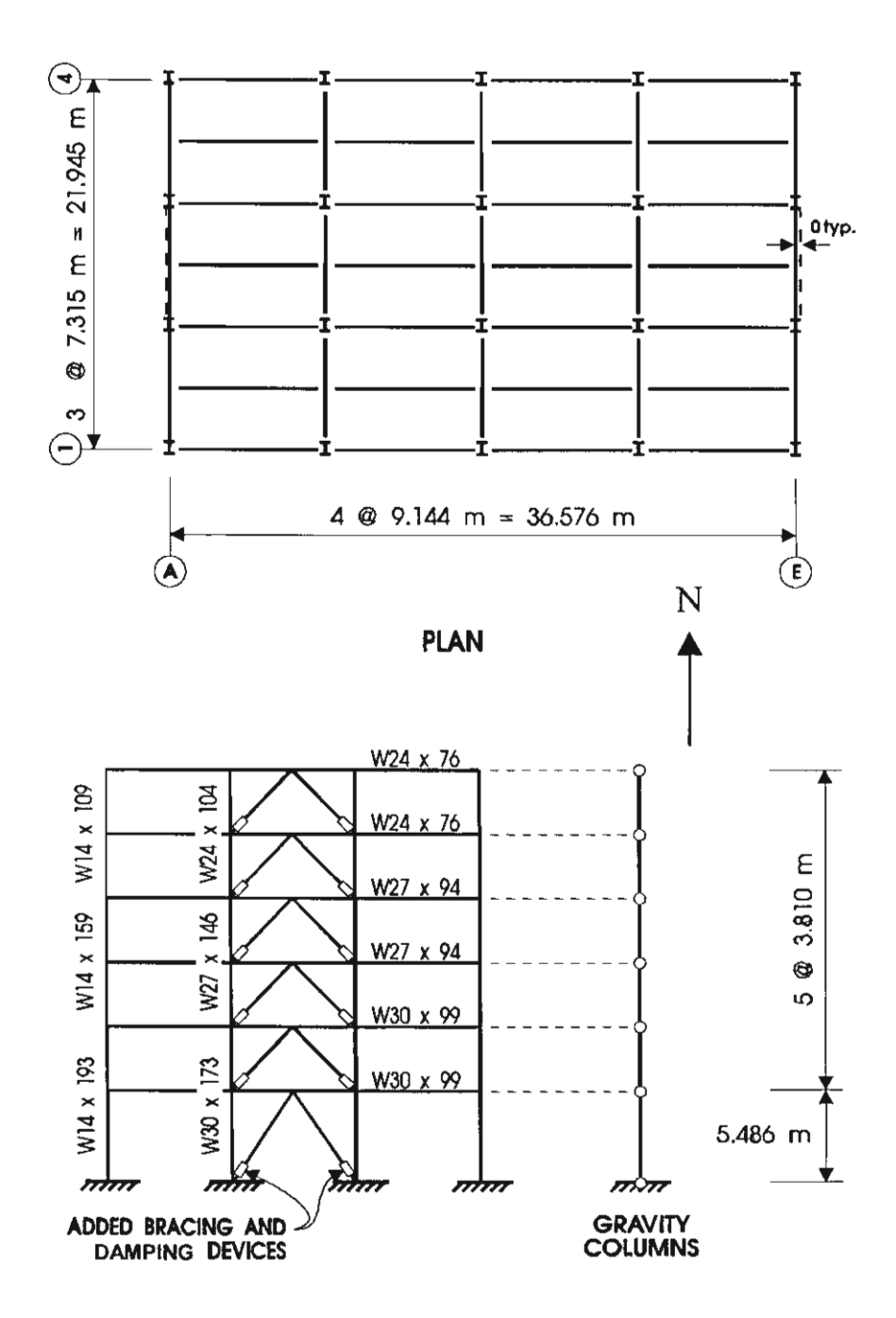


Fig. 1. Building and retrofit scheme

2.2. Model assumptions

Because of the symmetry of the studied building, only one exterior moment-resisting frame is modeled as a 2-D structure into the general-purpose nonlinear dynamic analysis program RUAUMOKO [Carr, 2000]. Floor slabs and architectural elements are excluded. The panel zones of the beam-column joints are assumed to have no panel shear deformation and yielding during strong excitations. This assumption represents the most critical condition for welded

beam-column joints because the hysteretic energy can only be dissipated through plastic hinging in the beams and the columns [Filiatrault *et al.*, 2001]. The inelastic response is assumed to concentrate in plastic hinges that could form at both ends of the frame members. Large displacement effect is also considered in the analyses. P-Δ effect from interior columns is included by introducing a pin-ended gravity column into the building model, which represents all interior columns. Total gravity loads acting on the interior columns are applied to the gravity column. Both the exterior frame and the gravity column are constrained to undergo the same lateral displacement at each floor, which represents a rigid floor diaphragm assumption. Bi-linear moment-curvature relation with a curvature-hardening ratio of 2% is assigned for all columns.

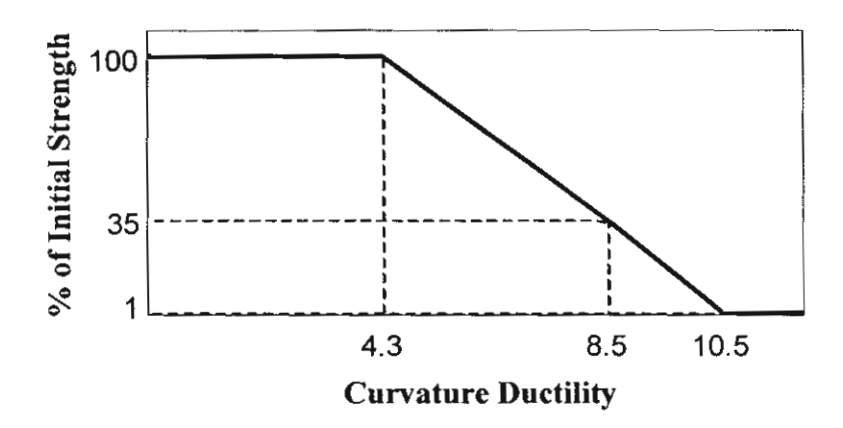


Fig. 2. Flexural strength degradation model

The flexural strength degradation model shown in Fig. 2 is introduced at both ends of all beams to account for the brittle behaviour of welded beam-to-column connections. Fracture initiates at curvature ductility of 4.3, corresponding to plastic rotation of about 0.01 rad in all beam sections of the studied structure, and the strength drops to 1% of the initial value at curvature ductility larger than 10.5. The strength degradation factor used here is the same as Filiatrault *et al.* [2001], which was obtained from a statistical review of different full-scale tests on beam-column joints, and it is assumed to be independent in positive and negative bending. Only fractures at the beam-to-column interfaces are considered. Then, an elasto-plastic moment-curvature relation is specified for all beam elements to prevent an increase in the flexural strength after fractures occur. Note that the connections are assumed to have no loss in shear capacity when weld fractures occur. An elasto-plastic force-displacement relation is also assigned for all friction-brace elements. The load at the yield plateau is specified by the slip load of each damper. The fundamental vibration period of the original building is 1.304 sec and is reduced to 0.649 sec after being retrofitted by the scheme described previously.

A mass proportional only damping model is adopted here because the rotational velocity at beam-to-column interface can increase significantly after fracture occurs. The large rotational velocity results in the increase in damping from the stiffness proportional portion of the global damping matrix, and this can violate the equilibrium condition at beam-column joints after weld fracture occurs [Filiatrault *et al.*, 2001]. The mass-proportional damping coefficient is taken as 0.5 sec⁻¹. The time step for nonlinear dynamic analyses is 0.0005 sec for all cases and a tolerance of 1% in the residual force vector is imposed for Newton-Raphson iteration to track the sudden

changes in stiffness due to joint fractures. Note that the slip loads of the friction dampers in the 2nd to 6th floors are 80% of slip load in the 1st floor. It is also assumed that the devices have sufficient slip lengths, so that no impact can occur.

The concept of Coulomb friction was adopted here to describe the hysteretic behaviour of the friction dampers, which can be formulated as:

$$F_S = \mu N \tag{1}$$

where F_S is a slip load of the damper, N is a normal force acting on the friction surface, and μ is a coefficient of friction. The friction devices will slip at a predetermined load exhibiting the well-known rigid-plastic hysteretic behaviour.

3. Earthquake Ground Motions

Accelerograms and pseudo-acceleration response spectra at 5% damping of all studied excitations are shown in Fig. 3. Three different long-distance earthquakes are considered here. First is a well-known long-distance earthquake, the 1985 Mexico city (SCT, E-W component) record. The SCT excitation was recorded on September 19, 1985 in Mexico city. The event's epicentral distance was about 400 km. It had a significantly narrow frequency band with a predominant period of 2.0 sec and peak ground acceleration about 0.17 times the gravitational acceleration (g). It is also a long-duration strong ground shaking which can have a significant effect on structures. To reduce the calculation time, only the 60-second range of the SCT record containing the peak acceleration value will be used in analysis. Second is the scaled 1995 Bangkok excitation. It was recorded on July 12, 1995 at the basement level of the Baiyoke tower whose fundamental vibration period is 2.5 sec. This event resulted from an earthquake whose epicenter was about 900 km away from Bangkok. Its predominant period is about 2.3 sec and it also contains other significantly longer and shorter period components. Its peak ground acceleration was scaled to the same value of SCT record.

The last long-distance ground motion is the scaled 1977 Romania (Bucharest, N-S component) earthquake. It was recorded on March 4, 1977 in the basement of the Research Institute building in Bucharest, Romania. The epicentral distance was about 150 km. The event had a narrow frequency band with a predominant period about 1.2 sec. Its peak ground acceleration was also scaled to 0.17g. The studied building was also subjected to the 1940 El Centro N-S component excitation which had been used extensively in many past studies. This signal was considered here for comparison purposes. Note also that the peak ground acceleration of the El Centro earthquake is about 2 times that of the other three records.

4. Numerical Results

In this section, the responses of the building under all four excitations are compared. The response parameters of interest are the peak interstory drifts, the number of yielded members and joint fractures, and the energy input and dissipated. The variation of these parameters with the slip load of the devices is investigated. The slip load of each device is varied between zero and

buckling strength of bracing member. Responses of the original building excluding weld fracture behaviour are also shown for comparison.

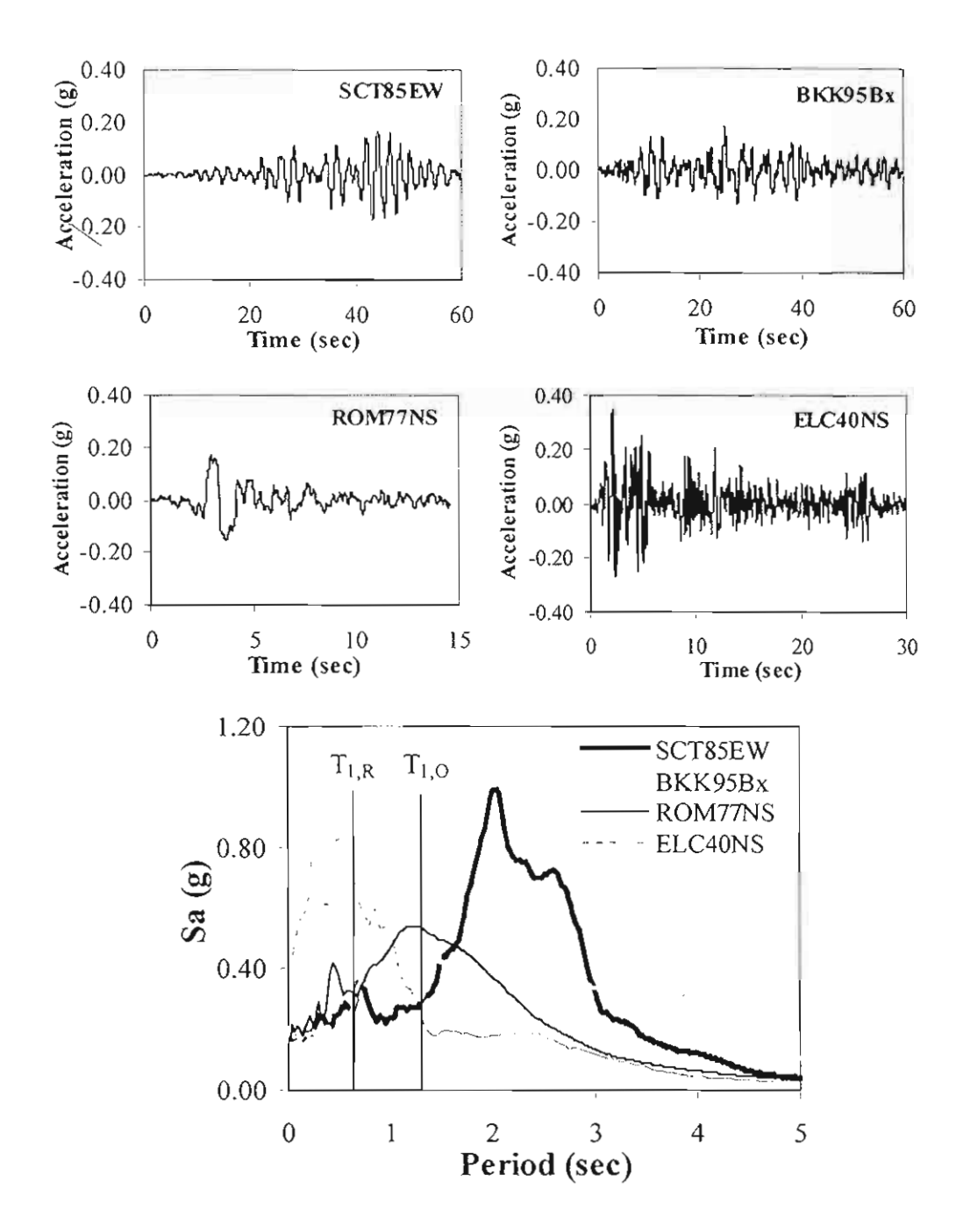


Fig. 3. Accelerograms and pseudo-acceleration response spectra at 5% critical damping

4.1. Peak interstory drift

The interstory drift can be an indicator for both structural and nonstructural damage. According to the performance criteria defined by the NEHRP seismic rehabilitation guidelines [ATC, 2000] for steel moment-resisting frames, maximum drift levels are 0.7% for immediate occupancy, 2.5% for life safety, and 5% for collapse prevention. Therefore, in this study, the 5% interstory drift is used as the collapse criterion. Fig. 4 shows the variation of peak interstory drift in each floor of the original structure neglected weld fracture effect. From the figure, the original building can survive all four earthquakes considered. The maximum interstory drifts, which are found in the first floor are 1.51%, 1.46%, and 0.81% resulting from the SCT, Romania, and El Centro excitations, respectively, while the maximum interstory drift of 1.14% is found in the second floor when the building is subjected to the Bangkok signal.

Fig. 5 shows the variation of peak interstory drift in each floor with the normalized slip load of the structure including weld fracture effect. The slip load is normalized by the buckling strength of the ground floor bracing element which equals to 3811 kN. The non-retrofitted building including joint fracture collapses under all excitations which is indicated by a peak storey drift of more than the 5% drift limit. Interestingly, even moderate long-distance earthquakes which have a peak ground acceleration only about half of the El Centro record can lead to the total collapse of the structure. This result indicates that weld fractures have a large effect on the performance of the structure and they must be taken into account.

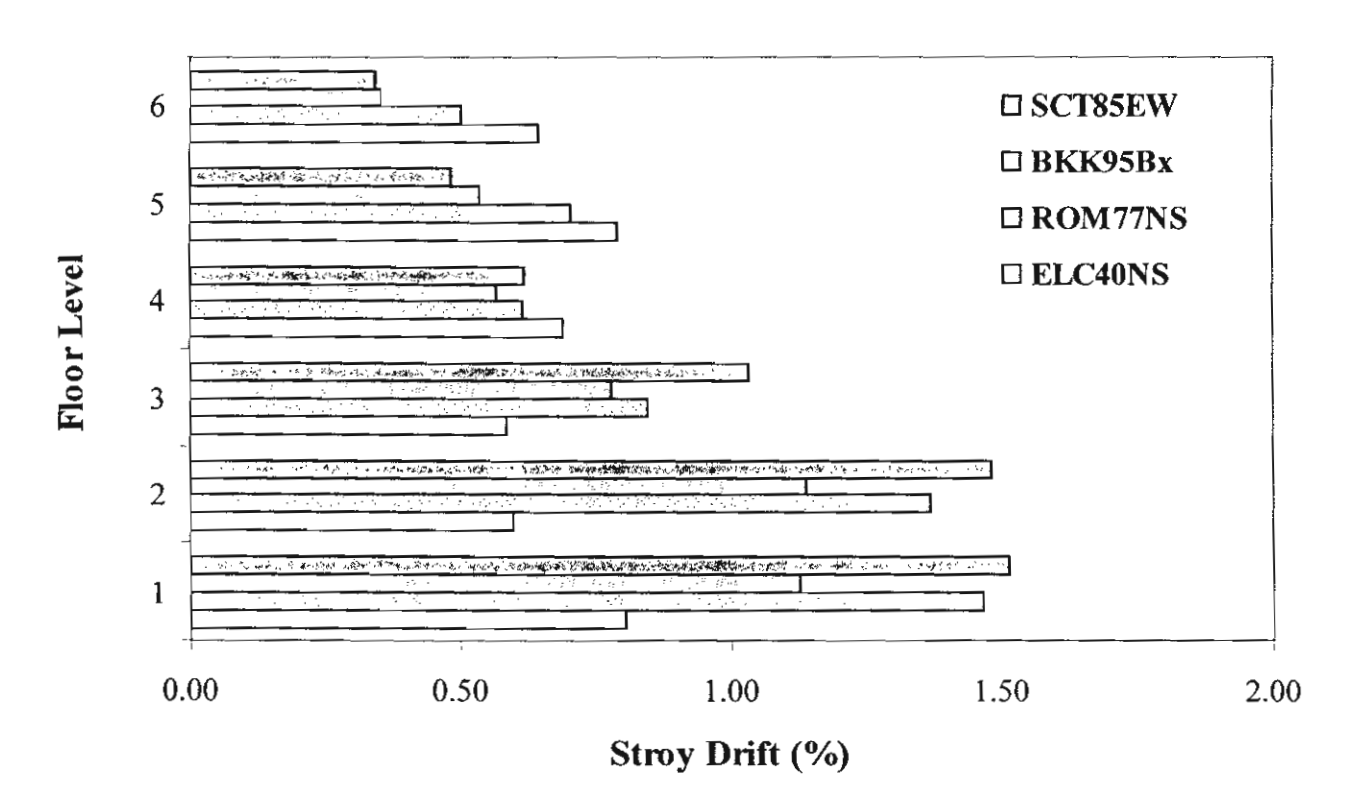


Fig. 4. Variation of peak interstory drift of the non-retrofitted building neglecting weld fracture effect

For a retrofitted structure including the effect of weld fracture, the building survives the El Centro earthquake at any slip load values, even under a very low normalized slip load of only 2.3%. However, it collapses under the SCT, Bangkok, and Romania ground motions as joint fractures take place at normalized slip loads less than 20.7%, 25.6%, and 19.7% for SCT, Bangkok, and Romania records, respectively. It is important to note that at a slip load close to these critical values, damages increase very rapidly. It should also be noted that larger earthquakes would require a higher critical slip load for collapse prevention. This is of practical significance in selecting the slip load of a friction damper to be sufficiently larger than the critical threshold values, and at the same time not too close to the buckling strength or the yield strength of the connecting elements; otherwise, the friction devices may not be effective to protect the structure. Past the threshold slip loads, responses of the buildings are sharply reduced. Peak interstory drifts are kept below 1% in all cases, which indicate that the retrofitted structure can survive all three long-distance excitations considered here. Note that there is an optimum slip load value in the case of the building subjected to the El Centro excitation. The optimum normalized slip load is 19.7% which is similar to the results obtained by Filiatrault et al. [2001]. On the other hand, for the three long-distance earthquakes, it seems that the performance of building improves for increasing slip loads. This would be caused by the characteristics of these studied accelerograms that have a frequency content concentrating in the low frequency zone. When joint fractures take place, the building will lose its stiffness and the resonant effect can occur. Then the additional stiffness induced by bracing system will play a more important role. Therefore, at a large slip load value, the devices are more difficult to slip. Then the building will be stiff and will respond for a longer time in the low spectral value zone resulting in a better performance.

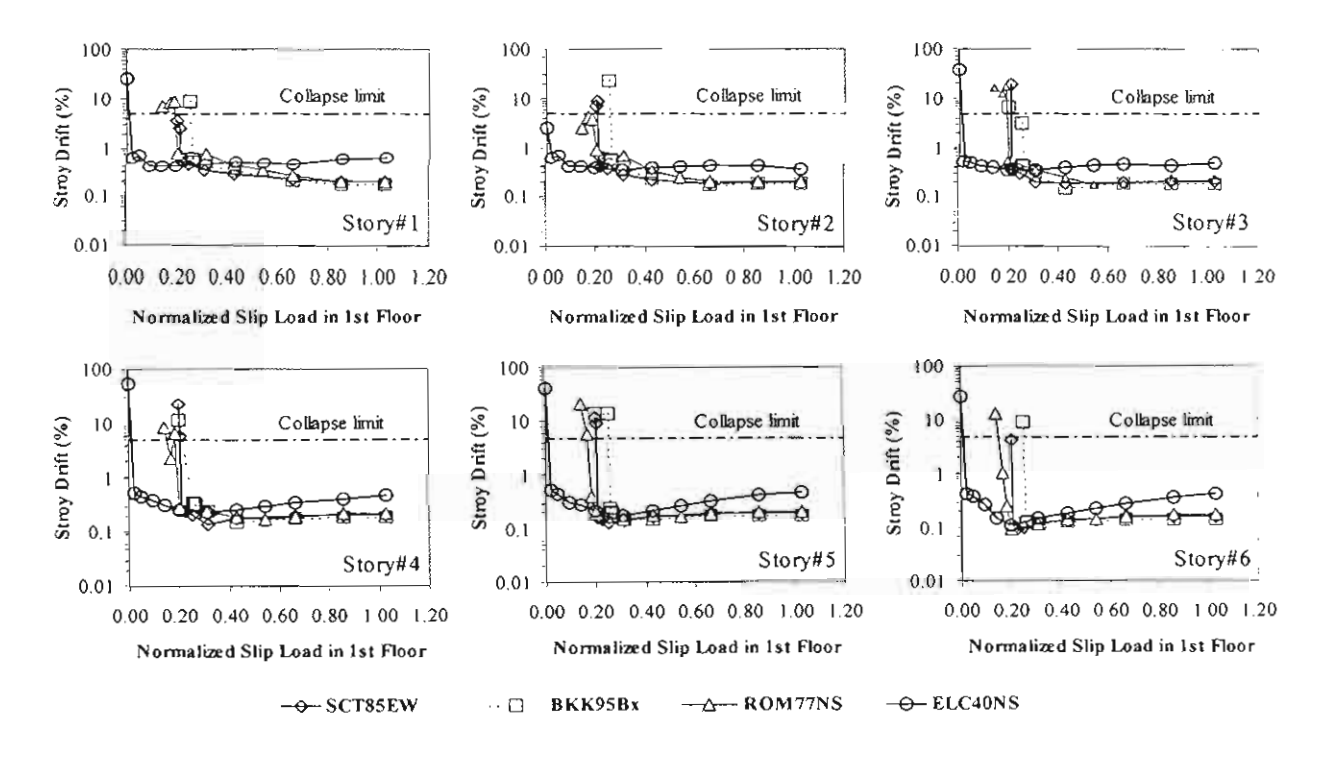


Fig. 5. Variation of peak interstory drift with normalized slip load of the building including weld fracture effect

However, if the slip loads reach the buckling or yield strength of the bracing elements, the performance of the system will decrease due to the buckling phenomena, or the failure of the bracing members. Note that buckling of the bracing members at the normalized slip load of 100% is neglected in this study.

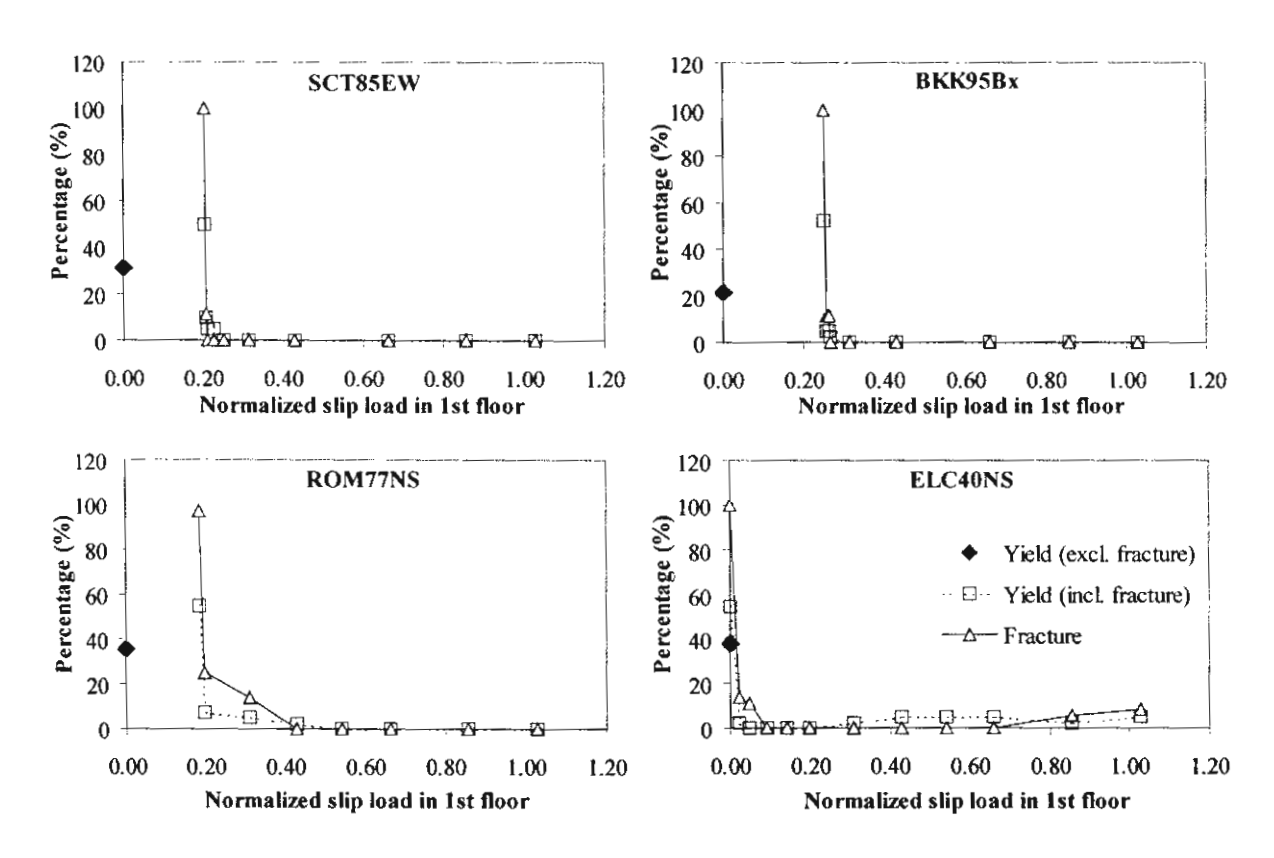


Fig. 6. Variation of the percentage of the yielded members and joint fractures with normalized slip load

4.2. Damage to the structure

Fig. 6 shows the percentage of yielded members and joint fractures for the original building neglecting weld fracture and for the retrofitted structure including weld fracture at each slip load value. For the numbers of yielded members, all members except the bracing elements and the gravity column are counted corresponding to a total of 42 members. The numbers of joint fractures are presented for each beam's end resulting in a total of 36 joints. For the original structure excluding weld fracture, the percentages of yielded members are 31%, 21.4%, 35.7%, and 38.1% when subjected to SCT, Bangkok, Romania, and El Centro ground motions, respectively. Although the building can survive all considered earthquakes, damages occur in many structural members which can lead to a high repair cost. Retrofit would be required for this structure.

For the retrofitted structure considering weld fracture characteristics, past the critical slip load value, the friction devices can reduce damages significantly. At the normalized slip load larger than 25%, 31.2%, and 54.2% when subjected to SCT, Bangkok, and Romania accelerograms,

respectively, all structural elements remain elastic and no joint failures occur. Similarly, for the retrofitted structure subjected to the El Centro record, the building remains elastic at the normalized slip load between 9.2% and 19.7%. Under all long-distance excitations, the studied building exhibits a sudden increase in damage at slip load less than the certain critical values indicated by failures of all joints in the building. Selection of the device's slip load would be very important for the structure having a possibility of weld fracture.

4.3. Energy ratio

In this section, the amount of energy dissipated by means of friction dampers for all analyses are presented. The results are shown in terms of the energy ratios, *INR* and *FDR*, defined as follows:

$$INR = \frac{E_I}{V_{BY} \Delta_Y}$$
 (2)

$$FDR = \frac{E_{FD}}{V_{BY} \Delta_{Y}}$$
 (3)

where *INR* is the seismic input energy ratio; *FDR* is the friction-damper dissipated energy ratio; E_I is the seismic input energy; E_{FD} is the energy dissipated by all friction dampers; V_{BY} and Δ_Y are the yield base shear and the top-floor yield displacement of the braced structure without dampers, respectively. Derivations of E_I and E_{FD} are given in Appendix A.

Fig. 7 shows a relation between base shear and top-floor displacement obtained from pushover analysis of the braced building, without dampers, including weld fractures. The same bracing system as in the previous numerical studies is employed. Lateral force distribution according to the UBC 1997 code is adopted here. The values of lateral forces in each storey as fraction of base shear are shown in Table 1. A monotonic increasing load is applied to the structure with linear increment of 200 kN/sec until the ultimate load is reached. The same time step as used in the previous numerical studies is chosen. From the analysis, the yield base shear is 6448 kN and the yield top-floor displacement of the brace structure is 79.0 mm.

Table 1. Lateral force distribution factors as a fraction of base shear for braced structure

Storey level	Height (m.)	Weight (kN)	Distribution factor
6	24.536	1815.53	0.2123
5	20.726	2514.80	0.2484
4	16.916	2514.80	0.2028
3	13.106	2514.80	0.1571
2	9.296	2514.80	0.1114
1	5.486	2599.13	0.0680

Note: Fundamental period of braced structure = 0.649 sec

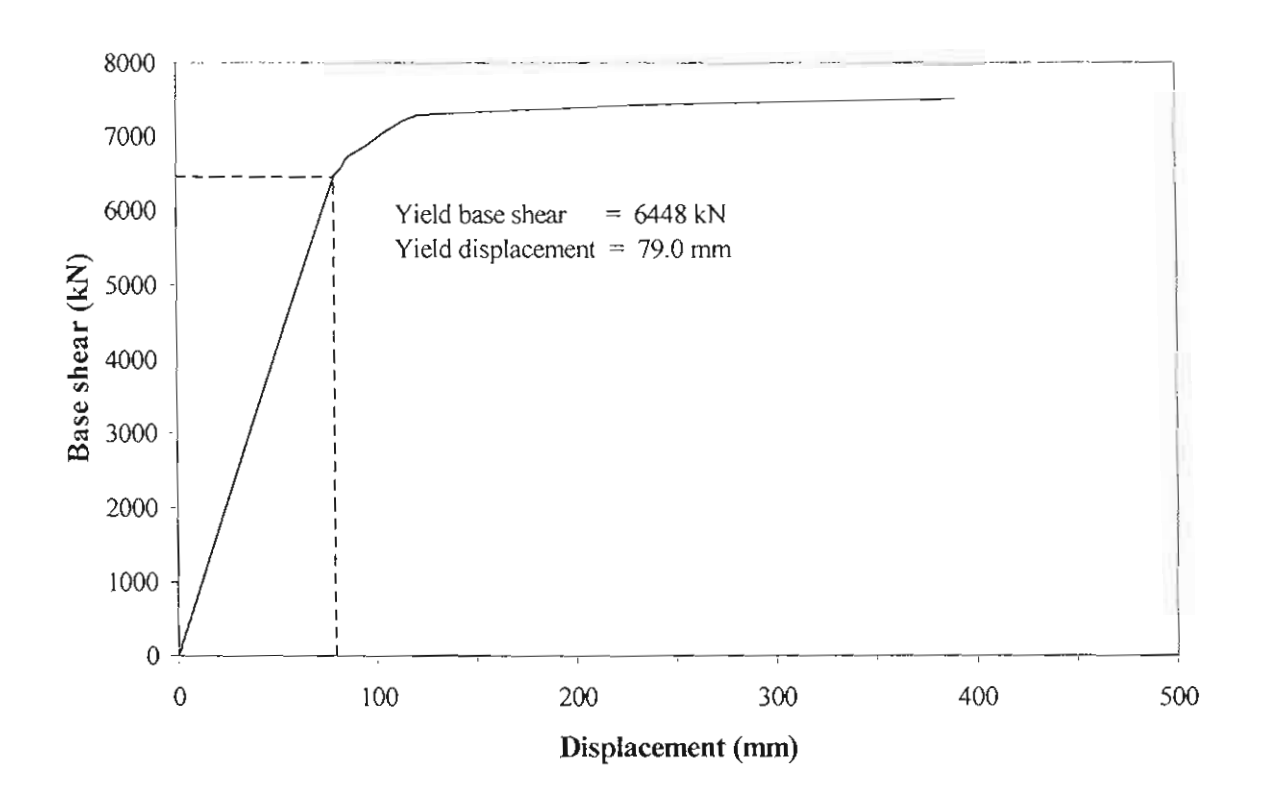


Fig. 7. Pushover analysis of the braced building without dampers including weld fracture effect

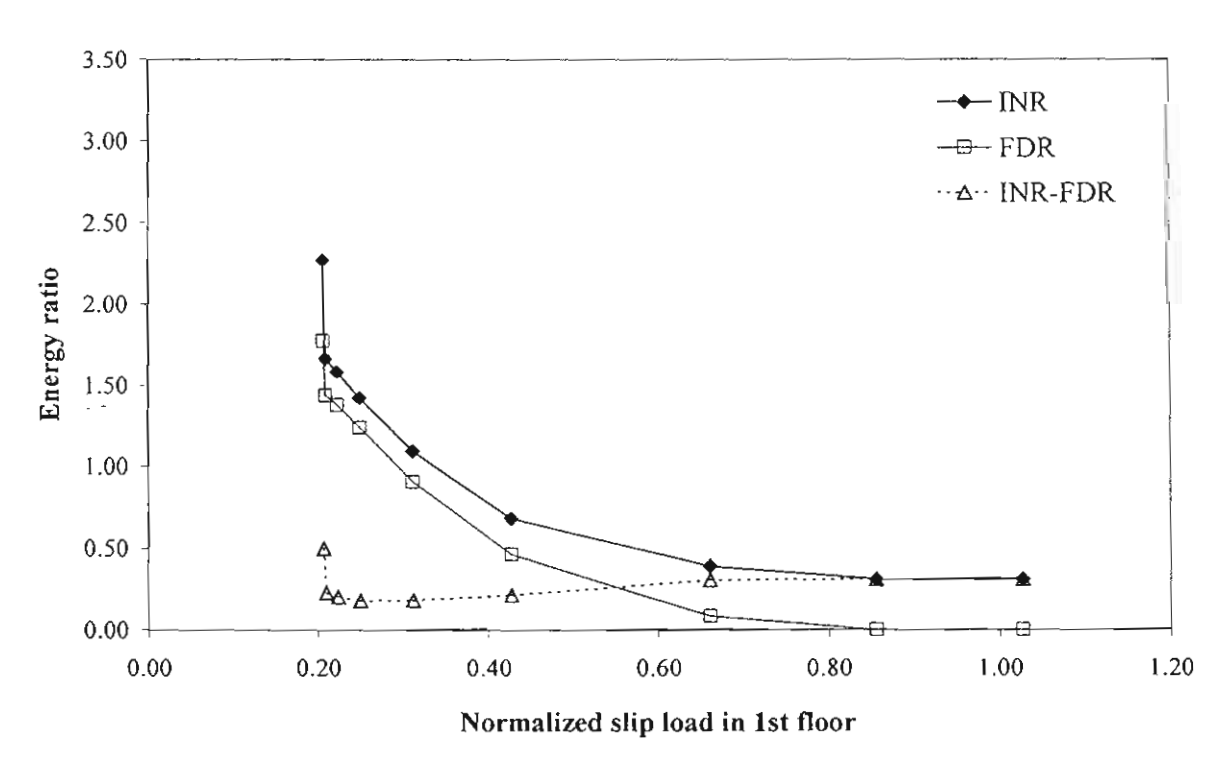


Fig. 8. Variation of energy ratio with normalized slip load: SCT85EW

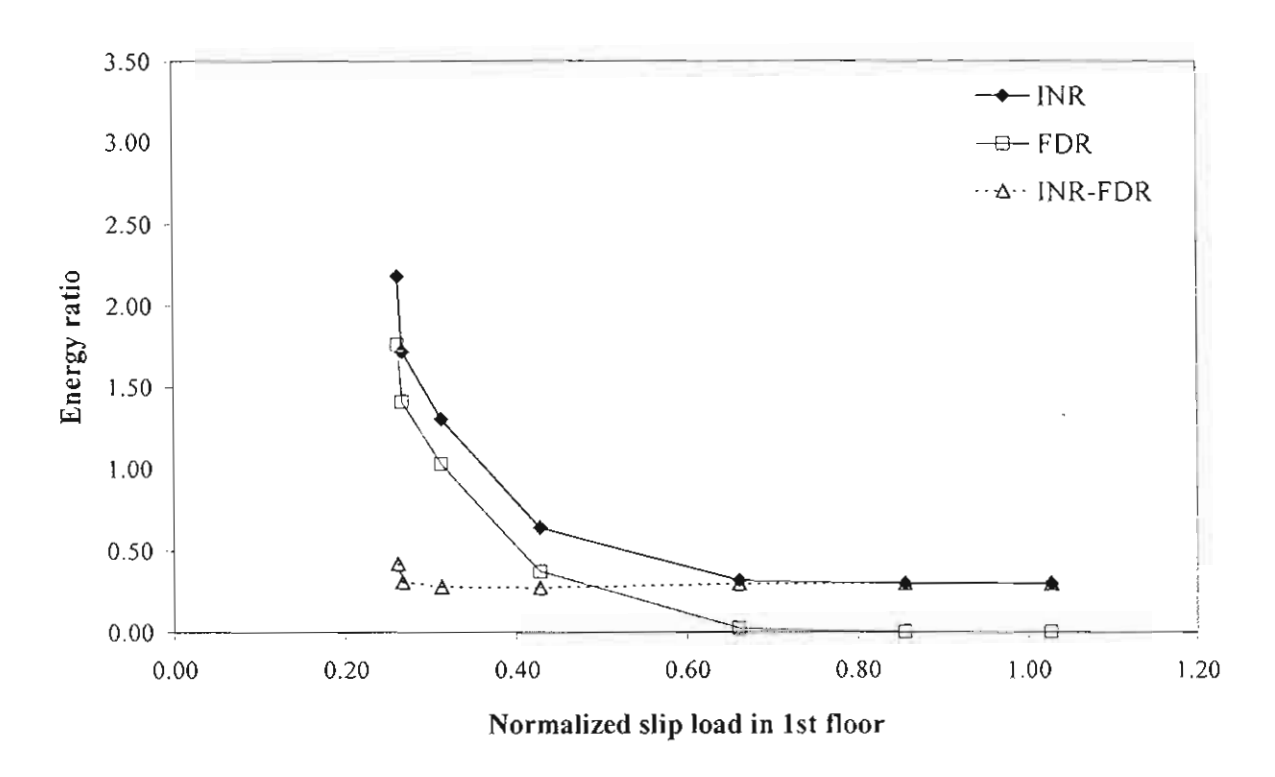


Fig. 9. Variation of energy ratio with normalized slip load: BKK95Bx

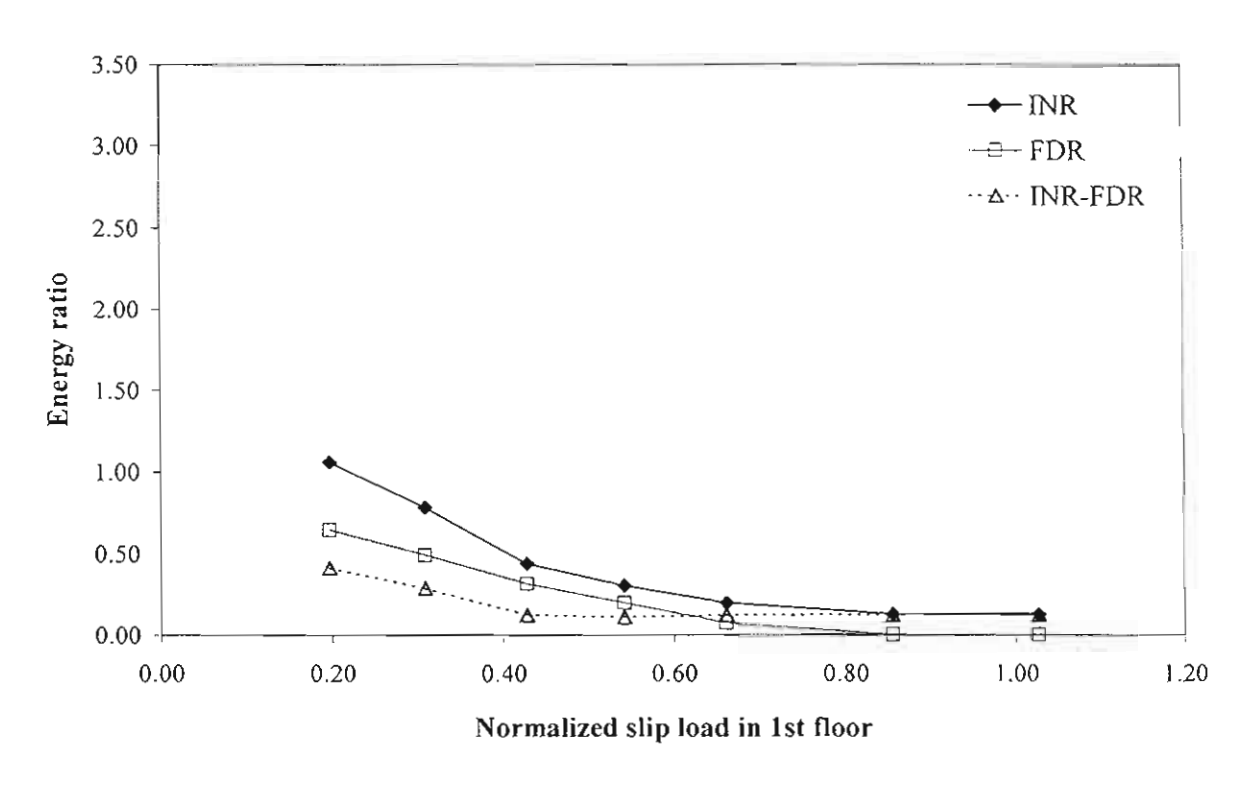


Fig. 10. Variation of energy ratio with normalized slip load: ROM77NS

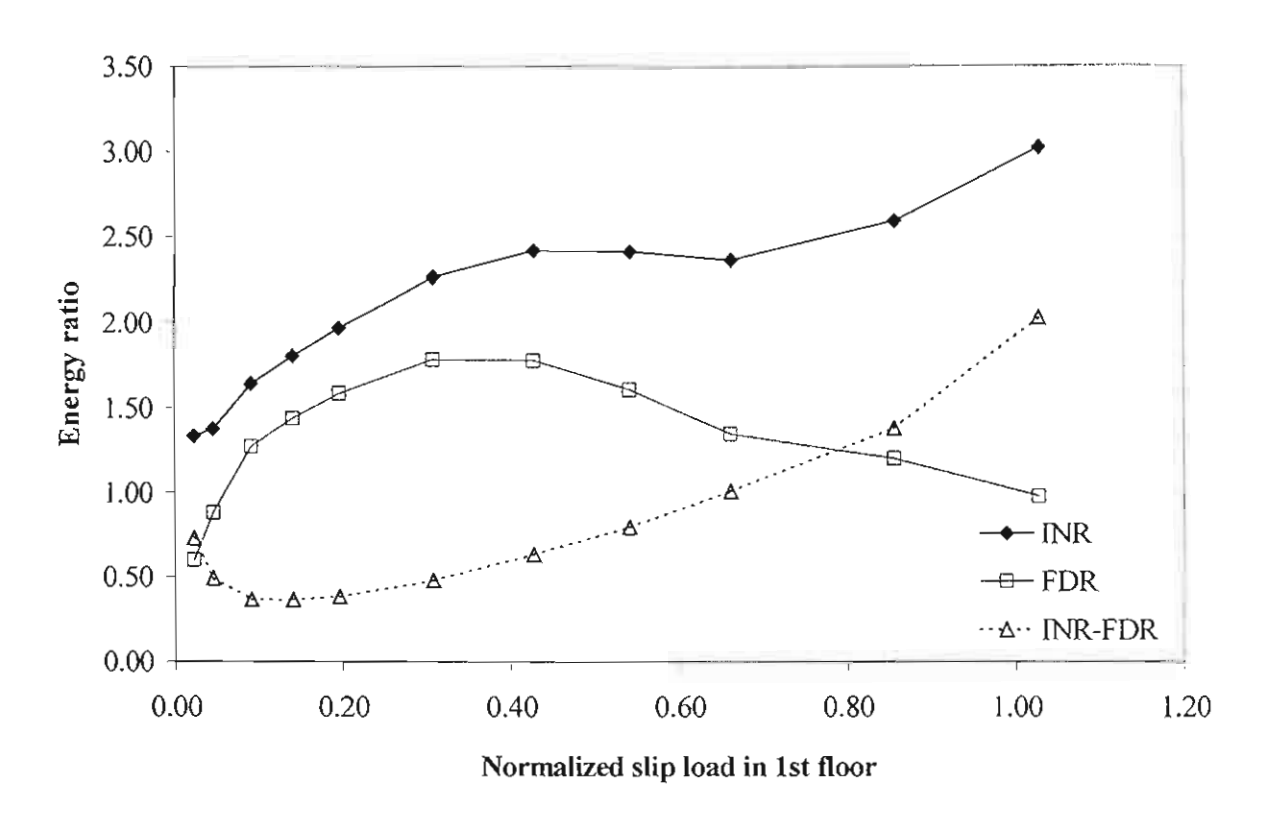


Fig. 11. Variation of energy ratio with normalized slip load: ELC40NS

Figs. 8 to 11 show the variations of the energy ratios with the normalized slip load in the first floor for building subjected to each excitation. The difference between the seismic input energy ratio (INR) and the friction-damper dissipated energy ratio (FDR) indicates the amount of energy dissipated by inherent damping and damage of the structure itself. It can also be considered as the performance index for the added friction dampers. Again, past the critical slip load, friction dampers can significantly reduce the energy fed to the primary structure. At the optimum points, the devices can absorb 87%, 58%, 65%, and 80% of the seismic input energy resulting from SCT, Bangkok, Romania, and El Centro signals, respectively. For El Centro, as expected, the performance of the damper decreases with increasing slip loads. For long-distance earthquakes at large values of slip load, the energy dissipated by the dampers vanishes indicating that the added dampers are not utilized. This is compensated by reduction of the seismic input energy because at high values of slip load, the system behaves as a fully braced structure resulting in the shift of a vibration period to the short period end of the response spectra which has low spectral values as shown in Fig. 3.

From the results obtained, it seems that only the added stiffness from the braces is sufficient for the building to resist the long-distance earthquakes considered. However, it should be noted that the buckling phenomena of bracing members are neglected in this study. If both the brace buckling and joint fractures occur, the stiffness of the system will sharply reduce and this could lead to a total collapse of the whole structure. Hence, addition of friction dampers will have the advantage of preventing buckling or damage to the bracing elements and give nearly equal or better performance compared to the traditional bracing system.

5. Conclusions

The performance of a friction damping system for retrofitting steel moment-resisting frames with weld fracture behaviour was investigated under three long-distance earthquakes: the 1985 Mexico city (SCT), the scaled 1995 Bangkok, and the scaled 1977 Romania ground motions. Responses of the building under the 1940 El Centro record were also shown for comparison purposes. The following conclusions can be drawn from this study:

- 1. The original building with joint fracture effect neglected can survive all considered excitations; however, retrofit would still be required.
- 2. The effect of weld fracture can lead to the collapse of the non-retrofitted structure under all excitations considered, even under moderate long-distance earthquakes which have a peak ground acceleration only about half of the El Centro accelerogram.
- 3. The building including joint fracture effect can survive all considered earthquakes with the addition of friction dampers at a certain critical slip load value.
- 4. It is important to pay attention to selecting the damper slip load to be sufficiently far away from the critical value and at the same time not too close to the buckling or yield strength of the connecting members.
- Addition of friction dampers will have the advantage of preventing buckling or damage to the bracing elements and give nearly equal or better performance compared to the traditional bracing system.

Acknowledgements

The writers are grateful to the Thailand Research Funds (TRF) for the TRF research scholar granted for this project.

Appendix A: Energy Formulation

Consider a multi-degree-of-freedom system equipped with friction dampers. Denoting \mathbf{u} as the vector of displacements relative to the base and $\mathbf{u}_g(t)$ is the horizontal ground displacement at any time t, the equations of motion can be written as:

$$\mathbf{M}\ddot{\mathbf{u}}(t) + \mathbf{C}\dot{\mathbf{u}}(t) + \mathbf{F}_{s}(t) + \mathbf{F}_{FD}(t) = -\mathbf{M}\mathbf{e}_{g}\ddot{\mathbf{u}}_{g}(t) \tag{A.1}$$

where M and C are the mass and damping matrices of the structure; F_s is the vector of the resisting forces provided by the main structure and F_{FD} is the vector of forces provided by the friction dampers. e_g is the displacement influence coefficient vector associated with a unit support displacement defined as follows:

$$\mathbf{u}_{t}(t) = \mathbf{u}(t) + \mathbf{e}_{\mathbf{g}}\mathbf{u}_{\mathbf{g}}(t) \tag{A.2}$$

where $\mathbf{u}_{t}(t)$ is the vector of total displacements.

Integrating the equations of motion with respect to the relative displacement vector **du** over the entire range of displacements, the energy equation can be obtained as follows:

$$\int d\mathbf{u}^{\mathsf{T}} \mathbf{M} \ddot{\mathbf{u}} + \int d\mathbf{u}^{\mathsf{T}} \mathbf{C} \dot{\mathbf{u}} + \int d\mathbf{u}^{\mathsf{T}} \mathbf{F}_{\mathsf{S}} + \int d\mathbf{u}^{\mathsf{T}} \mathbf{F}_{\mathsf{FD}} = -\int d\mathbf{u}^{\mathsf{T}} \mathbf{M} \mathbf{e}_{\mathsf{g}} \ddot{\mathbf{u}}_{\mathsf{g}}$$

$$E_{\mathsf{K}} + E_{\mathsf{D}} + E_{\mathsf{S}} + E_{\mathsf{FD}} = E_{\mathsf{I}} \tag{A.3}$$

The right side of Eq. (A.3), E_I , is the relative seismic energy input to the structure. For the terms on the left side, E_K is the kinetic energy of the mass associated with its motion relative to the ground; E_D is the energy dissipated by the inherent damping of the main structure; E_S is the total strain energy caused by deformations of the main structural elements and E_{FD} is the total energy dissipated by the added friction dampers. Based on these energy quantities, Eq. (A.3) is a statement of energy balance for the system.

References

Applied Technology Council [2000] "NEHRP Guidelines for the Seismic Rehabilitation of Buildings," Federal Emergency Management Agency (FEMA 354), Washington, DC.

Carr, A. J. [2000] "RUAUMOKO user's manual," Dept. of Civil Engrg., University of Canterbury, Christchurch, New Zealand.

EERI [1997] "Earthquake Hazard Slide Sets," Earthquake Engineering Research Institute, CA. (on CD-ROM).

Filiatrault, A. and Cherry, S. [1990] "Seismic design spectra for friction-damped structures," J. Struct. Engrg. ASCE 116(5), 1334-1355.

Filiatrault, A., Tremblay, R. and Wanitkorkul, A. [2001] "Performance evaluation of passive damping systems for the seismic retrofit of steel moment resisting frames subjected to near field ground motions," *Earthquake Spectra* 17(3), 427-456.

FitzGerald, T. F., Anagnos, T., Goodson, M. and Zsutty, T. [1989] "Slotted bolted connections in aseismic design for concentrically braced connections," *Earthquake Spectra* 5(2), 383-391.

Grigorian, C. E., Yang, T. S. and Popov, E. P. [1993] "Slotted bolted connection energy dissipators," *Earthquake Spectra* 9(3), 491-504.

Pall, A. S. and Marsh, C. [1982] "Response of friction damped braced frames," J. Struct. Div. ASCE 108(6), 1313-1323.

Pall, A. S. and Pall, R. [1996] "Friction-dampers for seismic control of buildings – A Canadian Experience," Proc. 11th WCEE, World Conf. Earthq. Engrg., Acapulco, Mexico, Paper No. 497.

Reinhorn, A. M., and Li, C. [1996] "Retrofit of concrete structures using supplemental damping devices," *Proc. 11th WCEE, World Conf. Earthq. Engrg.*, Acapulco, Mexico, Paper No. 78.

ภาคผนวก ง

บทความที่ตีพิมพ์ในการประชุมวิชาการนานาชาติ

- n. Pinkaew, T. "Vibration Control of Structures under Harmonic Excitation using Semi-Active Mass Dampers", Proceedings of the 13th ASCE-Engineering Mechanics Conference, The John Hopkins University, Maryland, USA., 1999.
- U. Lukkunaprasit, P. "Enhancement of Structural Performance for Moderate Seismic Risk Regions" Proceedings of the WG-1, Earthquake-Resisting Technologies for Civil Infrastructures, 3rd EQTAP Workshop, Manila, Philippines, 2000.
- O. Lukkunaprasit, P. "An Innovative Hook-Clip for Performance of Tied Columns in Developing Countries", Proceedings of the 12th World Conference on Earthquake Engineering, Auckland, New Zealand, 2000.
- Sittipunt, C., and Wood, S. L. "Development Details to Improve the Cyclic Response of Slender Structural Walls", Proceedings of the 12th World Conference on Earthquake Engineering, Auckland, New Zealand, 2000.
- a. Lukkunaprasit, P., and Thepmangkom, J. "Load History Effect on Cyclic Behavior of R.C. Tied Columns" Proceedings of the 14th KKNN Symposium on Civil Engineering, Kyoto, Japan, 2001.
- n. Teachavorasinskun, S., and Amornwithayalax, T. "Elastic Shear Modulus of Clays During Undrained Shearing" Proceedings of the 14th KKNN Symposium on Civil Engineering, Kyoto, Japan, 2001.

13th ASCE Engineering Mechanics Division Conference

The Johns Hopkins University Baltimore, MD, USA June 13-16, 1999

Conference Chairs

Roger Ghanem Nick Jones

National Steering Committee

Raouf Baddour

Allen Chwang

Ross Corotis

John Dempsey

Mark Hanson

Dimitrios Karamanlidis

Leon Keer

Loren Lutes

Sami Masri

Gilles Pijaudier-Cabot

Junuthula Reddy

Sunil Saigal

Howard Schreyer

Surendra Shah

Hayley Shen

Pol Spanos

Stein Sture

Stuart Swartz

Local Organizing Committee

Rajah Anandarajah

Jim Cox

Bruce Ellingwood

Poul Lade

Radoslaw Michalowski

Mike McCormick

Bob Scanlan

Vibration control of structures under harmonic excitation using semiactive mass damper

T. Pinkaew
Chulalongkorn University, Bangkok, THAILAND 10330
fcetpk@eng.chula.ac.th

Abstract:

A semi-active mass damper (SAMD) in which its damping can be varied is proposed to control the vibration of the structures under harmonic excitation. The objective is to produce a control system that provides a significant improvement over the conventional passive mass damper (TMD), but without the substantial penalties in cost, weight, and complexity as active damper. An optimal control law is formulated. A situation in which the damper can not vary beyond the certain range is also taken into account. The peak and steady-state amplitude responses are investigated in frequency domain. The obtained results are compared with those of TMD and it is found that the proposed SAMD can significantly reduce the peak response and also effectively suppress the steady-state response for broader band of excitation frequencies. The latter improvement is equivalent to the addition of mass about 300% on TMD.

Introduction

Structural vibration control has been one of the primary issues for some years. Active control is very efficient, but its implementation is very limited due to various mechanical and economical constraints. From this point of view, semi-active control is a promising alternative since it requires much less energy and it can potentially more efficient than passive control.

Karnopp, et. al. (1974) proposed the semi-active damping concept by using a variable damping device to generate the control force for vibration isolation. This semi-active control has been extensively studied in the field of automotive suspension control. To date, it has been successfully applied to a board class of vehicle vibration isolation problems ranging from military tanks to high-speed cars. An extension of the semi-active damping concept to structural control is found in the study of Hrovat, et. al. (1983). A TMD with an augmented variable damping device was proposed as a semi-active TMD for vibration control. Based on the numerical results of vibration control of a building subjected to a specific wind loading, the similar steady-state performance of semi-active TMD and active TMD was reported. However, there was no explicit study on the control performance of semi-active mass damper under harmonic excitation which is the common case in structural or mechanical control.

Optimal Semi-active Mass Damper

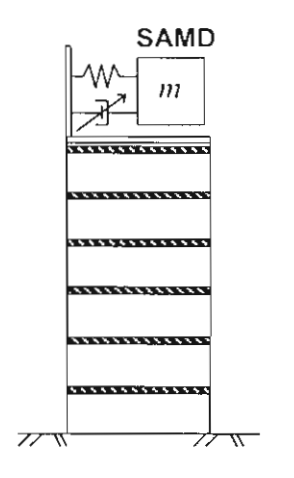


Figure 1. Structure-SAMD system

General Solution

A model representing a structure attached by the semi-active mass damper is shown in figure 1. This model can be expressed as a bilinear system in which the equations of motion are written in the following state-space description as

$$\dot{\mathbf{x}}(t) = \mathbf{A}\,\mathbf{x}(t) + \mathbf{B}\big(\mathbf{x}^{\mathsf{T}}(t)\,\mathbf{T}\big)\mathbf{v}(t) = \mathbf{A}\,\mathbf{x}(t) + \mathbf{B}\,\mathbf{u}_{sem}(t) \tag{1}$$

where $\mathbf{x}(t)$ is a state vector, \mathbf{A} is a characteristic matrix, \mathbf{B} is a control contribution matrix, \mathbf{T} is a transformation matrix, $\mathbf{v}(t)$ is an adjustable parameter vector, and $\mathbf{u}_{semi}(t) = \mathbf{x}^T(t)\mathbf{T}\mathbf{v}(t)$ is a semi-active control force produced by the variation of $\mathbf{v}(t)$. The objective is to find the parametric control $\mathbf{v}(t)$ that minimizes the well-known quadratic performance index

$$J_{semi} = \int_{0}^{\infty} \left[\mathbf{x}^{\mathsf{T}}(t) \mathbf{Q} \mathbf{x}(t) + \mathbf{u}_{semi}^{\mathsf{T}}(t) \mathbf{R} \mathbf{u}_{semi}(t) \right] dt$$
 (2)

subjected to the dynamic constraint, Eq.(1).

As obtained in the determination of optimal semi-active vehicle suspension system (Tseng and Hedrick 1994), it is convenient to first consider the optimal solution for fully-active system case. Then the corresponding semi-active optimal solution is determined by minimizing the variation of performance index which is deviated from its reference optimum due to the introduction of semi-active system. It is, therefore, helpful to relate the performance index of general semi-active system to that of the reference active system as

$$J_{semi} = J_{octive} + \int_{0}^{\infty} \left[\left(\mathbf{u}_{semi}(t) - \mathbf{u}_{opt}(t) \right)^{\mathsf{T}} \mathbf{R} \left(\mathbf{u}_{semi}(t) - \mathbf{u}_{opt}(t) \right) \right] dt$$
 (3)

where J_{active} is a constant function of initial state and \mathbf{u}_{opt} is the optimal control force of the reference active system. Instead of directly minimizing the whole integration, the control law is obtained by minimizing the instantaneous error resulted from the difference $(\mathbf{u}_{semi}(t)-\mathbf{u}_{opt}(t))$. This leads to the minimization of the function

$$L(t) = \left(\mathbf{u}_{semi}(t) - \mathbf{u}_{opt}(t)\right)^{2}$$
(4)

By equating the reaction forces of semi-active system with active system, the semi-active control force can be written as

$$\mathbf{u}_{semi}(\mathbf{t}) = u_{semi}(\mathbf{t}) = -(c(\mathbf{t}) - c_{\theta})\dot{z}(\mathbf{t}) \tag{5}$$

where now \mathbf{u}_{semi} becomes a scalar function, u_{semi} . z(t) = relative displacement across the variable damper, and c_0 = constant optimal passive damping.

Inequality Constraint on Damper Parameter

It is assumed that the variable damping coefficient c(t) can be varied in a range,

$$c_{\min} \leq c(t) \leq c_{\max}$$
 (6)

To find the optimal variation of damping coefficient which minimizes the performance measure Eq.(3) subjected to the inequality constraints Eq.(6), we define the Lagrangian (Bryson and Ho 1975)

$$H(c(t), \lambda_1, \lambda_2) = \frac{1}{2} L(c(t), k) + \lambda_1 f_1(c(t)) + \lambda_2 f_2(c(t))$$

$$\tag{7}$$

where $f_1(c(t)) = c(t) - c_{\text{max}} \le 0$ and $f_2(c(t)) = c_{\text{min}} - c(t) \le 0$ are the imposed inequality constraints and $\lambda_1, \lambda_2 \ge 0$ are the Lagrange multipliers.

The necessary condition for a minimum becomes

$$\frac{\partial H}{\partial x} = \frac{1}{2} \frac{\partial L}{\partial x} + \lambda_1 \frac{\partial f_1}{\partial x} + \lambda_2 \frac{\partial f_2}{\partial x} = 0$$
 (8)

By substituting Eq.(5) into Eq.(4) and then into Eq.(8), we get

$$c_{opt}(t) = \frac{\lambda_2 - \lambda_1}{\dot{z}(t)^2} + \frac{u_{opt}(t)}{\dot{z}(t)} + c_0$$
(9)

More precisely, we have an optimal variation of damping as

$$c_{opt}(t) = \begin{cases} c_{\text{max}}, & \text{if } c_d(t) \ge c_{\text{max}} \\ c_d(t), & \text{if } c_{\text{min}} \le c_d(t) \le c_{\text{max}} \\ c_{\text{min}}, & \text{if } c_d(t) \le c_{\text{min}} \end{cases}$$
(10)

where

$$c_d(t) = u_{opt}(t) / \dot{z}(t) + c_o \qquad \text{for} \quad \dot{z}(t) \neq 0$$
 (11)

and the sufficient conditions for minimum is ensured by Eq.(8) and $\frac{\partial^2 H}{\partial z^2} = (\dot{z}(t))^2 \ge 0$.

Vibration Control of a Single-degree-of-freedom System

Problem Formulation and System Properties

In the following numerical examples, a SAMD is employed to reduce the vibration of the main structure which is model by a SDOF system subjected to an harmonic excitation F (t) as shown in figure 2. The equations govern the vibration of the system are

$$(m_1 + m_2) \ddot{x}_1(t) + c_1 \dot{x}_1(t) + k_1 x_1(t) = F(t) - m_2 \ddot{z}(t)$$
 (12)

and
$$m_1\ddot{z}(t) + c_2(t)\dot{z}(t) + k_2z(t) = -m_2\ddot{x}_1(t)$$
 (13)

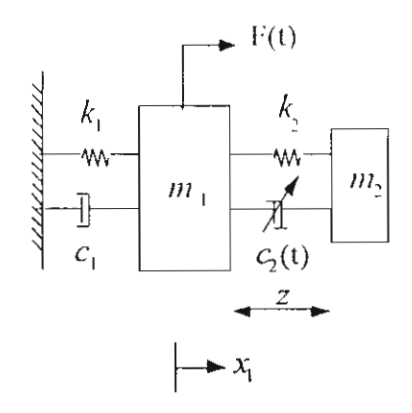


Figure 2. Structure-SAMD Model

where the time-dependent damping of the SAMD, c(t) is computed according to the control law derived in previous section.

Throughout the simulations, the main structure is assumed to have the natural frequency of 3.0 Hz and the damping ratio of 2.0 %. While the mass dampers are assumed to have the mass ratio of 3.0 %. The passive parameters of the TMD are optimized according to the excitation (Den Hartog 1956). Table (1) lists all the values of the system properties, which are used for the numerical model.

Table 1. System Properties

(i) main structure
$$m_1 = 1 \text{ kg}$$
 $k_1 = 355.30 \text{ N/m}$ $\xi_1 = 2.00 \%$ $\omega_1 = \sqrt{\frac{k_1}{m_1}} = 18.85 \text{ rad/s} (f_1 = 3.0 \text{ Hz})$ (ii) SAMD $m_2 = 0.03 \text{ kg}$ $k_2 = 10.05 \text{ N/m}$ $c_{2\text{min}} = 0$, $c_{2\text{max}} = 3.403 \text{ N-s/m} (\xi_2 = 300\%)$

Response under Harmonic Excitation

It is known that for a nonlinear system the response magnification factor may depend on the excitation or the system response may not be even periodic. Nevertheless, it is demonstrated that (1) the response of the eqs.(12) and (13) to periodic excitation is

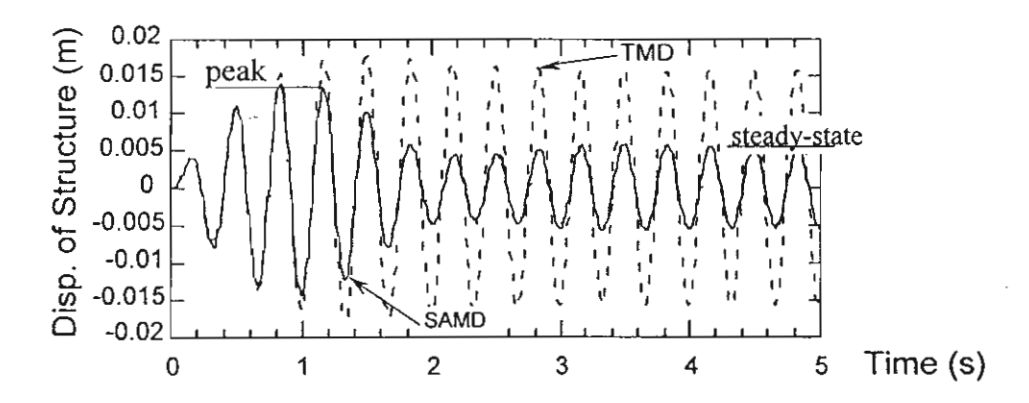


Figure 3. Typical Harmonic Responses under TMD and

periodic with the same period as excitation, and (2) the amplitude ratio is independent of excitation amplitude (Hac and Youn 1992). Therefore the following comparison of the control performance in frequency domain is meaningful.

Figure (3) shows the typical time histories of the structure subjected to harmonic excitation under TMD and SAMD. Assuming that the system starts from rest, the steady-state amplitude and the peak amplitude are defined as shown in this figure for SAMD case.

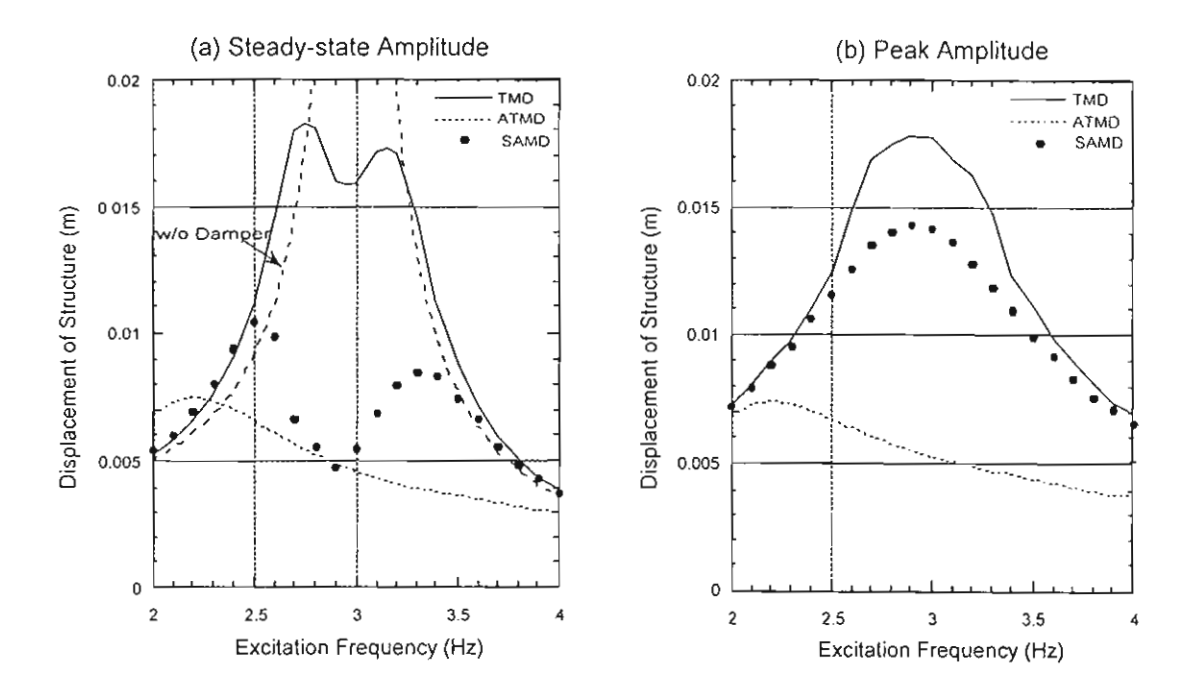


Figure 4. Frequency Responses (a) Steady-state Amplitude and (b) Peak Amplitude

Figure (4a) plots the steady-state amplitudes of the structure controlled with TMD, ATMD, and SAMD, within the frequency range of 2.0-4.0 Hz. The figure indicates that significant improvement of steady-state amplitude reduction of the structure, comparing to TMD, can be achieved via SAMD. Beside the amplitude reduction, the figure also reveals that SAMD has broader frequency band of suppression. More precisely, the suppression band of SAMD becomes about 2 times broader than that of TMD. This is equivalent to the increasing of mass of TMD by 300 percents. Figure (4b) plots the peak amplitudes of the structure within the same frequency range. It is found that SAMD markedly improves the peak amplitude response of structure over TMD case especially around the resonant frequency. It is clearly from these two figures that, in both cases, ATMD exhibits highest control performance. However, its implementation is known to be very costly.

Conclusion

An optimal control law which minimizes the quadratic performance index for a semi-active mass damper is formulated and applied to control the vibration of SDOF-structure. Through the computer simulation, the control performance of the semi-active mass damper is studied and compared with that of TMD under harmonic excitation. The obtained results reveal that the proposed SAMD can significantly reduce the peak response and also effectively suppress the steady-state response for broader band of excitation frequencies. In particular, the latter improvement is equivalent to the addition of mass about 300% on TMD. This is often unfeasible for passive system implementation.

Generally, simulation results indicate that the semi-active mass damper which is usually cheaper than the active damper system offers a substantially better performance than the passive TMD. Consequently, it represents a very attractive alternative for vibration control of structures subjected to harmonic-liked disturbances.

Acknowledgment

The author wishes to thank Prof. Dr. P Lukkunaprasit of Chulalongkorn University for his valuable comments and discussions. Also he gratefully acknowledges the support of Thailand Research Fund under contact RTA/03/2540.

References

- Bryson, A.E., and Ho, Y.C. (1975), *Applied Optimal Control*, John Wiley and Sons, Inc., New York.
- Den Hartog, J.P. (1956), Mechanical *Vibrations*, 4th. Edition, McGraw-Hill Book Company, New York.
- Hac, A. and Youn, I. (1992), "Optimal Semi-Active Suspension with Preview Based on a Ouarter Car Model", Trans. ASME, J. of Acoustics and Vibration, 144, 84-92.
- Hrovat, D., Barak, P., and Rabins, M. (1983), "Semi-Active Versus Passive or Active Tuned Mass Dampers for Structural Control", ASCE, J. Engrg. Mech., 109, 691-705.
- Karnopp, D.C., Crosby, M.J., and Harwood, R.A. (1974), "Vibration Control Using Semi-Active Force Generators", *Trans.* ASME, *J. Engrg. for Industry*, **96**, 619-626.
- Tseng, H.E. and Hedrick, J.K. (1994), "Semi-Active Control Laws-Optimal and Suboptimal", *Vehicle System Dynamics*, **23**, 545-569.